REPORT CDOT-2022-02 February 2022

Earth Pressure Assessment and Optimization of Type-7 Barrier GRS Walls

APPLIED RESEARCH & INNOVATION BRANCH

Nien-Yin Chang

Hien Manh Nghiem

Shin-Chung Wang

Aziz Khan

Technical Report Documentation Page

1. Report No.	2. Government Accession No.	3. Recipient's Catalog No.
CDOT-2022-02		

4. Title and Subtitle	5. Report Date
Earth Pressure Assessment and Optimization of Type-7 GRS Walls – Earth Pressure for Type-7 GRS Wall	February 2022
	6. Performing Organization Code

7. Author(s)	8. Performing Organization Report No
Nien-Yin Chang, Hien Manh Nghiem, Shing-Chun Wang, Aziz Khan	. UCD-CGES-2022-001

9. Performing Organization Name and Address	10. Work Unit No. (TRAIS)
The Regents of the University of Colorado Center for Geotechnical Engineering Science, Department of Civil Engineering, University of Colorado Denver 1201 Larimer St, Denver, CO 80204	11. Contract or Grant No. R218.01 Type 7 GRS

12. Sponsoring Agency Name and Address	13. Type of Report and Period Covered
Colorado Department of Transportation - Research 2829 W. Howard Pl. Denver CO, 80204	Final
	14. Sponsoring Agency Code

15. Supplementary Notes

Performed in cooperation with the Federal Highway Administration

16. Abstract

The construction of Type-7 Barrier Geosynthetic Reinforced Soil Wall (T7B-GRSW), much like bridge abutments, bridge approach, and retaining walls, the adoption of Geosynthetic Reinforced Soil (GRS) technology provides much-needed space-saving. In the early 20th century, before the invention of GRS (or MSE) technology, earth retaining structures had to resist immense earth pressures and massive earth retaining structures were required and the block facing and panel walls were impractical, and the wall construction took a much longer time. Nowadays, the adaptation of GRS technology significantly reduces wall pressures, block and panel facings become feasible for saving cost and construction time.

The further cost and time saving is accomplished with truncated base wall construction, as reported in the CDOT study on the base bearing pressure distribution in truncated base walls. This study on T7B-GRS walls utilizes the truncated-base design concept to achieve wall pressure reduction, reinforced concrete wall shape optimization, and space utilization efficiency with a much-reduced wall cross-section. T7B-GRS walls enhance sustainable geo-construction and make wall construction more nature-friendly. In low winter temperatures, the winter freeze and thaw cycles accelerate the GRS block facing wall distress and compromise the wall longevity, as shown in the GRS block facing wall distress along the Berthoud Pass. Besides, their repairs are both challenging and costly. The T7B-GRSW combines the functionality of wall and barrier in one wall system with the full benefit of GRS technology. So, T7B-GRSW is a superior design concept.

17. Keywords	18. Distribution Statement
T7B-GRS wall, earth pressure assessment, optimum wall cross-section, finite element analysis, geosynthetic reinforced soils	This document is available on CDOT's website https://www.codot.gov/programs/research

19. Security Classif. (of this report)	20. Security Classif. (of this page)	21. No. of Pages	22. Price
Unclassified	Unclassified		

ACKNOWLEDGEMENT

The Colorado Department of Transportation sponsored this study, and the Center for Geotechnical Engineering Science (the Center) research team (TEAM) at the University of Colorado Denver greatly appreciates the sponsorship. The TEAM appreciates the comments from the following panelists: Aziz Khan, Shing Chun (Trever) Wang, Panel Chair, Bridge Design and Management (BDM), Ryan Sullivan-Hope, Teddy Meshesha, Matt Greer, CO Division of FHWA, Daniel Alzamora, FHWA Resource Center, Dave Thomas, Materials and Geotechnical Branch. The TEAM includes the following members: Nien-Yin Chang, PI, Hien Manh Nghiem, Co-PI, and doctoral graduate students: Bach Pham and Shile Dong. The Center acknowledges the devotion of the TEAM members to this study.

TABLE OF CONTENTS

LIST OF FIGURES

LIST OF TABLES

1. PROBLEM DESCRIPTION AND ENGINEERING SIGNIFICANCE

General The construction of Type-7 Barrier Geosynthetic Reinforced Soil Wall (T7B-GRSW), much like bridge abutments, bridge approach, and retaining walls, the adoption of Geosynthetic Reinforced Soil (GRS) technology provides much-needed space-saving. Just imagine in the early nineteen hundred before the invention of GRS (or MSE) technology, all earth retaining structures would have to resist larger earth pressures. Thus, block facing and/or panel walls will be impractical and the construction would take much longer time. Nowadays, GRS technology is widely adopted to achieve effective space utilization and saving of soils used as construction materials. This certainly enhances sustainable geotechnical construction and makes geotechnical construction more nature friendly. In the region of lower winter temperatures, while GRS block-facing walls are easier to construct, their longevity is frequently compromised. For instance, many GRS block-facing walls along the Berthoud Pass suffered great distress under repeated freeze-thaw action. Their repairs are both challenging and costly. Besides, the T7B-GRSW combines the functionality of walls and barriers in one wall system with the full benefit of GRS technology (Chang et al., 2004). So, T7B-GRSW is an excellent design concept.

Vehicular Impact Load Resistance Now, one can reap the benefit of GRS technology to enhance the safety of the T7B-GRS wall under highway vehicular impact loads. GRS wall lateral earth pressure and base bearing pressure dictate the wall design, and GRS reduces lateral earth pressure due to its greatly enhanced lateral stiffness of GRS mass. Combining GRS technology with the truncated base wall design further enhances the feasibility of the T7B-GRSW concept by construction cost reduction.

This study calls for the replacement of block facing with the reinforced concrete (RC) facing, precast or cast-in-place, whichever is more cost-effective. This RC facing enhances the vehicular impact load resistance, as demonstrated in the author's earlier study (Chang et al., 2004), in which the barrier is supported on an independent moment slab.

This study addresses the safety and performance of T7B-GRSW, where the safety of the rail-wall system in an integral design further enhances the safety of the impact rail. CDOT engineers frequently discuss the feasibility of adopting truncated GRS walls as a means of saving construction costs. Their concerns have been addressed in a final study report on truncated GRS wall base bearing distribution (Chang et al., 2020b). The concept of the truncated GRS wall is

again an integral part of this study. To answer the demand, the Staff Bridge has issued worksheets to address the design of truncated GRS walls with precast concrete facings and steep cuts behind the GRS backfill. The worksheet covers a truncated base self-standing GRS wall with a maximum design height of 8'-6" (Figs. 1 and 2).

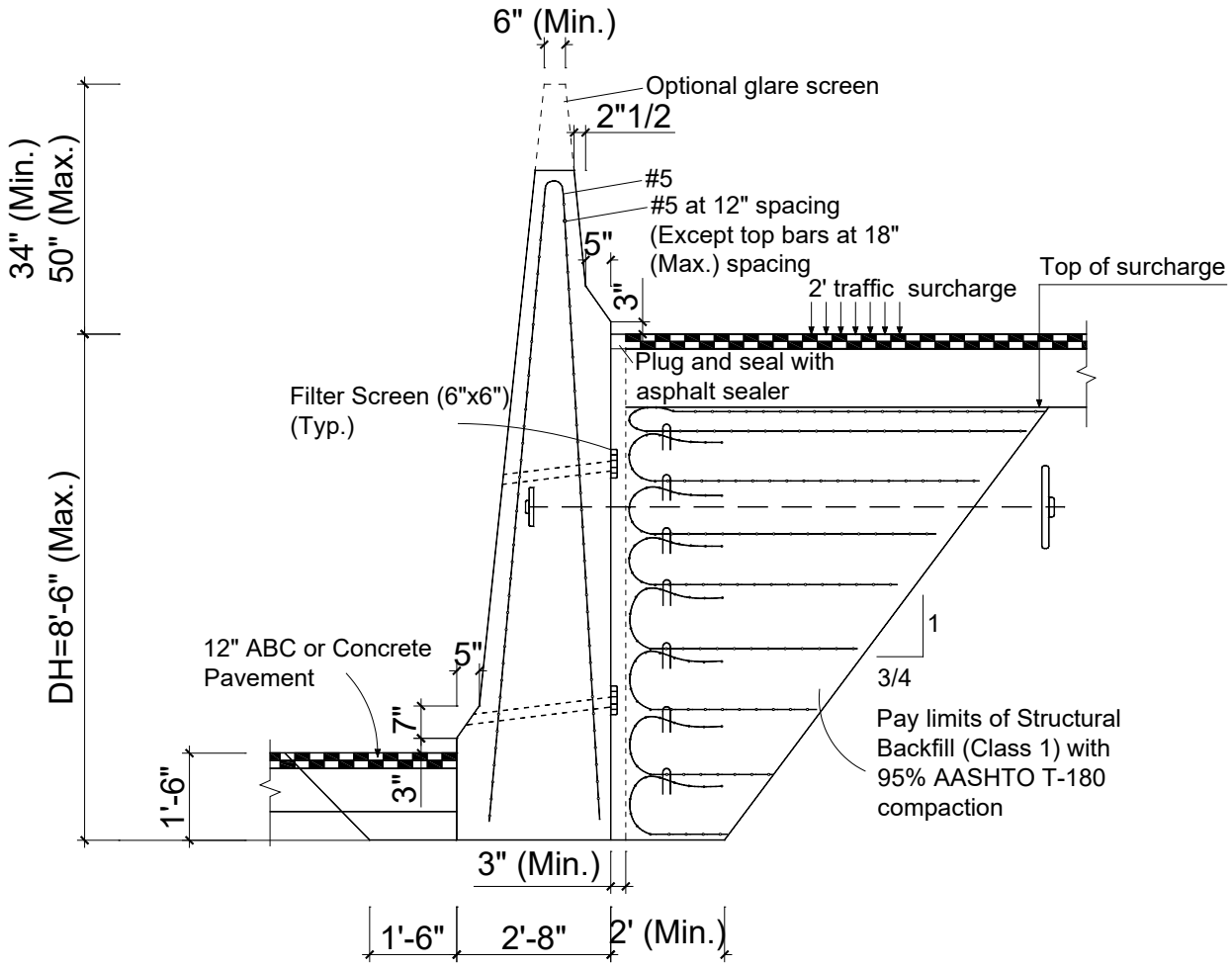

Figure 1. Type I with 3" sand-filled gap and wrap-around geosynthetic

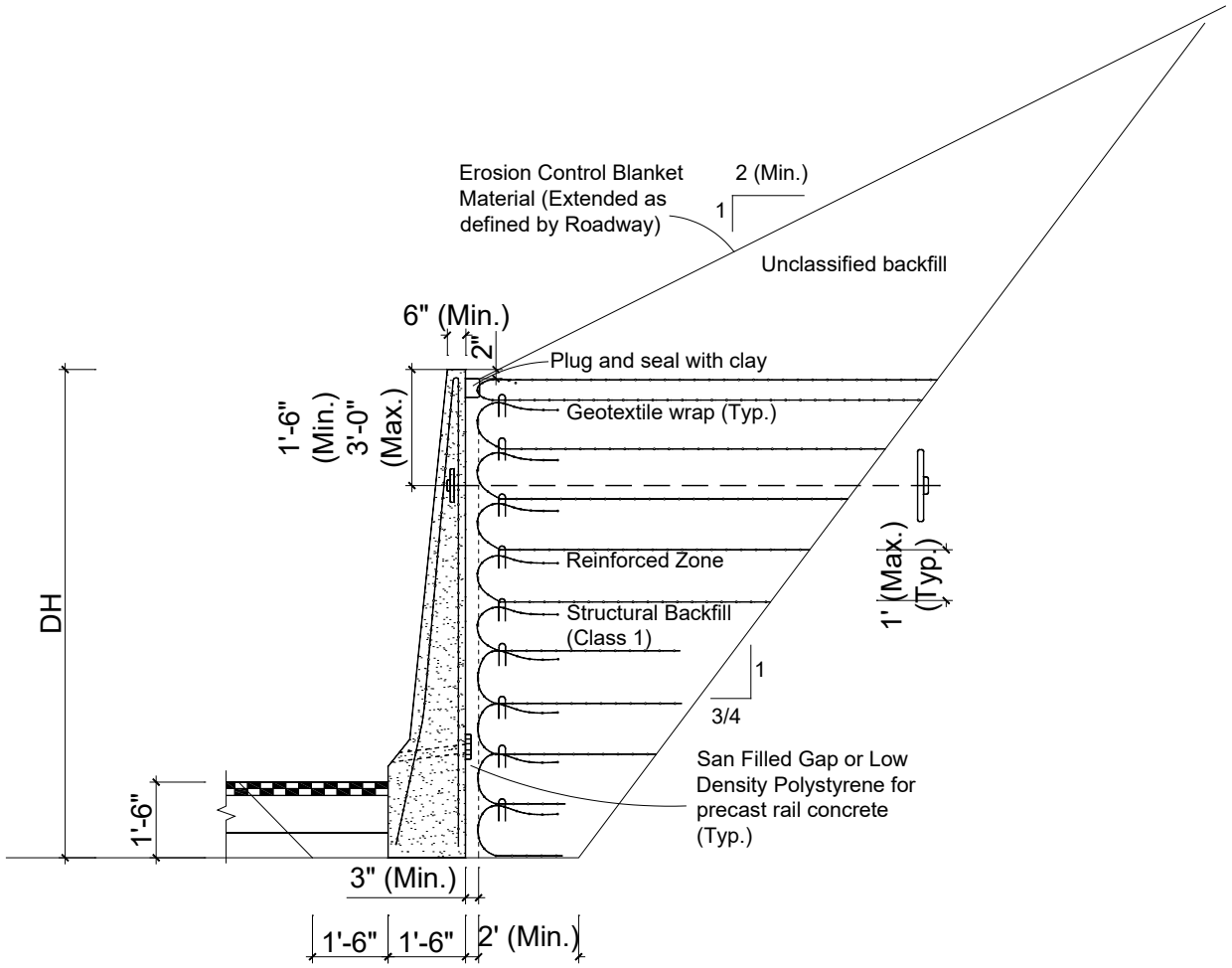

Figure 2. Type II with 3" sand-filled gap and wrap-around geosynthetic

Effects of 3-inch Gap with/without Sand Backfill and with/without wrap-around

By filling the gap (or space), with sands, between the facial element and the wrap around the GRS wall, the reinforced concrete facial element experiences a small earth pressure, and the wall height is conservatively limited to 8'-6". However, the construction of the wrap-around and sand-filled gap slows down the GRS wall construction, and it is desirable to eliminate the wrap-around (Figs. 3 and 4). This proposed study examines some safety and performance concerns of the design, which are addressed through laboratory experiments and numerical analyses. To study the safety and performance of GRS walls without wrap-around and 3-inch sand-filled gap requires accurate earth pressure measurement through a large model (or full-scale) experiment of T7B-GRS walls with precision measurement of earth pressure instrumentation during and after construction.

Although the earth pressure with one-foot geosynthetic spacing might be of concern for the barrier stability during compaction, the problem can be addressed through a large-scale model test with earth pressure instrumentation, particularly when there is a need for extending the wall design height beyond the 8'-6" limit.

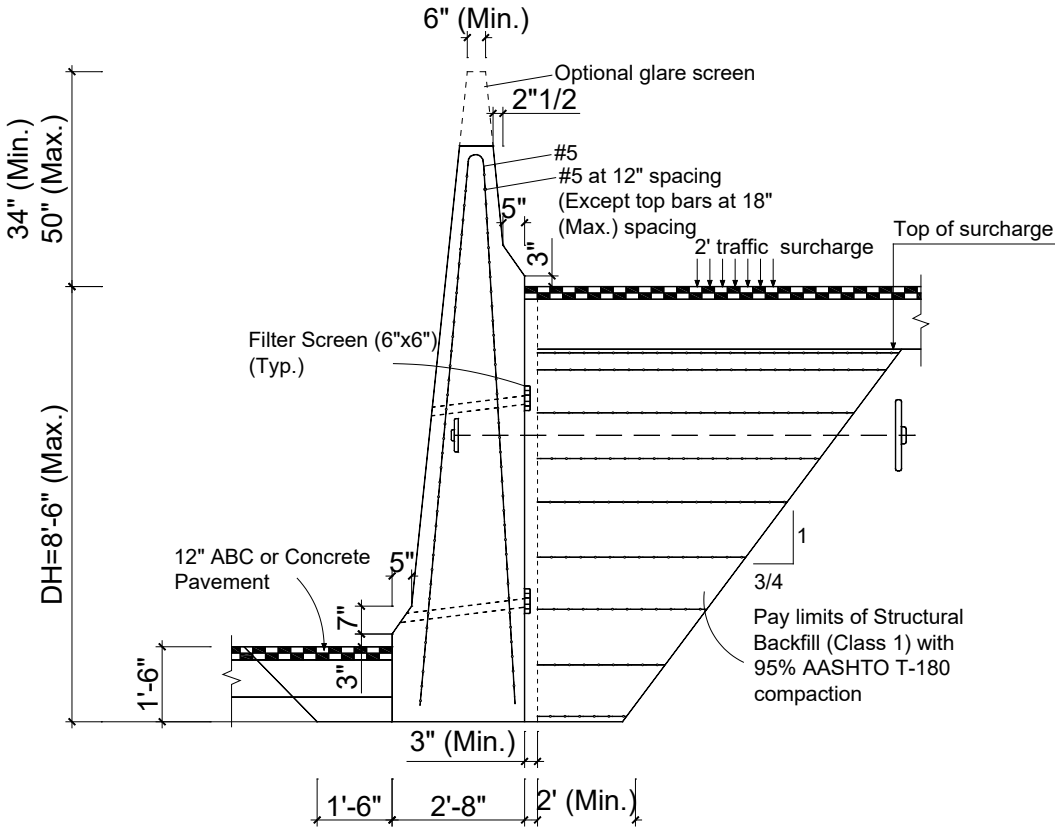

Figure 3. Type I with geosynthetic 3" from the back face of facing

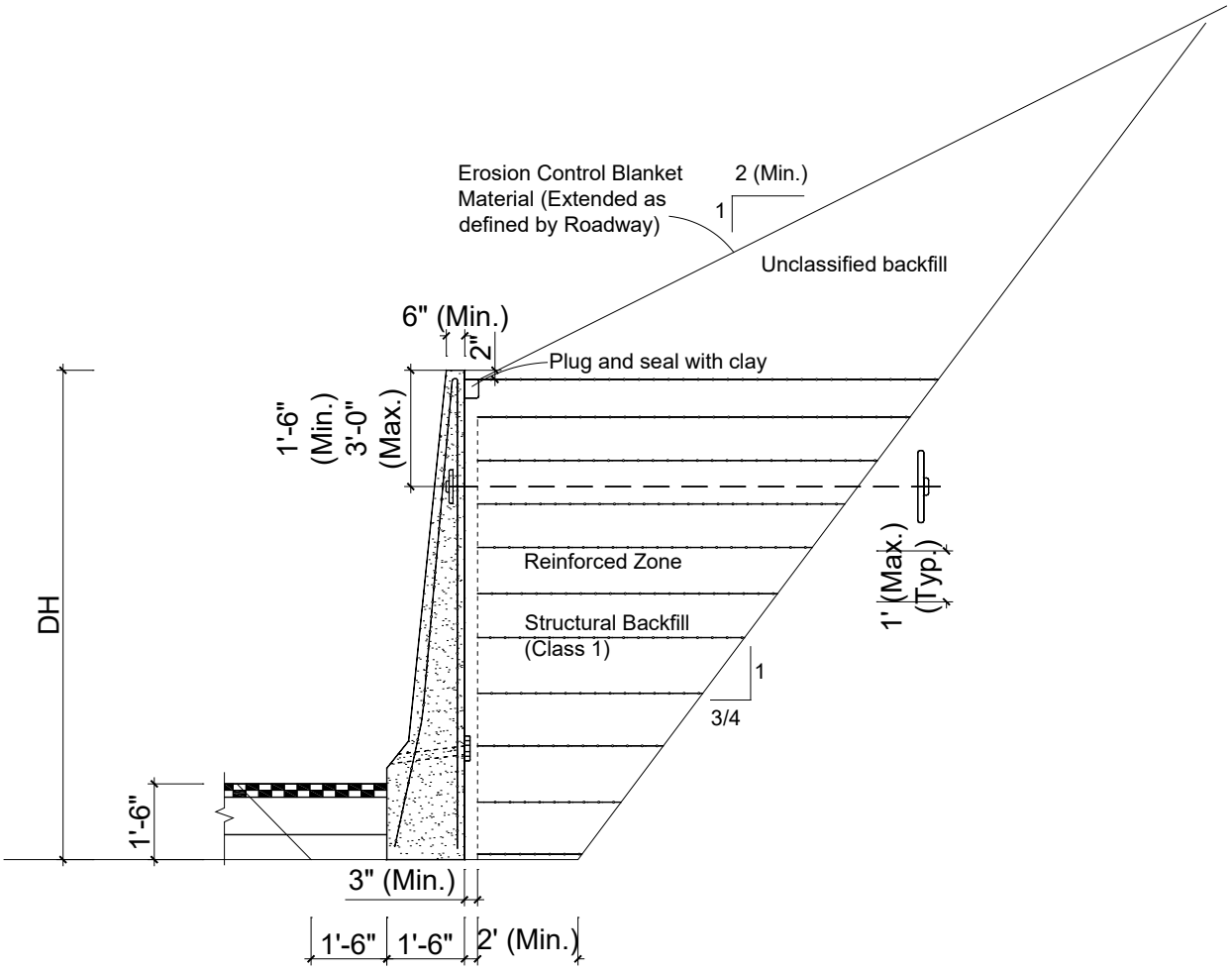

Figure 4. Type II with geosynthetic 3" from the back face of facing

Maximum Wall Height via Large Scale Model Tests and Finite Element Analyses

While the height of the Tiger Cage is limited to six feet, airbags with a maximum air pressure of 14 psi are capable of simulating a height increase of 14 feet (if backfill soil unit weight is about 150 pcf), which is more than enough to simulate the maximum wall height of 8'-6" specified in the CDOT Worksheet. The Center for Geotechnical Engineering Science (CGES) study team at the University of Colorado Denver, briefed as TEAM, investigated various issues, including the maximum wall height. The maximum design height of 8'-6" was based on Rankine Earth Pressure Theory without the benefit of GRS (or MSE). Currently, AASHTO provides earth pressure equations corresponding to wall types. For example, AASHTO Equation 3.11.5.3-1 presents the active lateral earth pressure coefficient K_a:

$$K_a = \frac{\sin^2(\theta+\varphi)}{\Gamma\left[\sin^2\theta\sin(\theta-\delta)\right]} \tag{1}$$

in which:

$$\Gamma = \left[1+\sqrt{\frac{\sin(\varphi+\delta)\sin(\varphi-\beta)}{\sin(\theta-\delta)\sin(\theta+\beta)}}\right] \tag{2}$$

Where δ is friction angle between fill and wall (degrees); β is the angle of fill to horizontal as shown in Fig. 5 (degrees); θ is the angle of the back face of the wall to the horizontal as shown in Fig. 5 (degrees); and φ is the effective angle of internal friction (degrees).

And the passive lateral earth pressure coefficient is given by AASHTO Equation 3.11.5.4-1 as:

$$p_p = K_p\gamma_s z + 2c\sqrt{K_p} \tag{3}$$

where K_p is the coefficient of passive lateral earth pressure; γ_s is the unit weight of soil; z is depth below the soil surface; c is soil cohesion.

In Eq. (1), the active pressure is only considered for cohesionless soil. Equations 3 presents passive lateral earth pressures with the first term related to internal friction angle and the second term related to soil cohesion. These equations can be generalized in a simple approach of Terzaghi's trial wedge method. To properly assess earth pressure, the cohesion component or the second term in Eq. (3), though important, is commonly ignored by the wall designer for conservatism. However, the major contribution of GRS is a cohesive parameter because GRS contributes minimally to the friction angle of GRS. The lab experiments showed the friction angle of GRS is nearly no different from the soil friction angle. So, soil backfill with tensile inclusions, such as geosynthetics or steel welded wire meshes, will contribute to equivalent cohesion in the following earth pressure equations:

$$\overline{p}_a = K_a\sigma_v - 2c_e\sqrt{K_a} \tag{4}$$

$$\overline{p}_p = K_p\sigma_v + 2c_e\sqrt{K_p} \tag{5}$$

where $\overline{p}_a$ an $\overline{p}_p$ active and passive lateral earth pressures of GRS, respectively; σ_v is vertical pressure; and c_e is equivalent composite soil cohesion. The details of inclusion effects need to be evaluated by model tests and finite element analyses. CDOT designs and builds 30+ major earth retaining walls annually with T7B-GRS walls for roadside safety improvement at locations with two-face Jersey barrier walls for avoiding glare in the median and maintaining a crash-rated shoulder Jersey barrier wall. This research has high returns and will result in rapid implementation. A new design policy with worksheets will be formulated for maintaining uniformity in design details and the design of safer and more reliable walls.

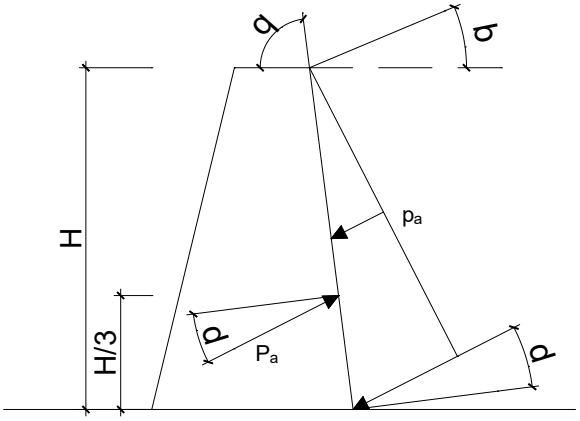

Figure 5. Active lateral earth pressure (AASHTO, 2017)

In CDOT MSE/GRS worksheet B-504-S7, the extended height of the T7B-GRSW can be applied either for roadway grade separation at a median or as cut walls for a widened shoulder. During design or construction on rock/very competent soil (OSHA construction and global stability requirements), this worksheet may be applicable and can derive immediate benefit to the State. Besides earth pressure, bearing capacity and bearing pressure distribution are also important design elements when using a truncated wall with a narrow base. Currently, a tied rod with a dead-man anchor at 5'-0" spacing is required for both rail impact and conservatism about uncertain earth pressure. Contemporary AASHTO MSE wall design guidelines are unclear in addressing earth pressure when utilizing T7B-GRS walls. CDOT with this proposed research will assess the real earth pressure applied to the reinforced concrete barrier facing, establish a reasonable earth pressure for soil with tensile inclusions, and provide the maximum design height of T7B-GRS walls.

OBJECTIVES OF THIS PROPOSED STUDY

The objectives of this study are as follows:

1. Evaluate the effects of backfill with and without a sand-filled gap and wrap around on Type 7 Barrier GRS walls earth pressures,
2. Provide an optimum wall shape and reasonable width of truncated GRS wall base under gravitational force,
3. Comparisons of numerical modeling and lab model test results for GRS wall earth pressure and performance.
4. Evaluate the validity of the SSI2D finite element analysis program for the analysis of T7B-GRSW behaviors by comparing the results of the model tests and numerical analysis results,
5. Evaluate the maximum application height for CDOT GRS Wall Worksheet B-504-S7,
6. Effect of Vehicular impact load on the T7B-GRS wall design,

RESEARCH APPROACH AND TASKS

Approach To design T7B-GRS walls, engineers need information on backfill and bedrock properties, wall dimensions, geosynthetic properties, lateral earth pressures, the geometry of excavated bedrock with truncated base, loading conditions, etc. Finite element analysis programs can be used to analyze a complex GRS wall system. However, they need to be calibrated against the performance of full-scale walls and/or large-scale model walls. Only when validated, it can be used to predict the performance of a real physical wall system. This proposed study will develop and use the SSI2D program, validate it against large-scale model test results of bridge abutments, truncated-base GRS walls, GRS wall lateral earth pressures, etc. Finite element analysis results using GRSW will be compared with the performance measurement results of large-scale model test results of T7B-GRS walls with different excavated bedrock slopes. When validated, the SSI2D program will be used to analyze the performances of different T7B-GRSW's in parametric studies. The analysis results are then used to formulate the earth pressure function for GRS walls, which is then used to provide shear and moment distributions for the T7B-GRS wall design.

Both finite element analyses and large-scale model tests can help us better understand the performance of T7B-GRS walls. The Center for Geotechnical Engineering Science (CGES) has a large-scale wall model test facility of a stiff steel cage, Tiger Cage. The Tiger Cage has been used successfully for several CDOT/FHWA sponsored studies on GRS walls, MSE wall earth pressures, GRS-IBS abutment, truncated based bearing pressures, etc. It will be used again in this proposed study. In model tests, behaviors of test walls will be monitored via a comprehensive instrumentation program, as described in a later section of the proposal. In summary, the CGES has comprehensive test apparatuses for evaluating properties of soil backfills, rocks, and geosynthetic, for large-scale model tests, the computation equipment for numerical analysis for use in this proposed study.

Study Tasks The tasks needed to accomplish the above-stated objectives includes:

1. Review of literature on the performance of Type 7 Barrier GRS walls under gravitational and vehicular impact loads,
2. Review of GRS earth pressure theories and synthesize the results,
3. Model tests of T7B-GRSWs for earth pressures and wall system performance with sand-filled gap and wrap around with a selected truncated base width,
4. Model tests of T7B-GRSWs for earth pressures and wall system performance without sand-filled gap and wrap around with a selected truncated base width and comparison with those in Item 2,
5. SSI2D finite element analyses of T7B-GRSWs under the conditions as indicated in Items 3 and 4, and comparisons,
6. Develop optimum wall shape and reasonable width of truncated GRS wall base under gravitational force,
7. Comparisons of numerical analysis and lab model test results for GRS wall earth pressure and performance,
8. Evaluate the validity of the SSI2D finite element analysis program for the analysis of T7B-GRSW behaviors by comparing the results of the model tests and numerical analysis results,

9. Evaluate the maximum application height for CDOT GRS Wall Worksheet B-504-S7,
10. Recommendation for code improvement.

2. LITERATURE REVIEW

2.1. Introduction

The GRS walls were constructed with different facings, such as modular bocks, incremental, full-height concrete panels, and wrapped-face geosynthetic. The studies of GRS walls with hard facing such as modular bocks, incremental, full-height concrete panels were reported by many researchers in the literature as Abu-Hejleh et al. (2000), Wu (2001), Elias et al. (2001), Adams et al. (2011, 2012), Nicks et at. (2013). The performance of the block-facing walls was reported by Abu-Hejleh et al. (2000), Rahmouni et al. (2016), Saghebfar et al. (2017), Abu-Farsakh (2019), etc. in both field instrumentation and numerical analyses.

Different types of geotextile reinforcement were wrapped around to form the exposed face of the retaining wall at the facing. The wrapped around facing could be a wire mesh material and the soil reinforcement was a geosynthetic product (e.g., Carrubba et al., 1999). The geotextile wrapped-face walls had also been used for the reinforced soil zone in two-stage false-facia wall systems (Bathurst, 2014). Yu et al. (2017) reported two full-scale instrumented wrapped-face walls that were constructed, tested, and monitored in a controlled indoor laboratory environment. Both wall types were identical except for the reinforcements. The first wall was reinforced with layers of welded wire mesh and the second wall used layers of a biaxial polypropylene geogrid. The results of numerical modeling using FLAC software were compared to the instrumented data in terms of lateral displacements, strains of reinforcements, and internal soil stresses.

These wrapped faces are subjected to ultraviolet light degradation or damage due to fire. To protect the wrapped-face walls, the hard facing can be attached after construction of the reinforced soil mass by shotcrete, attaching prefabricated facing panels made of concrete, wood, or other materials, or cast-in-place concrete. Precast elements can be cast in several shapes and provided with facing textures to match environmental requirements and blend aesthetically into the environment. Retaining structures using precast concrete elements as the facings can have surface finishes similar to any reinforced concrete structure. This multi-staging facing approach has multiple advantages where GRS is protected from physical weathering and environmental actions.

The Type-7 Barrier GRS Wall was designed by combining the functionality of walls and barriers in one wall system with the full benefit of GRS technology (Chang, Lee, and Wang, 2004). The replacement of block facing with the reinforced concrete (RC) facing, precast or cast-in-place,

whichever is more cost-effective. This RC facing enhances the vehicular impact load resistance, as demonstrated in the author's earlier study (Chang and Oncul, 2003), in which the barrier is supported on an independent moment slab. The performance of T7B-GRSW, where the safety of the rail-wall system is an integral design, enhances the safety of the impact rail. According to the design worksheet B-504-S7, the backfill soil is crushed rock class 1 compacted to 95% under AASHTO T-180. The geosynthetic reinforcement shall be biaxial woven geotextile fabric with a minimum average strength value of 4600 lb./ft. based on ASTM D4595 and with a minimum 6" overlap between rolls. The geosynthetic is wrapped around behind the cast-in-place concrete wall. A gap of 3" between geosynthetic and concrete wall is filled by sand or polystyrene of low density to reduced lateral pressure from soil mass.

Presently, no theoretical and experimental study was performed for the Type-7 Barrier GRS Wall. Chang et al., (2020a) reported a performance GRS-IBS system using sheet pile as the facing. The GRS produces lateral pressure on the facing similar to that on the Type-7 Barrier GRS Wall when the geosynthetic is not wrapped around.

2.2 Lateral earth pressure

The lateral forces that act between the retaining structures and the soil mass being retained are caused by lateral earth pressure. The lateral strain in the soil will alter its lateral stress condition. The lateral stress is dependent on the magnitude and direction of the lateral strain. The final lateral stress is limited by two failure conditions: 1) At active failure state when the wall moves away from the soil mass, and 2) At passive failure state when the wall moves into the soil mass. At zero lateral strain, the existing undisturbed state is referred to as the at-rest state. The lateral stresses corresponding to active, passive, and at-rest states are referred to as the active, passive, and at-rest pressures. The lateral pressure can be expressed in terms of the vertical pressure as follows:

$$\sigma_h = K\sigma_v \tag{6}$$

where σ_h is the horizontal stress; σ_v is the vertical overburden stress; and K is the coefficient of lateral pressure, which is a function of the retained soil properties, the type of retaining structures, and the strain in soil. The coefficients of lateral pressure corresponding to the active, passive, and at-rest states are denoted as K_a, K_p and K_0, respectively.

As shown in Fig. 6 and Table 1, the coefficients of earth pressure are dependent on lateral wall movement. The strain for soil to reach passive failure is greater than that for it to reach active failure. For cohesionless soils, the necessary wall movement to induce the passive condition is four times larger than that inducing the active condition, and it is about two times for cohesive soils. When the predicted wall movement is less than the value required to fully mobilize active or passive pressure, the earth pressure coefficient can be determined based on curves similar to those shown in Fig. 6.

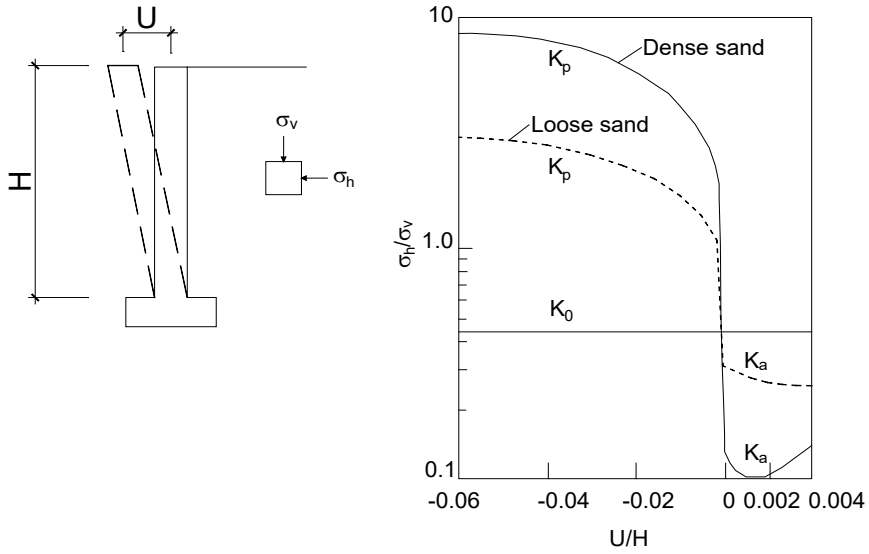

Figure 6. Effect of wall movement on earth pressure

Table 1. Magnitudes of wall movement to reach failure (NAVFAC DM7.2, 1982)

Soil type	U/H	
	Active	Passive
Dense cohesionless	0.0005	0.002
Loose cohesionless	0.002	0.006
Stiff cohesive	0.01	0.02
Soft cohesive	0.02	0.04

The lateral pressure on the GRS facing is governed by compaction-induced pressure, confining effects, surcharge loads, the movement of the facing, and internal forces from geosynthetic. Many researchers studied the lateral pressure of GRS on the block-facing wall. Currently, there is no research on GRS lateral pressure on continuous stiff and flexible facing, such as cast-in-place concrete and sheet pile.

2.3 At rest earth pressure

When the wall is stiff or lateral displacement of the wall is small/not allowed, the lateral at-rest earth pressure prevails. When the wall is not allowed to move, the stresses in the soil are under elastic equilibrium with no shear stress. Horizontal stress is related to vertical stresses as the following equation:

$$\sigma_h = K_0 \sigma_v \tag{7}$$

where K_0 is the coefficient of lateral earth pressure at rest.

For cohesionless soils, K_0 may be estimated by Jaky (1944) equation:

$$K_0 = 1 - \sin\varphi \tag{8}$$

where φ is angle of internal friction.

When cohesionless soils are in the unloading or pre-consolidated states, K_0 can be estimated by the following equation:

$$K_{0,OC} = K_{0,NC} OCR^{\alpha} \tag{9}$$

where $K_{0,OC}$ is the coefficient of lateral earth pressure at rest of over-consolidation soils; OCR is over-consolidation ratio; α is an empirical coefficient, $\alpha \approx \sin\varphi$; $K_{0,OC}$ is coefficient of lateral earth pressure at rest of normally consolidated soils;

For a stiff wall such as thick concrete, culvert box, or U-wall structures, lateral displacement is closed to zero, and the coefficient of lateral earth pressure is approximated as the lateral earth pressure at rest. For flexible walls such as pile-supported concrete cantilever or sheet pile cantilever walls, which may experience limited lateral displacement are commonly designed for

earth pressures between the at-rest and active conditions.

2.4 Active and passive pressures

Active and passive pressures are developed when a failure zone developed behind the wall resulting from wall-soil system forward movement. The failure zone is typically bounded by the back face of the wall and a failure surface through the soil mass along which the soil stress state has reached a failure condition. The magnitudes of the active and passive earth pressures are also affected by the wall geometry, wall stiffness and friction properties of its back face, and the characteristics of the retained soil such as geometry, properties, stratification, and groundwater conditions.

Rankine (1857) developed a theory of lateral earth pressure in conditions of failure in the back of a retaining wall based on the concept of plastic equilibrium. In this theory, there exists no friction between the retaining wall and soil, and the ground surface is horizontal. The earth pressure on the wall is at rest before the retaining wall moves. The stress condition in the soil can be represented by the Mohr's circle with a diameter of $\left|\sigma_{\max}-\sigma_{\min}\right|$, where $\sigma_{\max}$ and $\sigma_{\min}$ is maximum and minimum stresses, respectively. When the retaining wall moves away from the soil, the horizontal stress decreases while the vertical stress condition is unchanged. The Mohr's circle grows larger and intersect with the failure line at a point when the soil stress condition is at failure. This type of failure is called active failure, and the lateral pressure on the retaining wall is determined as follows:

$$p_a = K_a\sigma_v - 2c\sqrt{K_a} \tag{10}$$

where K_a is the coefficient of active lateral earth pressure, $K_a = \tan^2\left(45^0 - \varphi/2\right)$.

When the retaining wall moves into the soil, the horizontal stress increases while the vertical stress stays constant. When the Mohr's circle intersects with the failure line at a point with the failure envelope, the soil stress condition is at a passive failure condition. The passive pressure can be computed as:

$$p_p = K_p\sigma_v + 2c\sqrt{K_p} \tag{11}$$

where K_p is the coefficient of passive pressure.

2.5 Lateral earth pressure with GRS backfills

Lateral earth pressure on retaining walls with GRS backfill was studied by many researchers in both experimental and theoretical studies. The reinforcing elements are both connected or not connected to the wall face (Wu et al. 2015). Abu-Hejleh et al. (2001) reported an instrumentation project of GRS-IBS abutment for Meadows and Founders bridge near Castlerock, CO that carries Colorado State Highway 86 over U.S. Interstate 25. This bridge is the first major bridge in the United States built on footings supported by a geosynthetic-reinforced system with Colorado Class I backfill for gravelly soils and without the use of traditional deep foundations (piles and caissons). The GRS abutment was heavily instrumented with pressure cells for measuring earth pressures. Adams et al. (2011) also indicated in their report that the pressure cells installed behind the back wall of each abutment in the Tiffin River Bridge to measure lateral pressures between the superstructure and the GRS due to seasonal temperature-induced expansion and contraction of steel girders (Fig. 7). Saghebfar et al. (2017) presented the performance of the in-service GRS-IBS abutment of Maree Michel Bridge with block facing (Fig. 8). Pressure cells were installed in the south abutment to measure the stress distribution along the block-facing wall. Chang et al., (2020a) reported a comprehensive instrumentation program to monitor the performance of Abutment #4 of the unique CDOT Region 1 Twin Bridge over the Smith Road and Union Pacific Rail Road (UPRR) on I-70 (Fig. 9). In the design plan, the abutment performance was to be fully monitored where earth pressure cells were used to monitor the change and distribution of earth pressures in the vertical and lateral directions. Wu (2001) proposed that the bin pressure diagram between two reinforcement layers is near zero at the reinforcement elevation. It increases with depth below the reinforcement before decreasing. Soong and Koerner (1997) proposed a similar concept for MSE walls where the reinforcement is connected to the middle of the back face of the wall facing. While the reinforcements stabilize most of the soil mass through interface friction, Soong and Koerner (1997) postulated that there is a small zone of soil bearing against the wall facing that is not restrained by the reinforcement mobilized friction.

Figure 7. Pressure cells behind the back wall on Tiffin River Bridge (Adam et al., 2011)

Figure 8. GRS-IBS abutment of Maree Michel Bridge (Saghebfar et al., 2017)

Figure 9. Facing wall of the GRS Abutment #4 (Chang at al., 2020a)

The wall design procedure according to Elias et al., (2001) is only applied to a facing wall that connects directly to the reinforcement so it cannot be used for a separated facing wall such as Type-7 Barrier GRS Wall. As a result, the cast-in-place concrete wall should be checked individually for the external failure mechanism including 1) Sliding on the base; 2) Overturning; 3) Bearing capacity.

CDOT parameters used in MSE Wall LRFD (CDOT 2018) are shown in Table 2 (from B-504-H2).

Active earth pressure coefficient:

$$K_a = \frac{1-\sin\varphi}{1+\sin\varphi} \tag{12}$$

At rest earth pressure coefficient:

$$K_0 = 1-\sin\varphi \tag{13a}$$

$$K_r(z) = K_0 - \frac{z}{20}(K_0 - K_a) \text{ if } z < 20', \text{ otherwise } K_r(z) = K_a \quad (13b)$$

Resultant of soil weight and surcharge:

$$R_v(z) = (\gamma_v \gamma_{soil} z + LS\gamma_{soil} LLSurg)\, RL(z) \quad (14)$$

Overturning moment:

$$M_0(z) = \frac{1}{6} K_a \gamma_h \gamma_{soil} z^3 + \frac{1}{2} K_a LS\gamma_{soil} (LLSurg) z^2 + \frac{1}{2} K_a \gamma_{HMA,Max} hma \frac{HMAthk}{12} \quad (15)$$

Righting moment:

$$M_r(z) = \frac{1}{2} R_v(z) R_L(z) \quad (16)$$

Eccentricity of resultant:

$$e = \frac{RL(z)}{2} - \frac{M_r(z) - M_0(z)}{R_v(z)} \quad (17)$$

Overburden with LS

$$\sigma_{v1}(z) = \gamma_v \gamma_{soil} \left(z - \frac{HMAthk}{12} \right) + \gamma_{HMA,Max} \gamma_s \frac{HMAthk}{12} + LS\gamma_{soil} LLSurg \quad (18a)$$

Overburden without LS

$$\sigma_{v2}(z) = \gamma_{soil} \left(z - \frac{HMAthk}{12} \right) + \gamma_s \frac{HMAthk}{12} \quad (18b)$$

Lateral pressure:

$$\sigma_H = K_a \sigma_{v1} GRSfactor \quad (19)$$

Equation 13b is used to determine the coefficient of lateral earth pressure for the GRS wall as it reduces from K_0 at the ground surface to K_a at a depth of 20’ and keeps constant beyond. Figure 10 shows the variation of coefficient of lateral earth pressure that is used in the CDOT Work Sheet CDOT (2018). In this equation, no contribution from the reinforcement in reducing lateral pressures on the facing wall is considered.

Table 2. Parameters used in CDOT Work Sheet

Property	Value	Description
φ	34^0	Class I Backfill friction angle
Υ_{soil}	125 pcf	Unit weight with 95% AASHTO T180
Υ_h	1.5	The horizontal earth pressure factor
Υ_v	1.35	The vertical earth pressure factor
LS	1.75	Live load surcharge factor
$LL_{Surcharge}$	2’	Live load surcharge
d_{max}	2”	CDOT Class, I Backfill Max size
HMA_{thk}	10”	HMA thickness
hma	140 pcf	HMA unit weight
Υ_{HMA}	Max.=1.5 Min.=0.65	HMA design factor

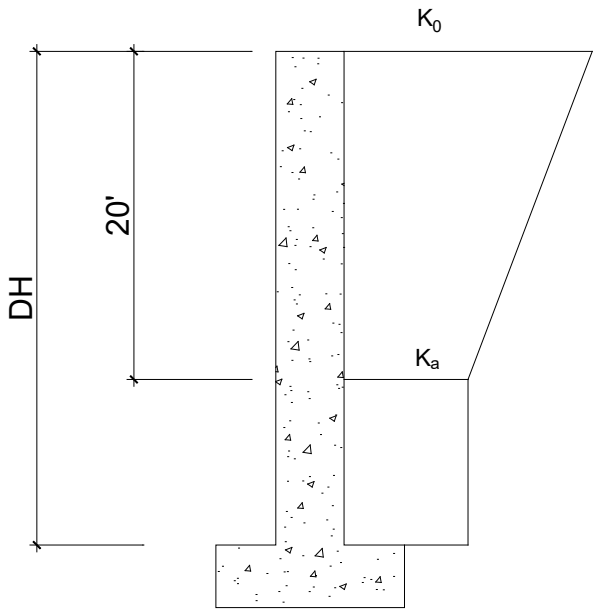

Figure 10. Coefficient of lateral pressure on facing wall

Under live load (surcharge) that is equivalent to 2’ of the backfill, the lateral pressures on the facing of a GRS wall will increase with increasing the surcharge. If the uniformly distributed load extensively acts on the ground surface, the load-induced lateral pressures can be calculated by Eqs.

(18a) and (19). If the live load is applied as a strip load that parallel to the concrete wall, according to linear elastic theory, the increase in lateral pressure can be approximated using the following equation:

$$\Delta\sigma_H = \left(LS\gamma_{soil}LLSurg\right)\frac{1}{\pi}\left[\alpha - \sin\alpha\cos\left(\alpha + 2\delta\right)\right] \tag{20}$$

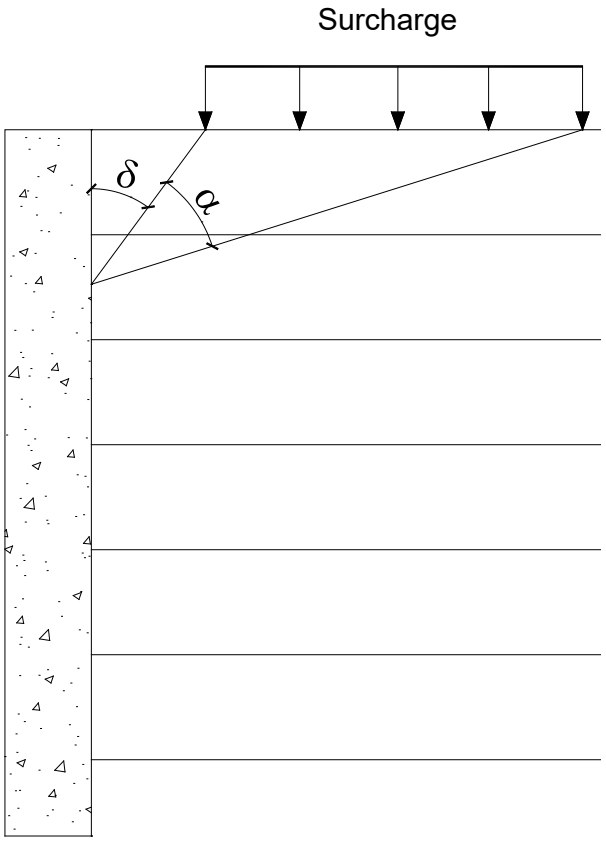

Figure 11. Lateral pressure on GRS wall with sloping backslope condition

3 LARGE-SCALE WALL MODEL TESTS

3.1 Tiger Cage

Under the joint sponsorship of CDOT and FHWA, the TEAM at the Center for Geotechnical Engineering Science (CGES) at the University of Colorado Denver designed and fabricated a stiff steel wall test cage, named Tiger Cage (Volmer et al., 2017) in 2013, and, since, has been used in several research projects, like GRS bridge abutment, GRS wall earth pressures, driven piles, and truncated base GRS wall. The T-cage is now a major geotechnical-structural teaching and research equipment used in wall and soil-pile-structure interaction teaching and research at the University

of Colorado Denver. Five different tests in different CDOT/FHWA sponsored projects were performed successfully with full instrumentation. The dimensions for the Tiger Cage are 2' in inside width x 6' in height x 12' in length. It was equipped with a stiff wall constructed of ¼" x 8" x 8" and ¼" x 4" x 8" rectangular steel pipes rotating about its lower end. The rotation is designed to induce active, at rest, and passive earth pressures to fulfill the project goal of earth pressure evaluation with GRS/MSE backfill. A large-scale model GRS wall with different facing can be constructed on top of the 5-ft GRS backfill. Each construction stage can be used for wall pressure measurement during compaction, active rotation, and passive rotation and also for establishing the load-settlement curve of GRS abutment under load. Before construction, thin latex membranes are used to cover the surface of the rotation and sidewalls of the Tiger Cage to reduce friction between soil and walls.

These projects with extensive instrumentation had generated greatly sought-after accurate performance measurement data to be used in improving the understanding of the pressure on T7B-GRSWs and further to update the T7B-GRSWs design specifications. Four tests will be performed to observe the wall performance and earth pressures. A concrete-model wall was cast with full instrumentation for pressure and wall performance monitoring.

3.2 Backfills

3.2.1 Triaxial Compression Tests of Colorado Class I Backfill

Several conventional triaxial compression tests were conducted in the Geotechnical/structural laboratory at the University of Colorado Denver. Samples were 6 inches in diameter, 12 inches in length. Dry soil was mixed with water to attain its optimum moisture content and compacted in a mold using the modified Proctor compaction. The triaxial compression tests were performed at confining pressures of 10psi, 20psi, and 30psi. Test results are shown in Fig. 12 without volume change measurement. From these tests, the soil strength parameters are determined and shown in Table 3. The method to determine the friction angle and cohesion is presented in Figs. 13 and 14. Two isotropic compression tests, one on dry soil and the other on moisture soil, were performed to assess the effect of moisture on volume change, Fig. 15. Both tests yielded similar results. This test is also used to determine the dilatancy angle, as shown in Figs. 16 and 17 and Table 3.

The Young's moduli can be determined from triaxial tests as follows:

$$E_i = K_L P_{atm} \left(\frac{\sigma_3}{P_a} \right)^{n_L} \tag{21a}$$

$$E_{ur} = K_{ur} P_{atm} \left(\frac{\sigma_3}{P_a} \right)^{n_{ur}} \tag{21b}$$

where E_i and E_{ur} are initial tangent modulus and unloading-reloading modulus, respectively, as functions of confining stress, σ_3; K_L and K_{ur} are loading and unloading-reloading moduli, respectively; P_{atm} is atmospheric pressure (used as a normalizing parameter); σ_3 is confining stress; and n_L and n_{ur} are exponents for defining the influence of the confining pressure on the moduli.

The Poisson's ratio is back-calculated from the coefficient of the lateral earth pressure at rest. The elastic parameters are presented in Table 4.

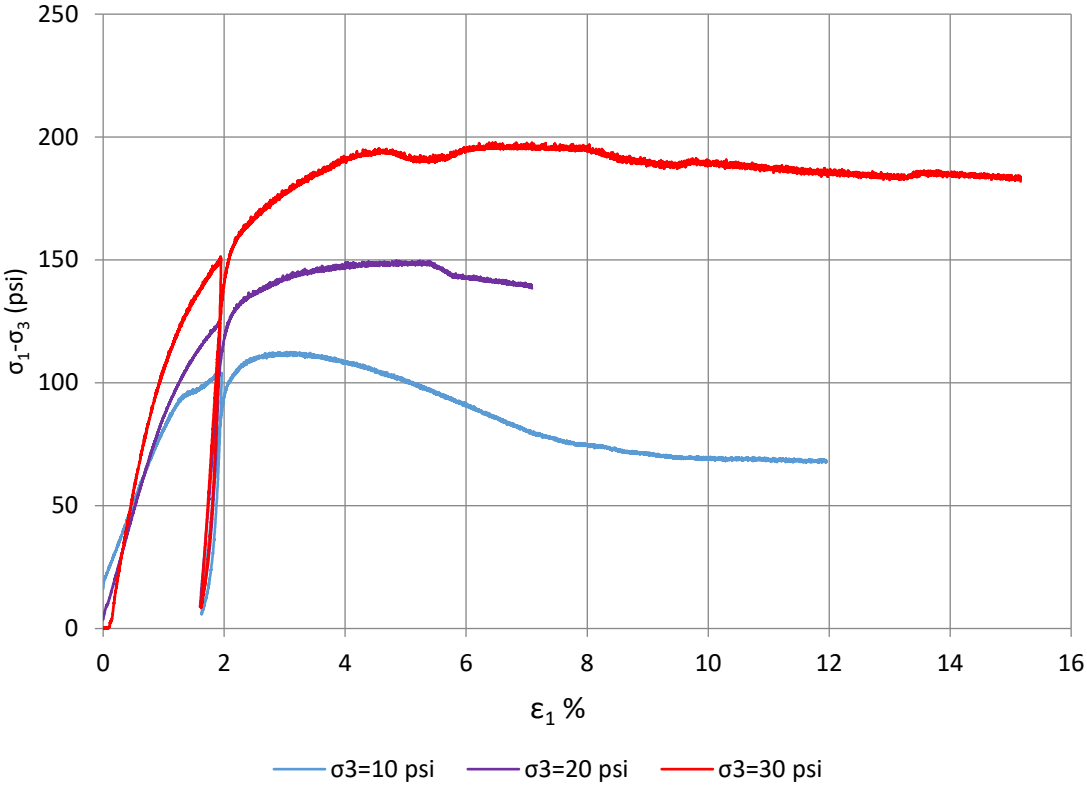

Figure 12. Triaxial test results

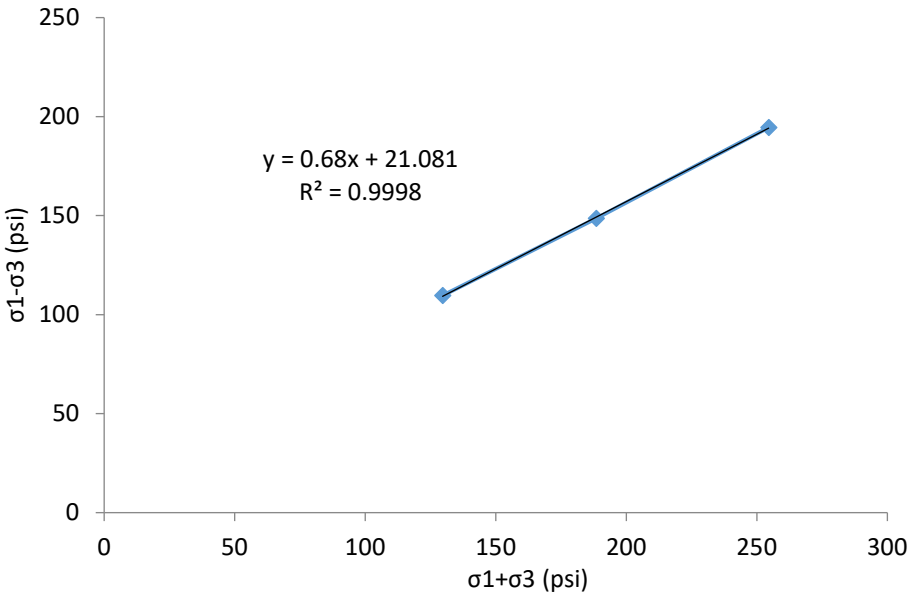

Figure 13. Determination of friction angle and cohesion

Table 3. Friction angle and cohesion from triaxial tests

Properties	Units	Value
Friction angle, ϕ	(^{0})	42.8
Cohesion, c	(psi)	14.4
Dilatancy angle, ψ	(^{0})	8.7

Table 4. Modulus from triaxial tests

Parameter	Value
K_L (Mohr-Coulomb)	532.4
K_L (Hyperbolic)	1300
n_L	0.477
K_{ur}	1975.6
n_{ur}	0.344
ν	0.145

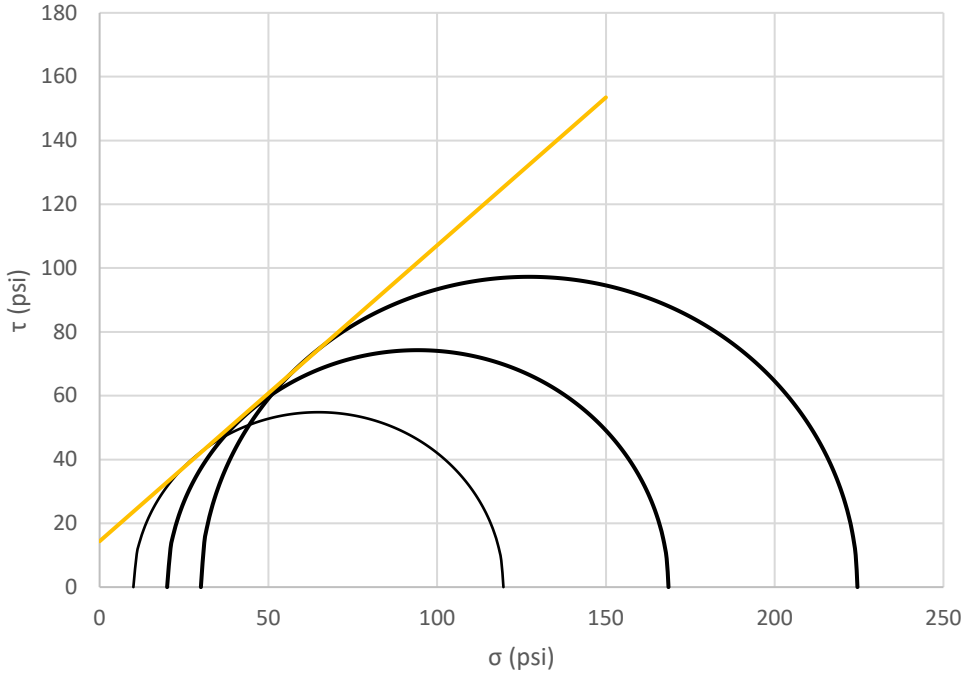

Figure 14. Mohr circle and failure line

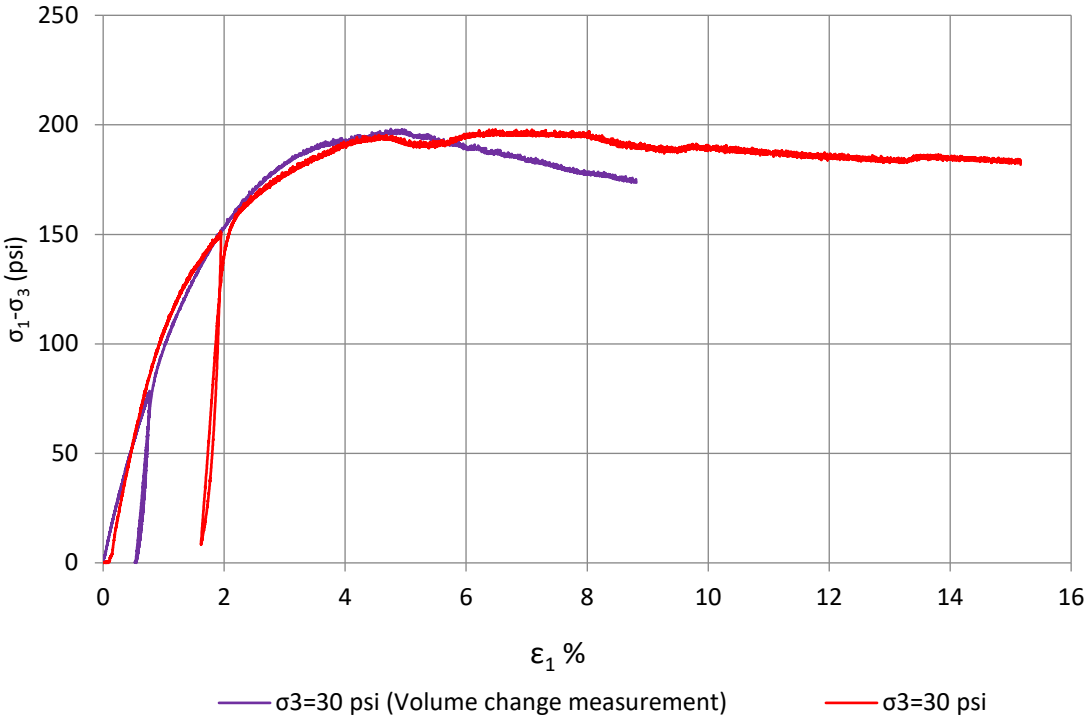

Figure 15. Comparison of triaxial compression tests (σ_3=30 psi)

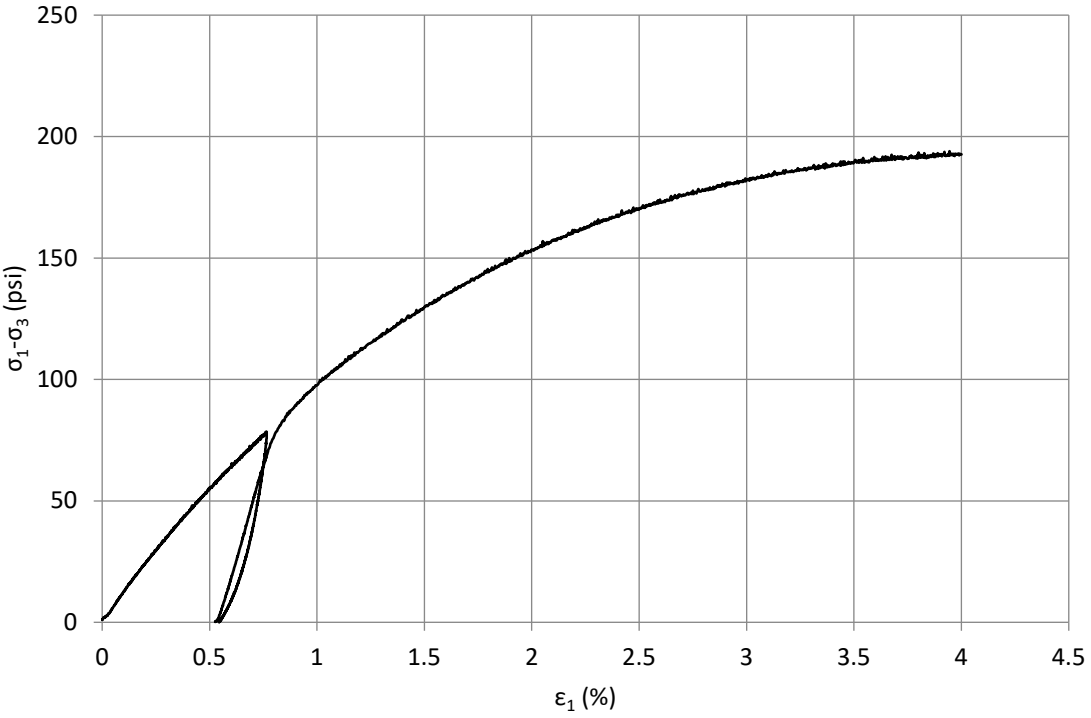

Figure 16. Triaxial test (σ_3 = 30 psi) with volume change measurement

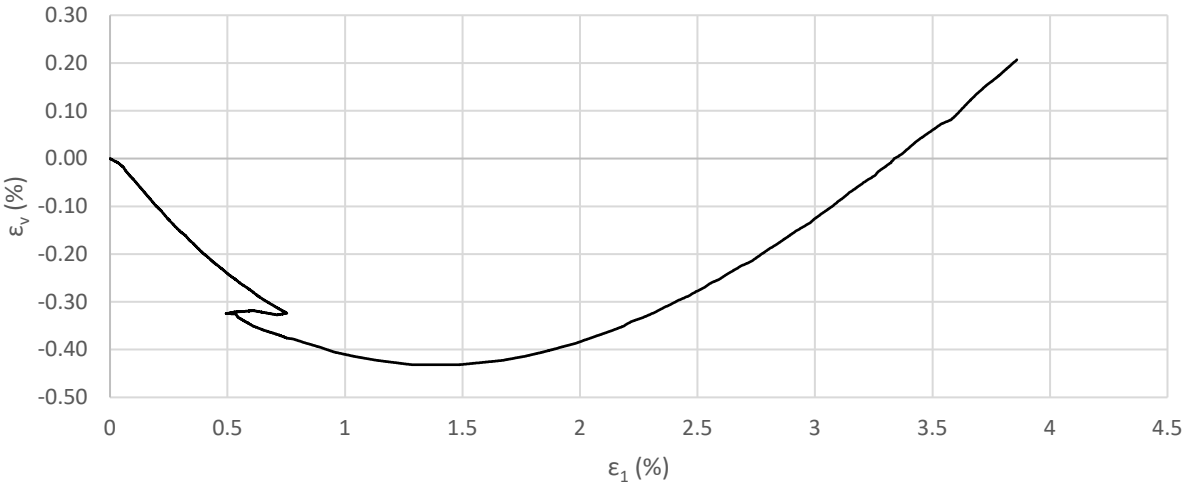

Figure 17. Volume change measurement

3.2.2 Oedometer Tests

The direct shear device is used for the one-dimensional compression test. Three samples of 12"x12"x7.94" were compressed under vertical load. The relationship between vertical pressure and vertical strain is shown in Fig. 18.

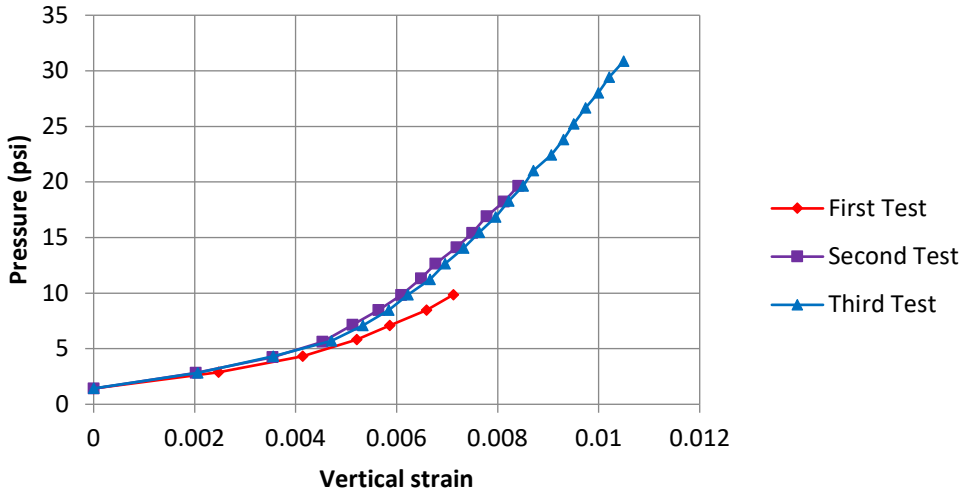

Figure 18. Oedometer tests

3.2.3 Direct Shear Tests

Three direct shear tests were conducted at different normal stresses to determine the shear strength of the soil. The soil sample after shearing is shown in Fig. 19. Shear stress-displacement curves are shown in Fig. 20 and vertical displacements and horizontal displacements curves are shown in Fig. 21.

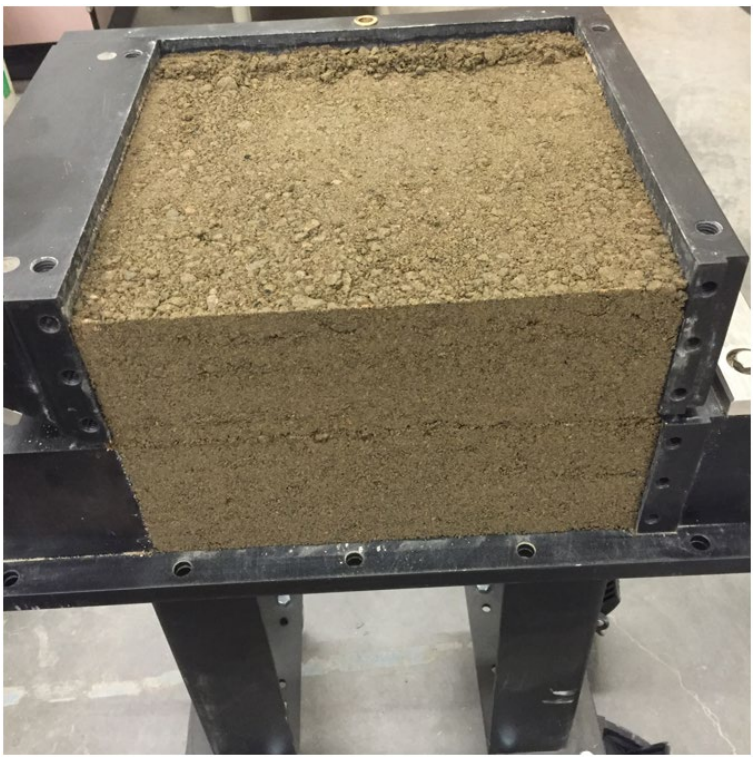

Figure 19. Soil sample after shearing

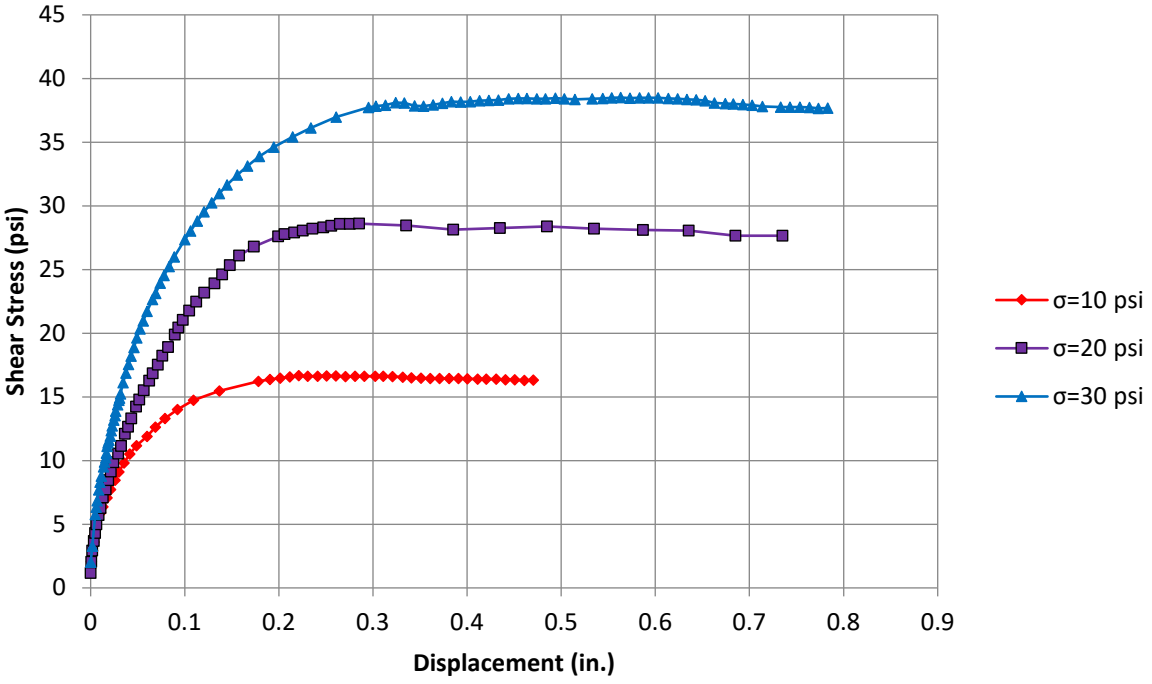

Figure 20. Shear stress and displacement curves

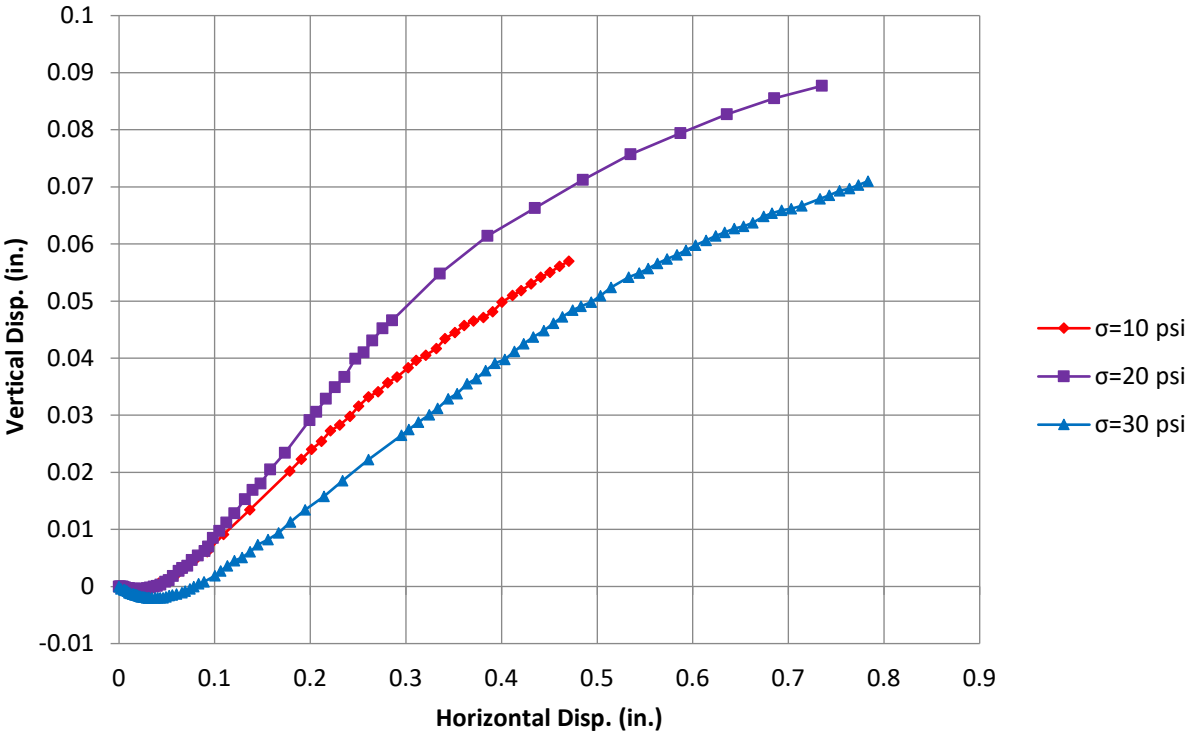

Figure 21. Vertical displacement and horizontal displacement curves

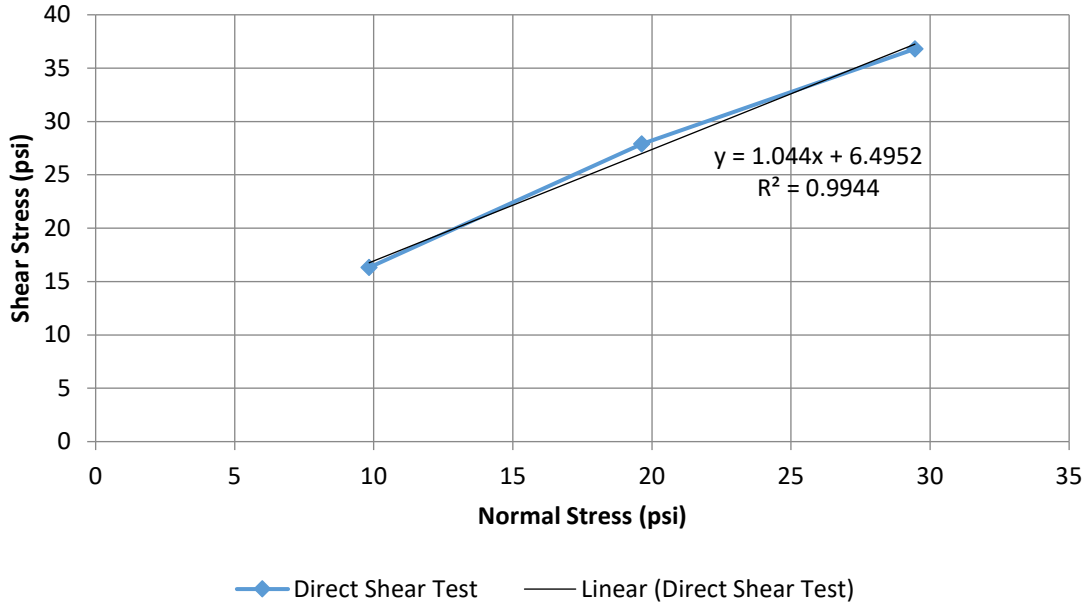

Figure 22. Determination of shear strengths

Using the Mohr-Coulomb criterion, $\tau = \sigma \tan\varphi + c$, friction angle and cohesion from these tests are calculated as shown in Fig. 22. Soil strength properties are shown in Table 5.

Table 5. Friction angle and cohesion from direct shear tests

Properties	Units	Value
Friction angle, ϕ	(^{0})	45
Cohesion, c	(psi)	6.49

3.2.4 The interface between Soil and Geosynthetic

The direct shear device was also used to determine the friction angle and cohesion of the interface between soil and geosynthetic. Figure 23 shows the failure line between soil and geosynthetic after a test. Test results are shown in Figs. 24 to Fig. 26.

Figure 23. Backfill with geosynthetic inclusion after shearing

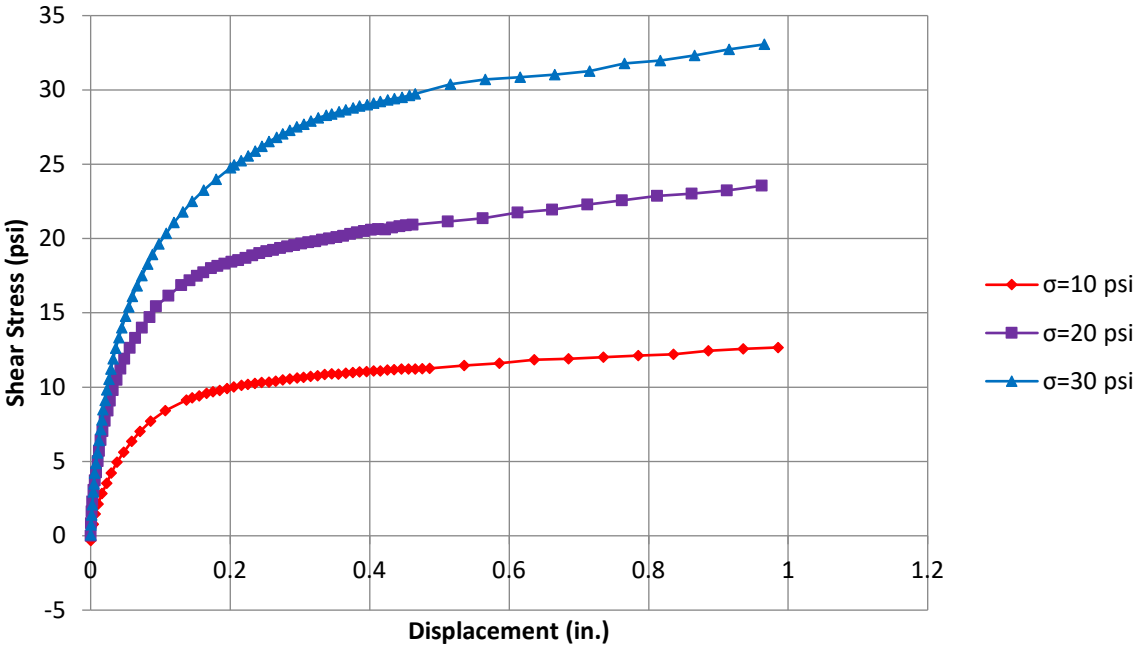

Figure 24. Shear stress and displacement curves for the backfill

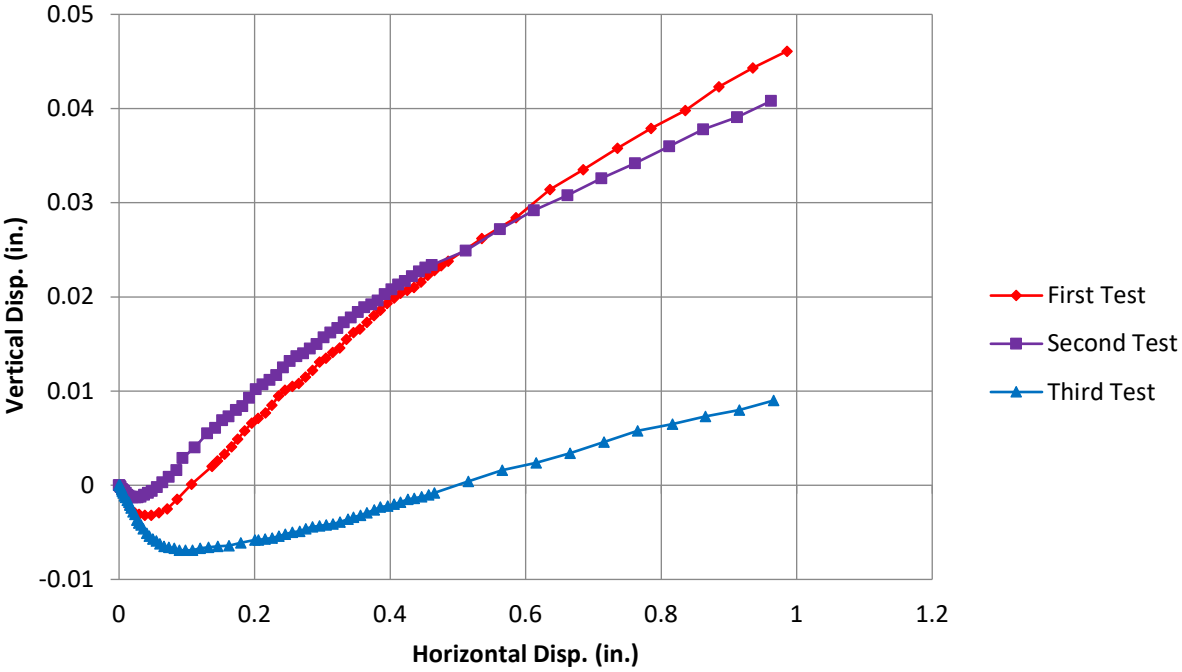

Figure 25. Vertical displacement and horizontal displacement curves

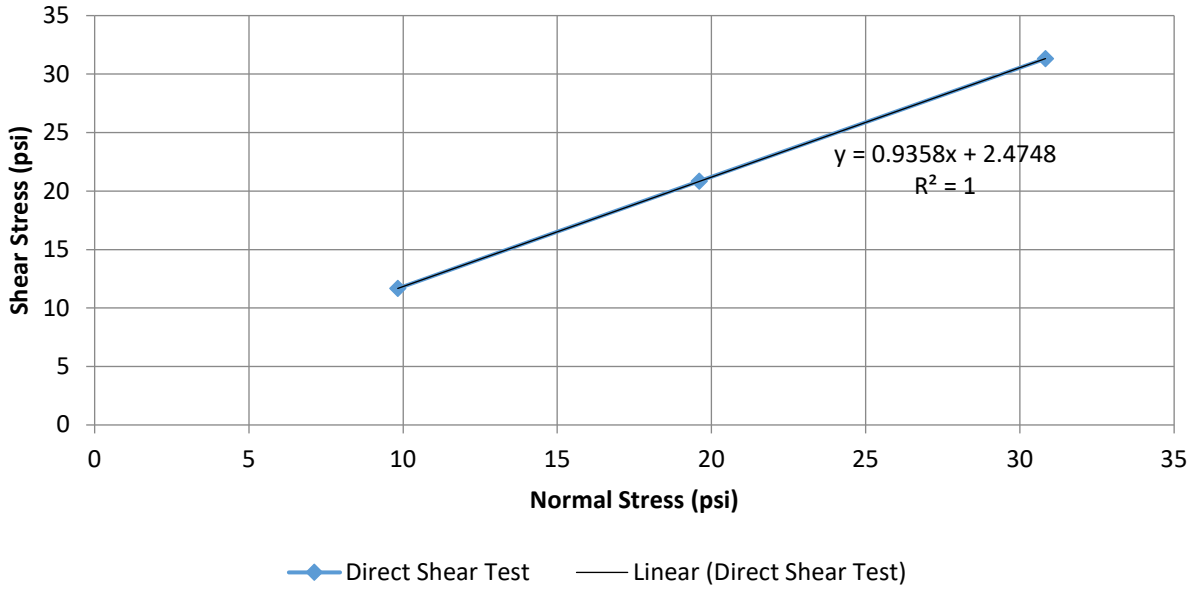

Figure 26. Interface shear strengths

Using the same method for soil, friction angle, and cohesion are computed from these tests for the interface as shown in Fig. 22 and also shown in Table 6 as below:

Table 6. Friction angle and cohesion of soil and geosynthetic interface

Properties	Units	Value
Friction angle, ϕ	(^{0})	43
Cohesion, c	(psi)	2.47

As can be seen, the frictional angle and cohesion of soil and soil-geosynthetic differ insignificantly.

3.2.5 Index Property Tests and Density-Moisture Relationship

Index properties and density-moisture relation of the backfill were also evaluated via corresponding tests and their results are:

1) **S**pecific gravity test gave the specific gravity value of 2.80,
2) Gradation analysis gave the following results: D_{60} = 3.64 mm, D_{30} = 1.05mm, D_{10} = 0.16 mm, C_u = 22.75 and C_c = 1.86.
3) Both Standard Proctor Compaction and Modified Proctor Compaction tests were

performed and their results are:

a. Standard Proctor Compaction Test: maximum dry density, γ_{dmax} = 131.5 pcf and

b. Optimum moisture content, ω_{opt} = 10%

c. Modified Proctor Compaction Test: maximum dry density, γ_{dmax} = 142 pcf and optimum moisture content, ω_{opt} = 6.5%

Details of the above tests were presented by Chang et al. (2020b).

3.3 Base foundation soil

The clay soil was compacted in the T-Cage used as the soil at the base of the GRS wall. The clayey soil was tested by using UU triaxial tests. Test results are shown in Fig. 27 and Table 7.

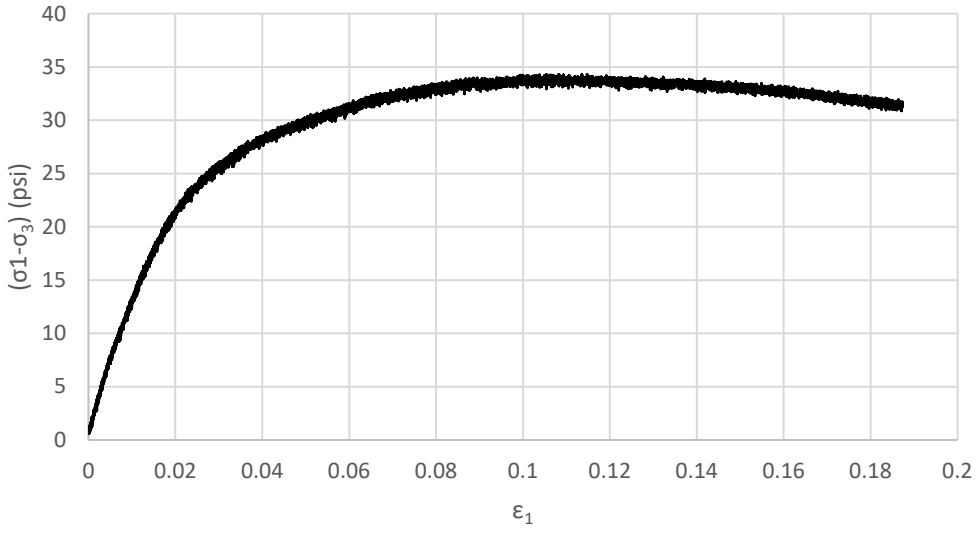

Figure 27. Stress-strain curve of the base foundation soil

Table 7. Properties of the base foundation soil

Properties	Units	Value
Young's Modulus	(psi)	4124
Undrained shear strength	(psi)	17
Poisson's Ratio	-	0.3

3.4 Wide-Width Tension Test of US4800 Geosynthetic

ASTM D 4595 requires the entire width of the sample to be clamped. The clamps are 8" x 2". The geosynthetic sample is 8" wide x 8" long (minimum). Since the entire width of the sample is held by the clamps, the test is considered to provide a true tensile strength, where the "pounds of force" is then divided by 8, multiplied by 12, and reported as pounds per foot.

Three geosynthetic samples with unloading-reloading are shown in Fig. 28. The sample dimensions are 8 in. in width and 12 in. in length. The properties of the geosynthetic used in analyses are shown in Table 8.

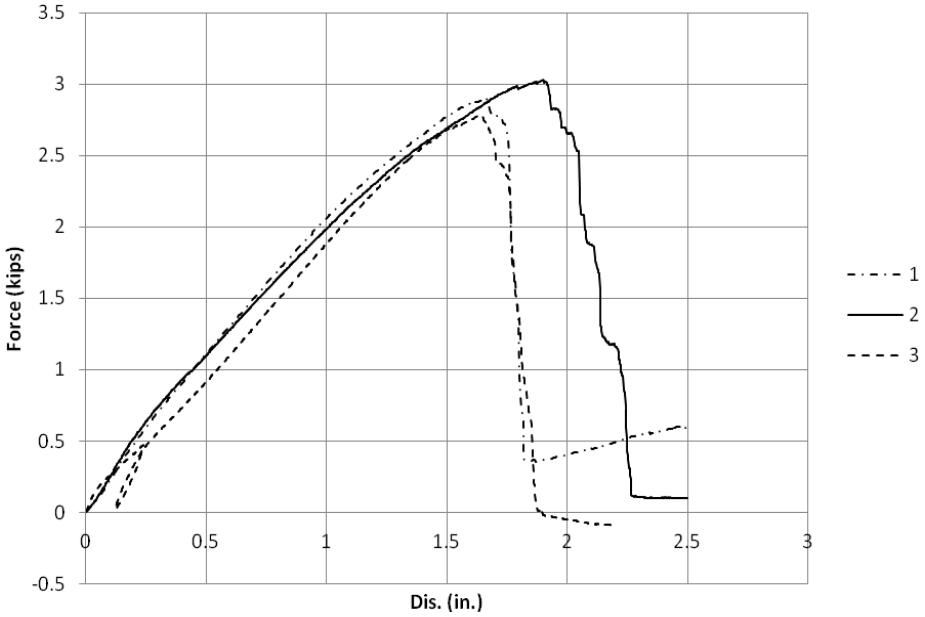

Figure 28. Load-displacement curves of geosynthetic from tension tests

Table 8. Geosynthetic properties

Properties	Unit	Value
EA_i	lb/ft [kN/m]	44250 [659]
EA_{ur}	lb/ft [kN/m]	69000 [1028]
Fmax	lb/ft [kN/m]	4353 [65]

3.5 Concrete wall

The dimension of the T7B-GRS wall is shown in Fig. 1 as the required design of the CDOT Work Sheet (CDOT 2018). The maximum height of the GRS wall is 8'-6". The design height of the GRS wall is varied from 34" to 8'-6" and the corresponding base width of the concrete wall from 2'-2.625" to 2'-8". The design base width is interpolated linearly with the design height. In this full-scale test, the height of the GRS wall is limited by the Tiger Cage' height and assigned as 4'-2" then the design base width obtained from linear interpolation as 2'-4", as shown in Fig. 29. The concrete wall properties are presented in Table 9.

Table 9. Concrete wall properties

Height (in.)	Width (in.)	Thickness at the base (in.)	Volume (in^3)	Weight (lb)
82	22	29	40040	3040

The concrete wall is cast using high strength concrete mix that can reach a compressive strength of 5000 psi after 28 days. Reinforcements provide more flexible strength for the concrete wall while bending moments may occur during installation, construction, and testing. Dimensions of the reinforcements shown in Fig. 29 were obtained from the design in Fig. 1. Several pictures of the concrete wall during and after casting including formwork and reinforcement installation are shown in Figs. 30 to 32.

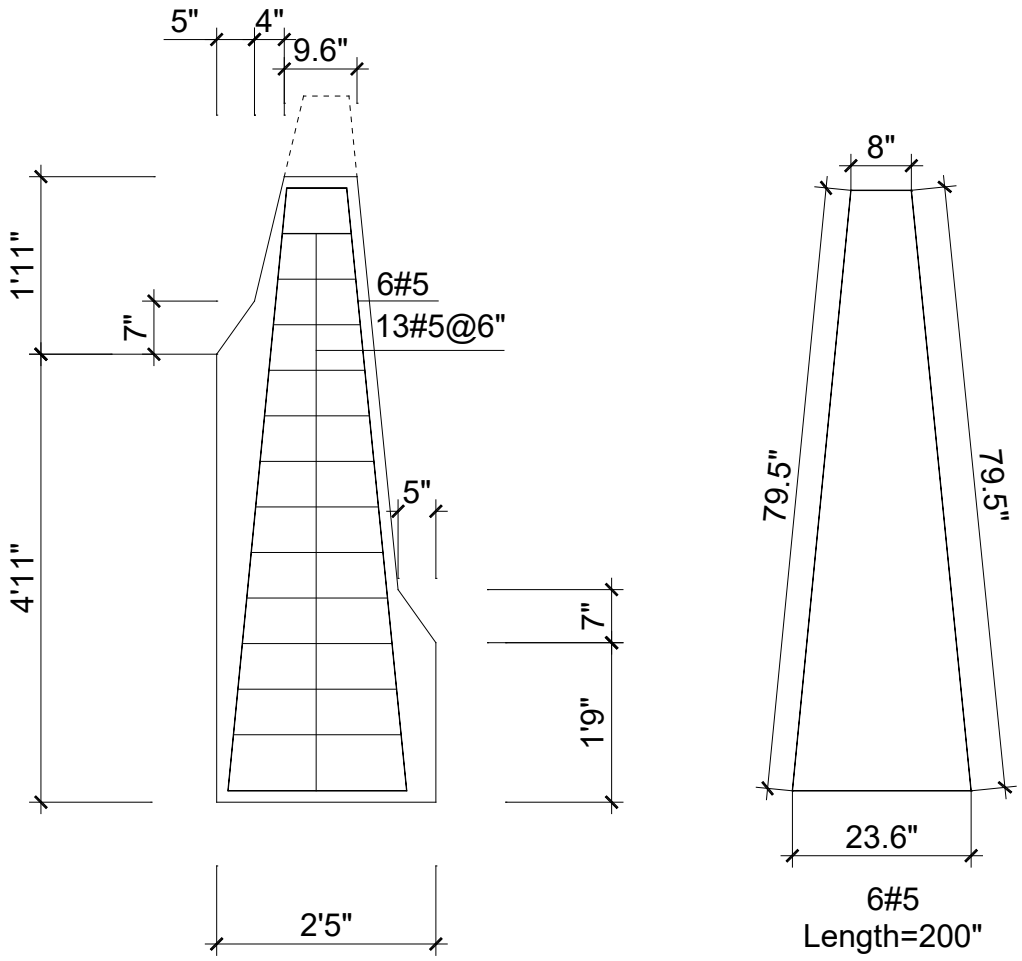

Figure 29. Detail of concrete wall of T7B-GRS wall for testing in T-Cage

Figure 30. Formwork and reinforcement of the concrete wall

Figure 31. Concrete wall after casting

Figure 32. Concrete wall in the vertical direction

3.6 Type 7 Barrier GRS wall model tests

The Type 7 Barrier GRS wall model tests will be conducted in the Tiger Cage located on a 20-ft x 30-ft test bay with a 10-ton overhead crane. The Team will perform four model tests (Table 10) with the arrangements as shown in Figs. 33 to 36. Four lateral and two vertical pressure cells, wall displacement transducers, and geosynthetic strain gauges were installed to measure the wall performance.

Table 10. Full-scale tests

No.	Geosynthetic spacing (in)	Geosynthetic style at facing
1	12	without wrap-around
2	12	with wrap-around
3	4	without wrap-around
4	4	with wrap-around

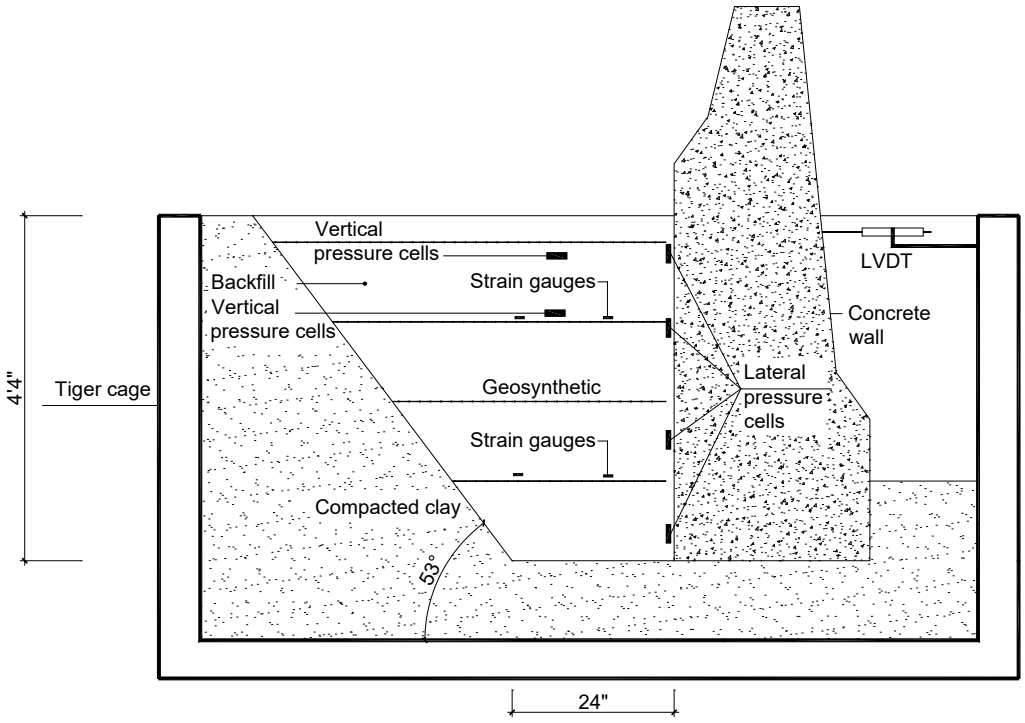

Figure 33. Model test of GRS wall with 3" distance from wall face to geosynthetic tip with 12" geosynthetic spacing (Test 1)

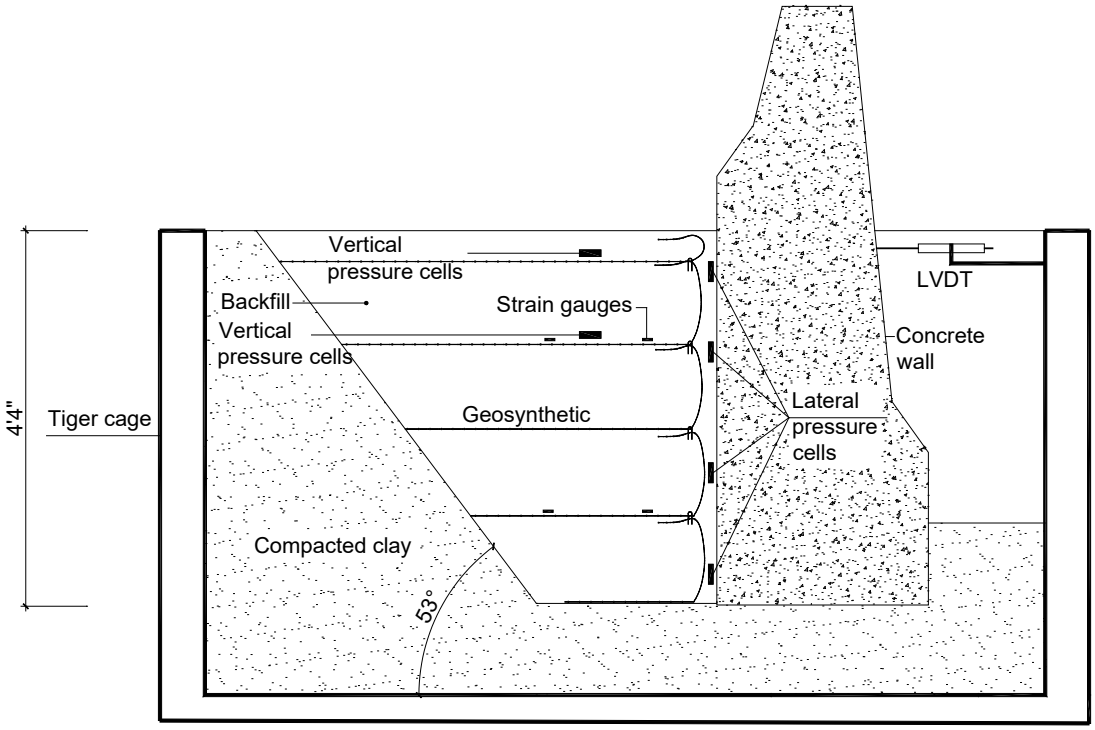

Figure 34. Model test of GRS wall with 12" spacing of wrapped around geosynthetic with (Test 2)

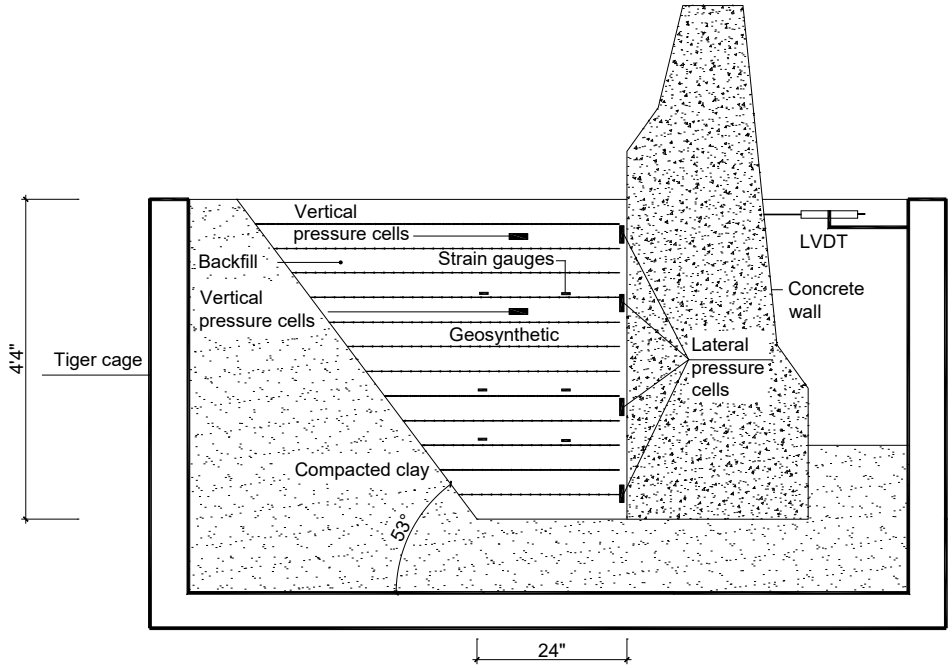

Figure 35. Model test of GRS wall with 3" distance from wall face to geosynthetic tip with 4" geosynthetic spacing (Test 3)

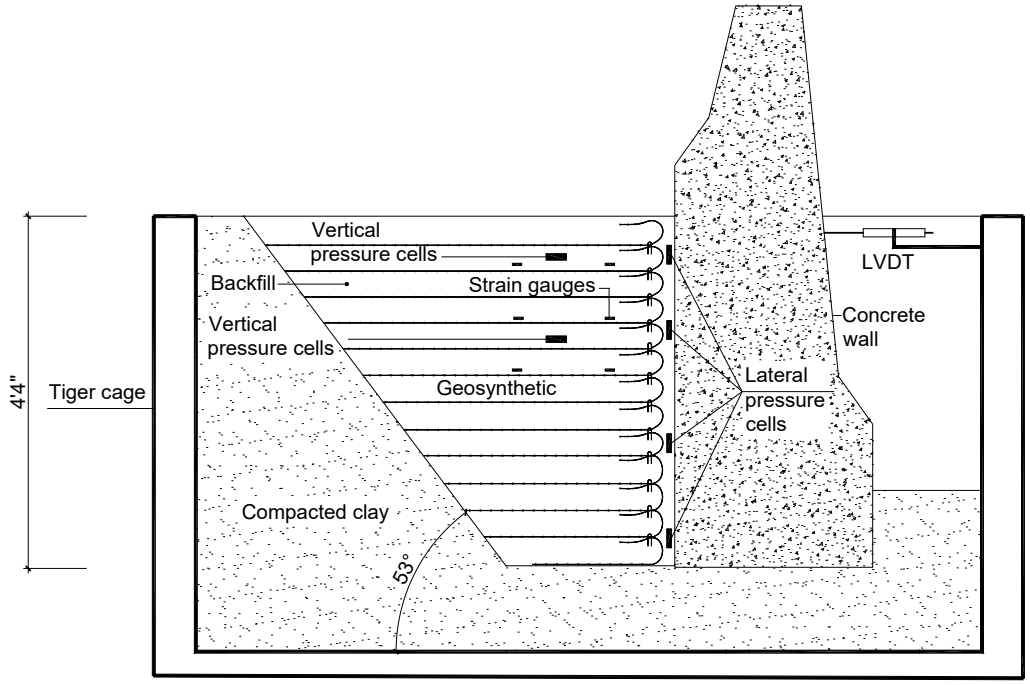

Figure 36. Model test of GRS wall with 4" spacing of wrapped around geosynthetic with (Test 4)

3.7 Instrumentation

3.7.1 Introduction

The experimental program consisted of instrumentation of the four T7B-GRS walls. To monitor and evaluate the wall performance, various types of instruments were installed in the T7B-GRS wall to record the measurement of interests. The measurements of interest are vertical pressures, lateral pressures and lateral displacement along the concrete wall, and distribution of strains along the geosynthetics.

Four load cells were installed below the concrete wall to measure the load transfer from soil to the concrete wall. Four other load cells were installed along the concrete wall to measure the lateral pressures. Two earth pressure cells with a semiconductor transducer were used to monitor vertical pressures. Two displacement sensors (LVDT) were installed laterally to monitor the lateral displacement of the concrete wall. Electrical resistant-type/foil-type-strain gauges were installed on the geosynthetics to measure the developed strains along the geosynthetics.

3.7.2 Pressure cells

Earth pressure cells are designed to measure stress in the soil acting on plane surfaces. Earth pressure cells used in these tests are the TP-101 series. Two earth pressure cells are installed to measure vertical pressure under abutment (Fig. 37).

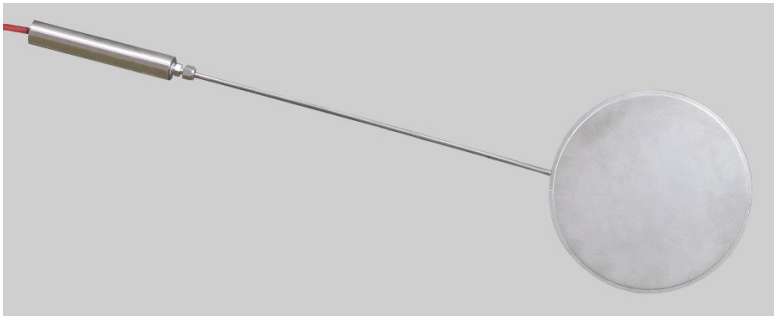

Figure 37. Earth pressure cell used to measure vertical stress

Pressure is calculated with the following equation:

$$p = mX + b \qquad (22)$$

where X is current in mA; m is a scale factor in kPa/mA, $m = 62.805$ kPa/mA; and b is offset in kPa, $b = -254.879$. The calibration factors are given in Table 11 for both pressure cells.

Table 11. Pressure cell calibration factors

Pressure cell	m (kPa/mA)	b (kPa)
TP2397	62.805	-254.879
TP2398	62.742	-256.450

3.7.3 Load cells

Four load cells were installed below the concrete wall (Fig. 38) to measure the load transfer from the compacted soil to the wall during construction and testing. They were calibrated before installation, and the calibration curves are shown in Fig. 39. The wall weight ~~is~~ measured by the

load cells after wall installation, as shown in Fig. 40, which is closed to the value given in Table 9.

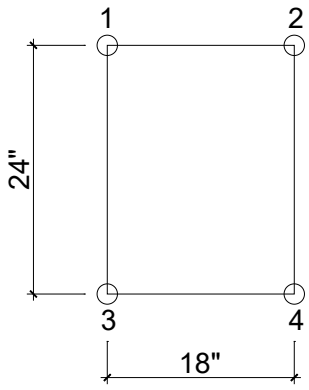

Figure 38. The load cells below the wall

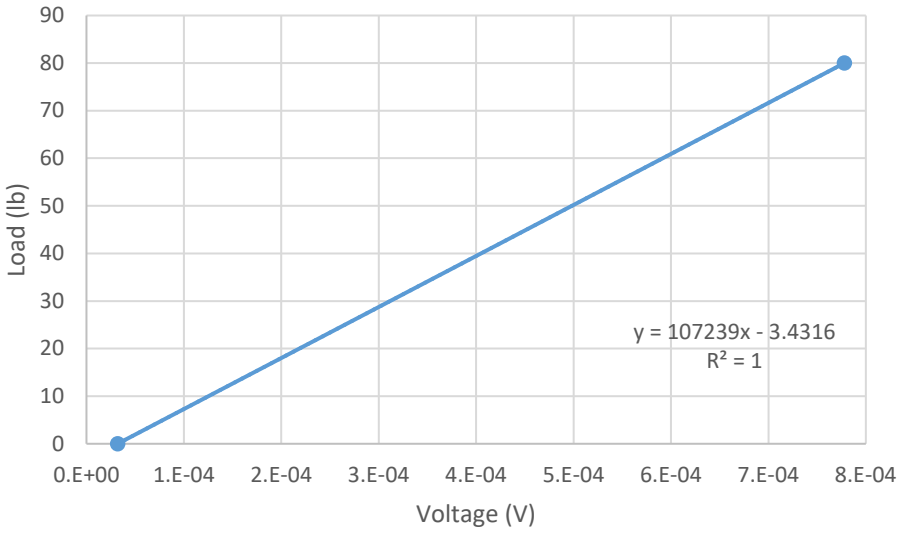

a) Load cell 1

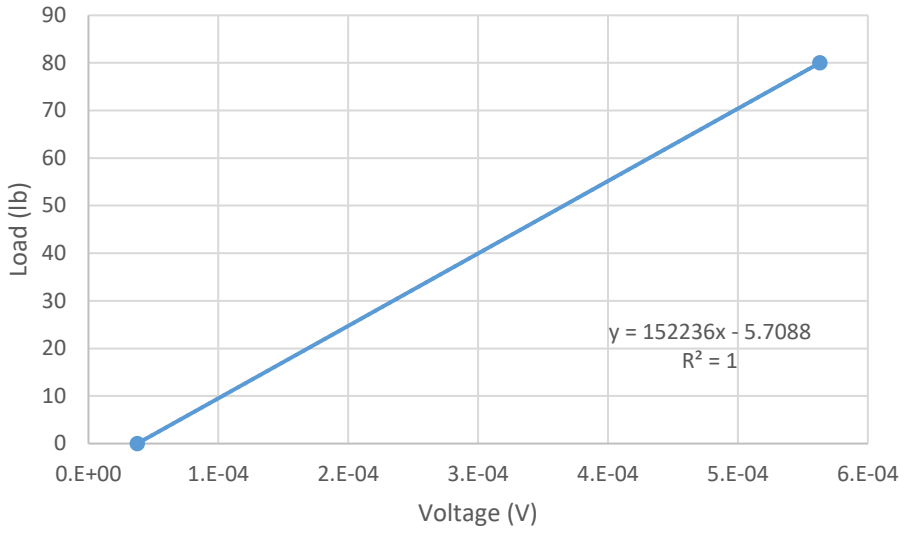

b) Load cell 2

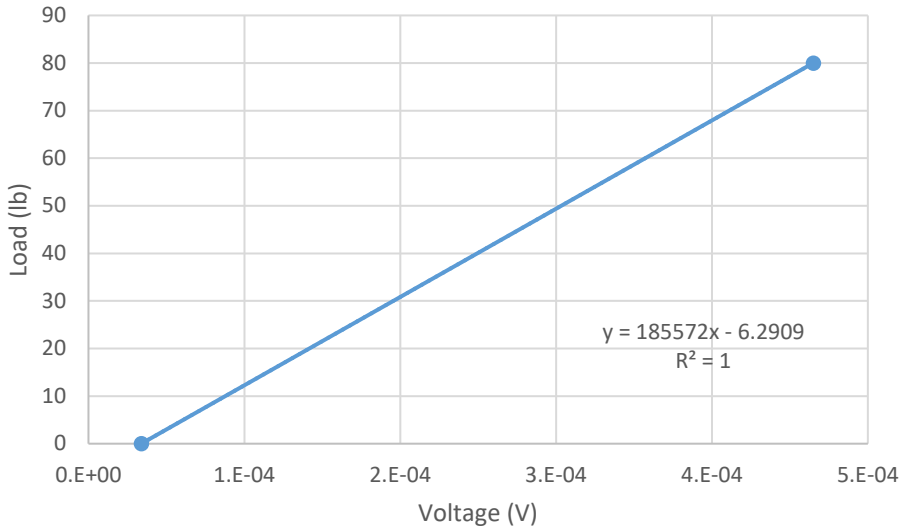

c) Load cell 3

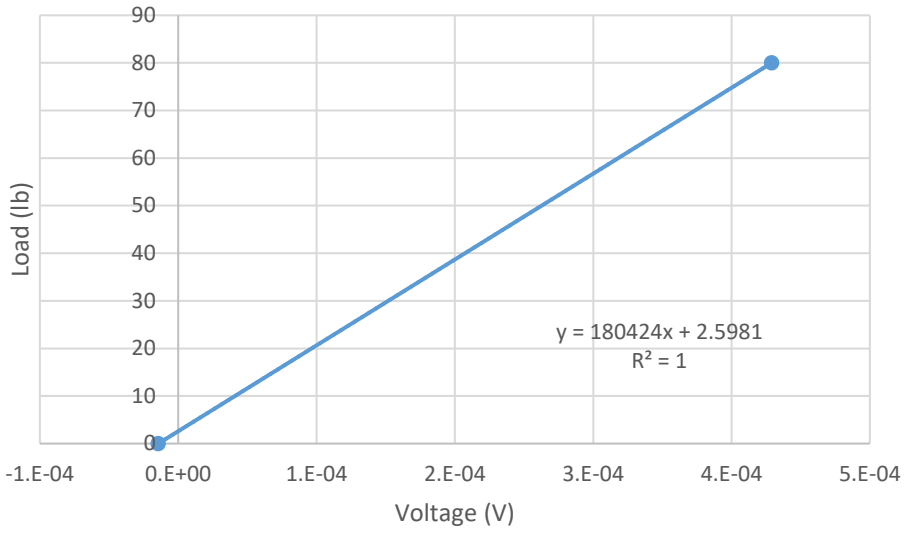

d) Load cell 4

Figure 39. Calibration curves for load cells

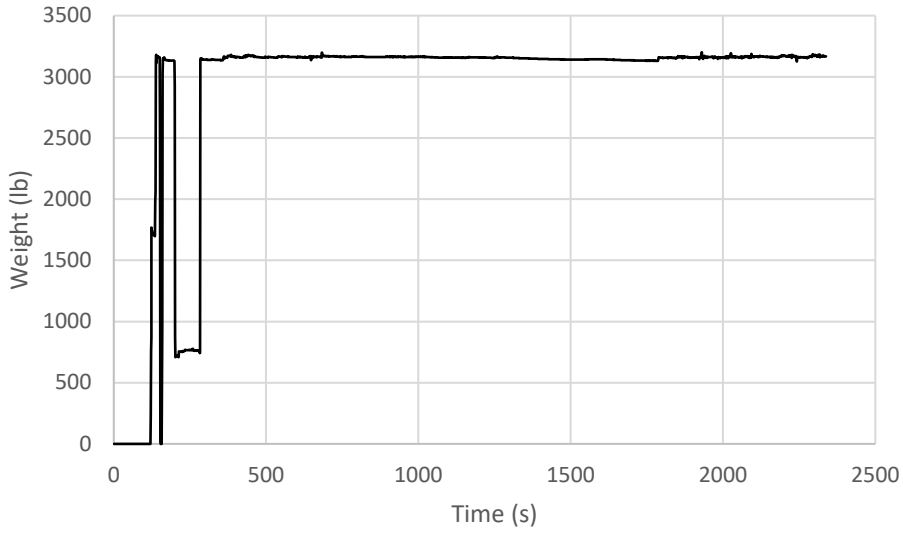

Figure 40. Concrete wall weight measured from load cells

3.7.4 Strain gauge on geosynthetic

The strain gauges were protected by Styrofoam to prevent punching from sharp particles of soil as shown in Fig. 41. Locations of all instruments are shown in Figs. 33 to 36.

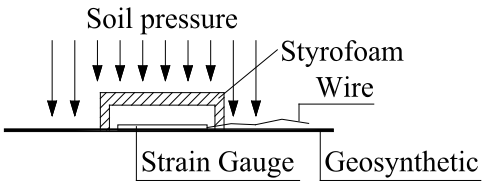

Figure 41. Strain gauge with protection

3.8 Construction Procedure

The chosen backfill was compacted in Tiger Cage to achieve the required density. The backfill was compacted in layers at the thickness of 4 in. and 12 in. as designated in Table 10 on full-scale tests. The backfill is compacted to reach a maximum density evaluated in the Modified Proctor tests. The full-scale model construction followed the following procedures:

1. Fill and compact the Colorado Class I backfill layers. When geosynthetic is wrapped around, a wooden plank is used to create a 3-inch gap between-the-concrete wall and geosynthetic as shown in Figure 42. The gap then is free filled with sand.

2. Install geosynthetic and load cells as shown in the instrumentation plan.

3. Repeat step 1 to step 2 until reaching the final layer.

4. The wooden plank is removed and the gap was filled with sand to complete the construction.

The nearly completed T7B-GRS wall is shown in Figs. 43 and 44.

Figure 42. Gap between concrete wall and wrap-around geosynthetic

Figure 43. Tiger Cage with T7B-GRSW model test

Figure 44. Wall top after soil compaction

3.9 Test results

3.9.1 Load transfer

The four load cells installed at four corners underneath the wall measured the load transfer from the backfill to the wall. Two load cells are near the inside face, and two others near the outside face of the wall as shown in Figs. 38 and 45. Based on the diagram in Fig. 45, the vertical load transfer to the concrete wall can be calculated as:

$$V = V_1 + V_2 \tag{23}$$

Overturning moment can also be predicted as the following equation:

$$M = Hd = V_1 L_1 + V_2 L_1 \tag{24}$$

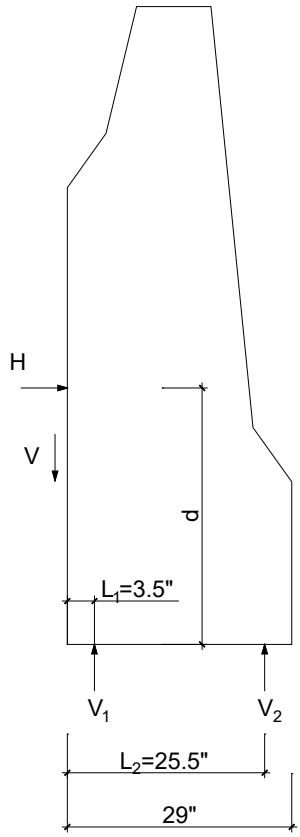

Figure 45. Applied load on concrete wall

The lateral resultant force cannot be determined accurately since its location is unknown. The only overturning moment can be calculated from the test data by using Eq. 24. Loads transferred to the concrete wall for all tests are shown in Figs. 46 to 49. It can be seen, for the tests with 12-inch

geosynthetic spacing, that the vertical load and overturning moment of test 1 (geosynthetic was not wrapped around) are higher than those of test 2 (geosynthetic was wrapped around).

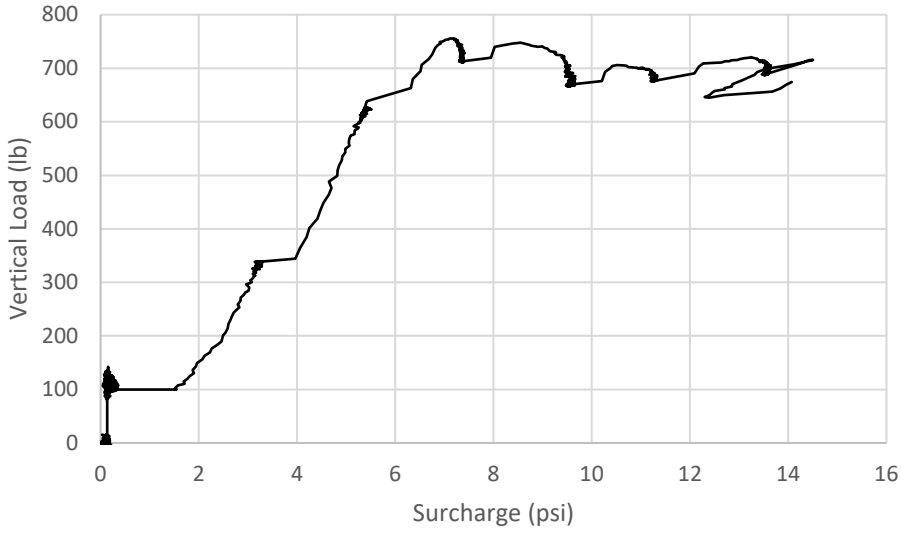

Figure 46. Vertical load transfers to the wall (test 1) without wrap-around geosynthetic

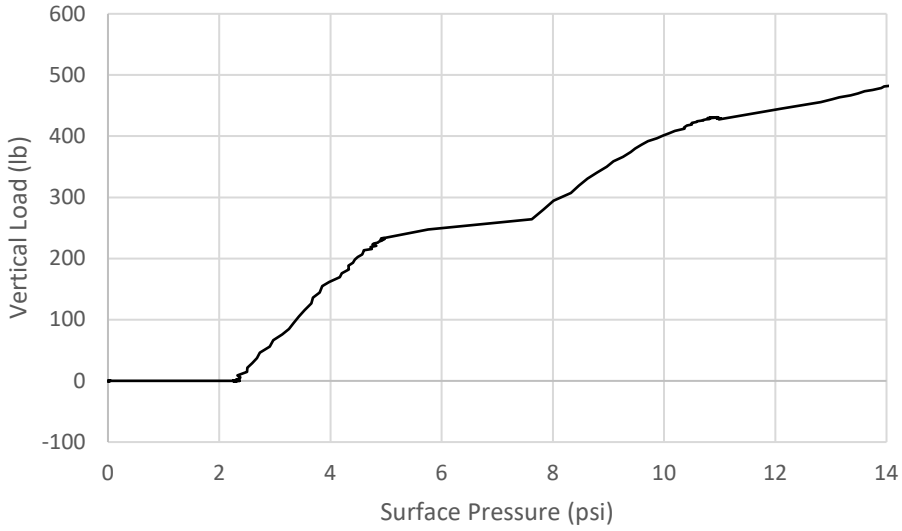

Figure 47 Vertical load transfers to the wall (test 2) with wrap-around geosynthetic

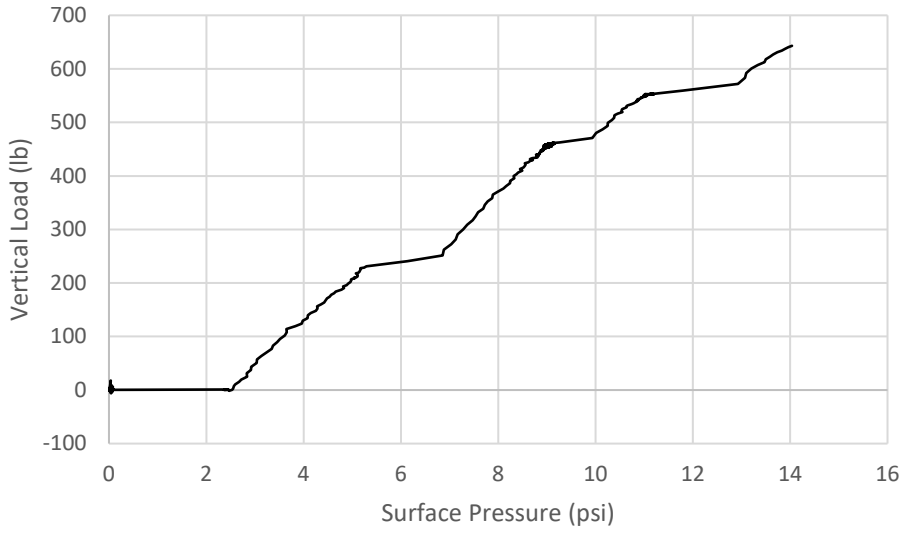

Figure 48. Vertical load transfers to the wall (test 3) without wrap-around geosynthetic

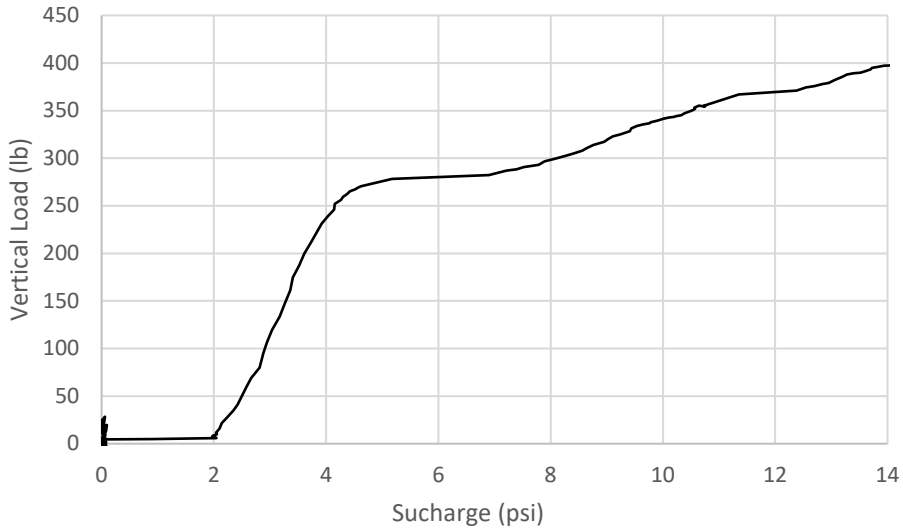

Figure 49. Vertical load transfers to the wall (test 4) with wrap-around geosynthetic

3.9.2 Lateral pressures

Four pressure cells were also installed vertically along the wall that faced soil mass. The pressure cells were numbered 1 to 4 from the bottom to the top of the concrete wall. Figure 50 depicts the measurements of the lateral pressures due to a surcharge of 14psi. The maximum pressures were observed above 26 in. depth for all cases. For the tests without wrap-around geosynthetic (tests 1 and 3), the spacing of geosynthetic has a significant effect on lateral pressures. As shown in Fig.

50, the test with 4 in.-spacing geosynthetic resulted in lower lateral pressures in comparison to those from the test with 12 in.-spacing geosynthetic. For the tests with wrap-around geosynthetics, the maximum lateral pressures also differed significantly.

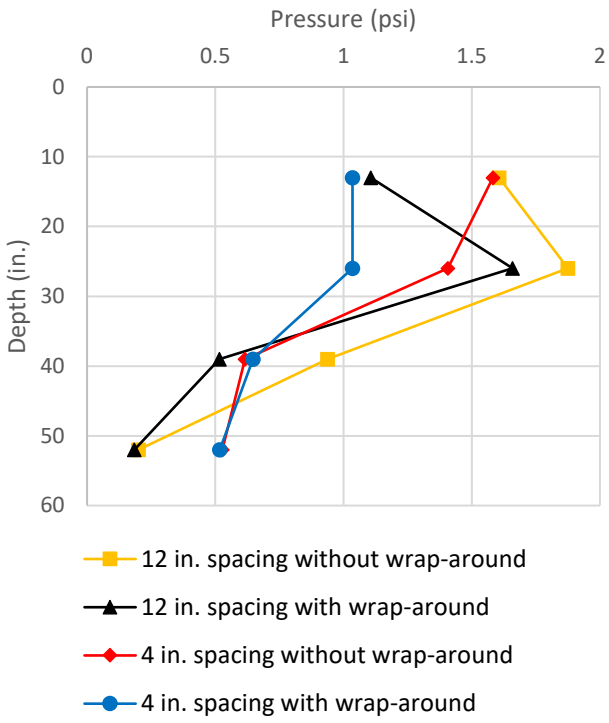

Figure 50. Lateral pressure

3.9.3 Lateral displacements

The concrete wall is very stiff so that no deformation occurs along the wall. Displacements at only two points on the wall were instrumented by LVDTs as shown in Fig. 51.

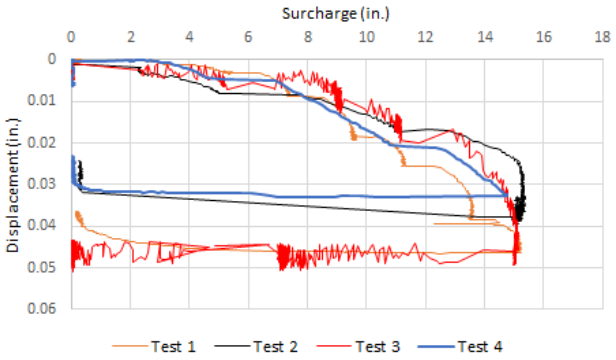

Figure 51. Displacements of concrete wall

4 FINITE ELEMENT ANALYSES

4.1 Introduction

Investigation of the GRS wall pressures requires a comprehensive numerical analysis program to simulate and check the measured performance as a cross-check effort to assure accurate computation and measurement. Since the deformation in the direction perpendicular to the cross-section of the wall is assumed to be zero, these three-dimensional structures can be simplified to a plane strain model. A general-purpose computer software, SSI2D was selected to serve the purpose. Chang et al. (2020a and 2020b) successfully developed plane strain, finite element models of steel-sheet-pile-facing GRS-IBS abutment and block-facing GRS wall, by using SSI2D. Analysis results of lateral and vertical pressures, lateral displacements were agreed well with the measurements of field instrumentation and full-scale model tests. It can be concluded that this numerical method is capable of effectively simulating the performance of the GRS wall.

4.2 Materials

The soil parameters are obtained from triaxial and oedometer tests of the Colorado Class I backfill (Chang et al. 2020b). The modified hyperbolic model was used in the analysis. All parameters for this model are presented in Table 12.

Table 12. Soil properties used in the analyses

Properties	Units	Value
Friction angle, ϕ	(^{0})	43
Cohesion, c	(psi)	14.4
Dilatancy angle, ψ	(^{0})	8.7
K_L	-	1300
n_L	-	0.477
K_{ur}	-	1975.6
n_{ur}	-	0.344
ν	-	0.145

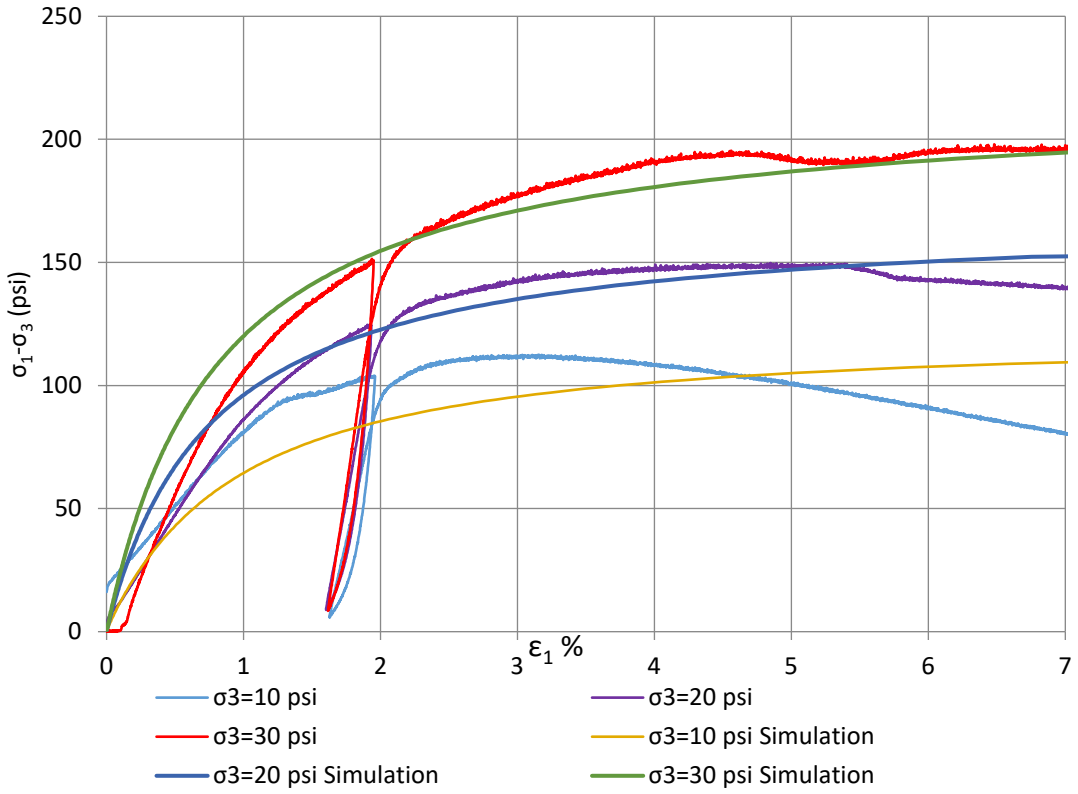

Figure 52. Comparison of stress-strain curves for the backfill

The geosynthetic reinforcement was modeled as a linear elastic perfectly-plastic material, in which three parameters are required (Fig. 53). The linear elastic perfectly-plastic model possesses a bilinear stress-strain curve. Note that the slope of the tensile load-strain curve is the product of modulus (e.g., Young's modulus E or tangent modulus E_t) and thickness of the geosynthetic. The tensile load is typically expressed in units of force per unit width of the reinforcement. Inversely, the modulus was calculated by dividing the slope of the tensile load-strain curve by the geosynthetic thickness. Similarly, the yield stress f_y for the bilinear model was found by dividing the yield tensile load by the thickness of the geosynthetic.

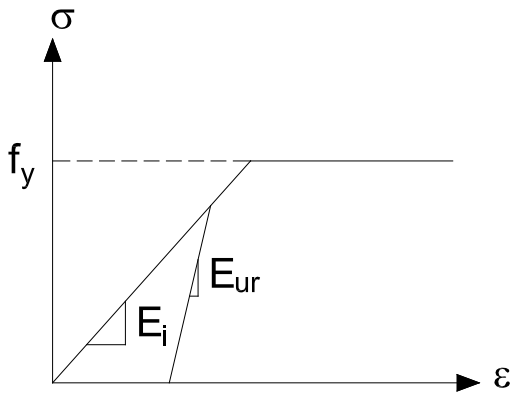

Figure 53. Stress-strain curve for geosynthetic

4.3 Finite element model of full-scale tests

Plane strain FE analysis was developed and verified using the results from the model tests of the fully-instrumented T7B-GRS walls. In the FE model, the soil and the cast-in-place concrete wall were represented by a plane strain second-order, 6-noded triangle elements to describe the stress-deformation behavior. The geotextile was represented by a special tension 2-noded elements to describe the axial forces. The interfaces between the backfill, foundation soil, and concrete wall were modeled using interface elements to model the soil-structure interface interaction of the thin zone of intense sharing interaction between soil and concrete wall at their contact. It is represented by a 6-joint element (also compatible with the soil element). Stage constructions were also modeled to take into account the effect of construction sequences. The analysis models and element meshes are shown in Figs. 54 and 55, respectively.

The following factors that may significantly contribute to the differences between FEA and full-scale tests are:

- Soil compaction: if soil density is not uniform, soil properties may be significantly different from those used as input data for the numerical analyses such as coefficient of lateral pressure at rest, Young's modulus, friction angle, and cohesion.
- Interface between soil and concrete wall: The interface properties between soil and concrete wall may not be determined accurately because they are dependent on the roughness surface of the concrete, backfill, and free-fill soils. Those properties mainly contribute to load transfer from soil to wall in both vertical and lateral directions.

- Boundary conditions of the concrete wall: the connection between the concrete wall and soil at the base is also very important. If the concrete wall rotates or moves, lateral pressure drops significantly.

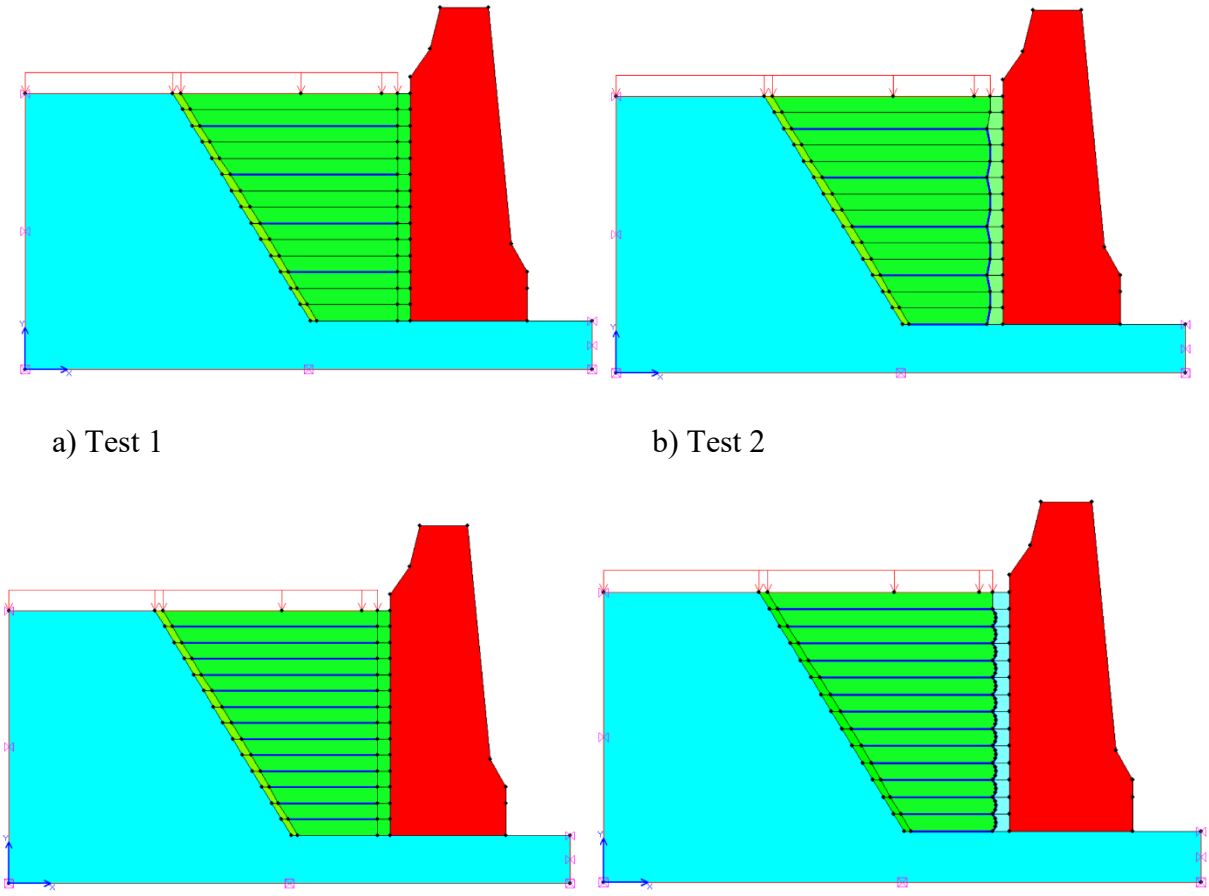

a) Test 1 b) Test 2

c) Test 3 d) Test 4

Figure 54. Finite element model

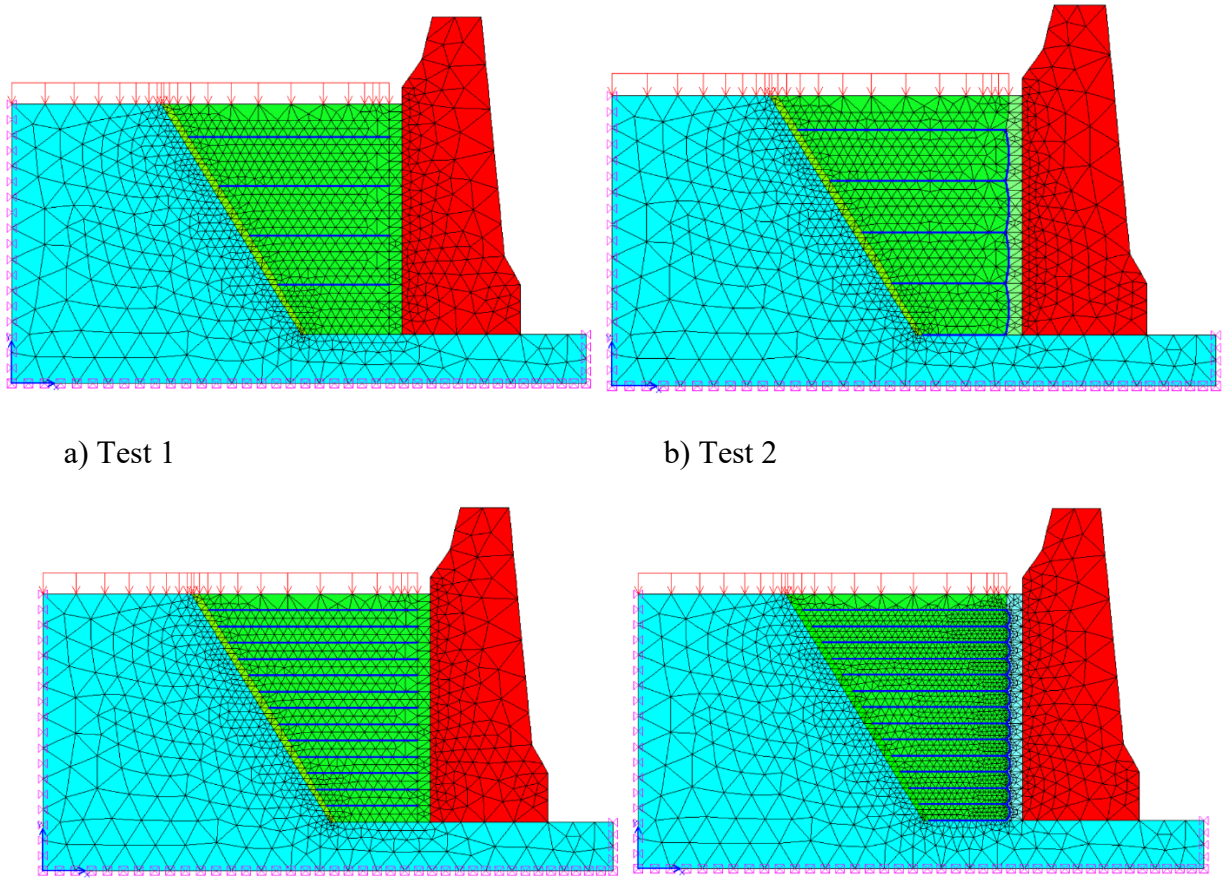

a) Test 1 b) Test 2

c) Test 3 d) Test 4

Figure 55. Finite element meshes

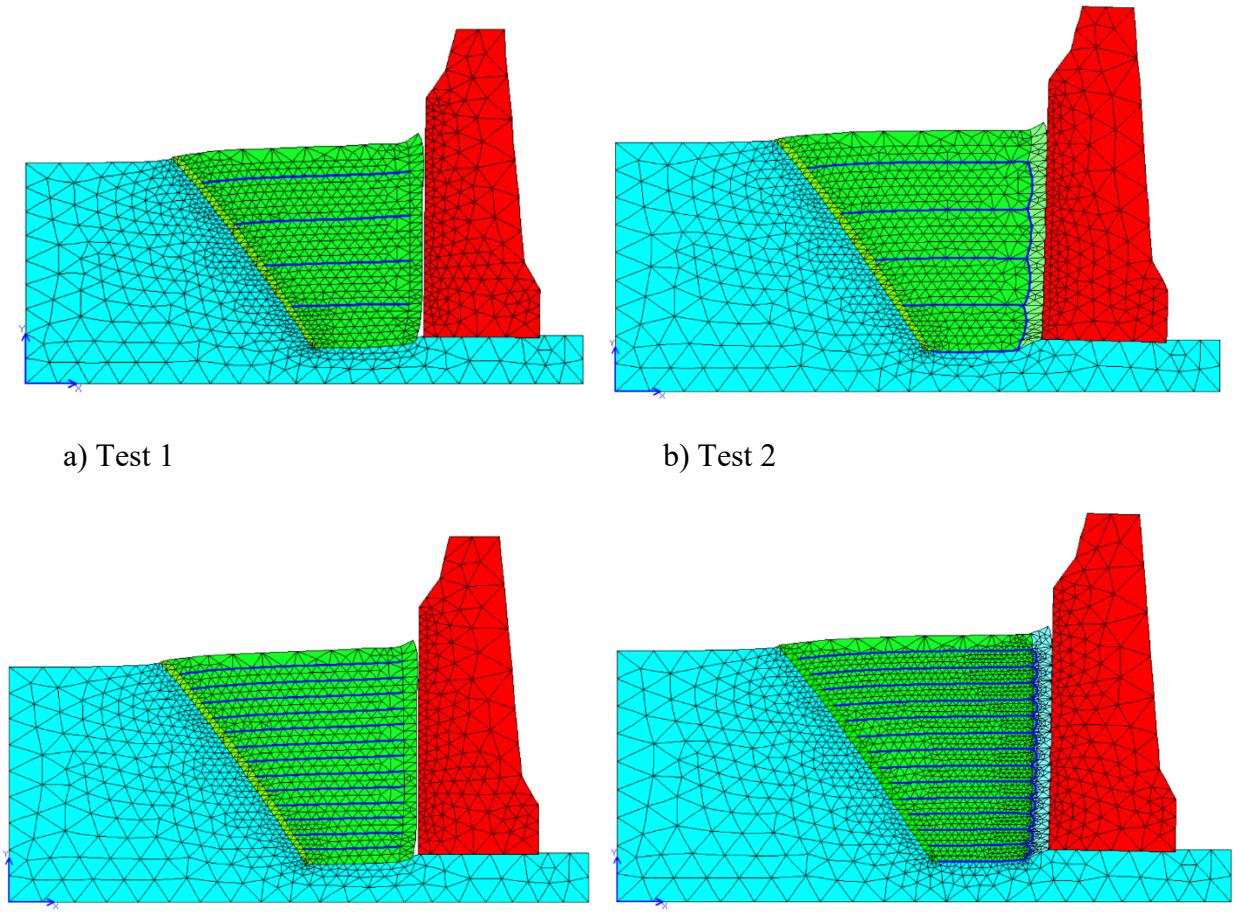

a) Test 1 b) Test 2

c) Test 3 d) Test 4

Figure 56. Displacements of wall and soil

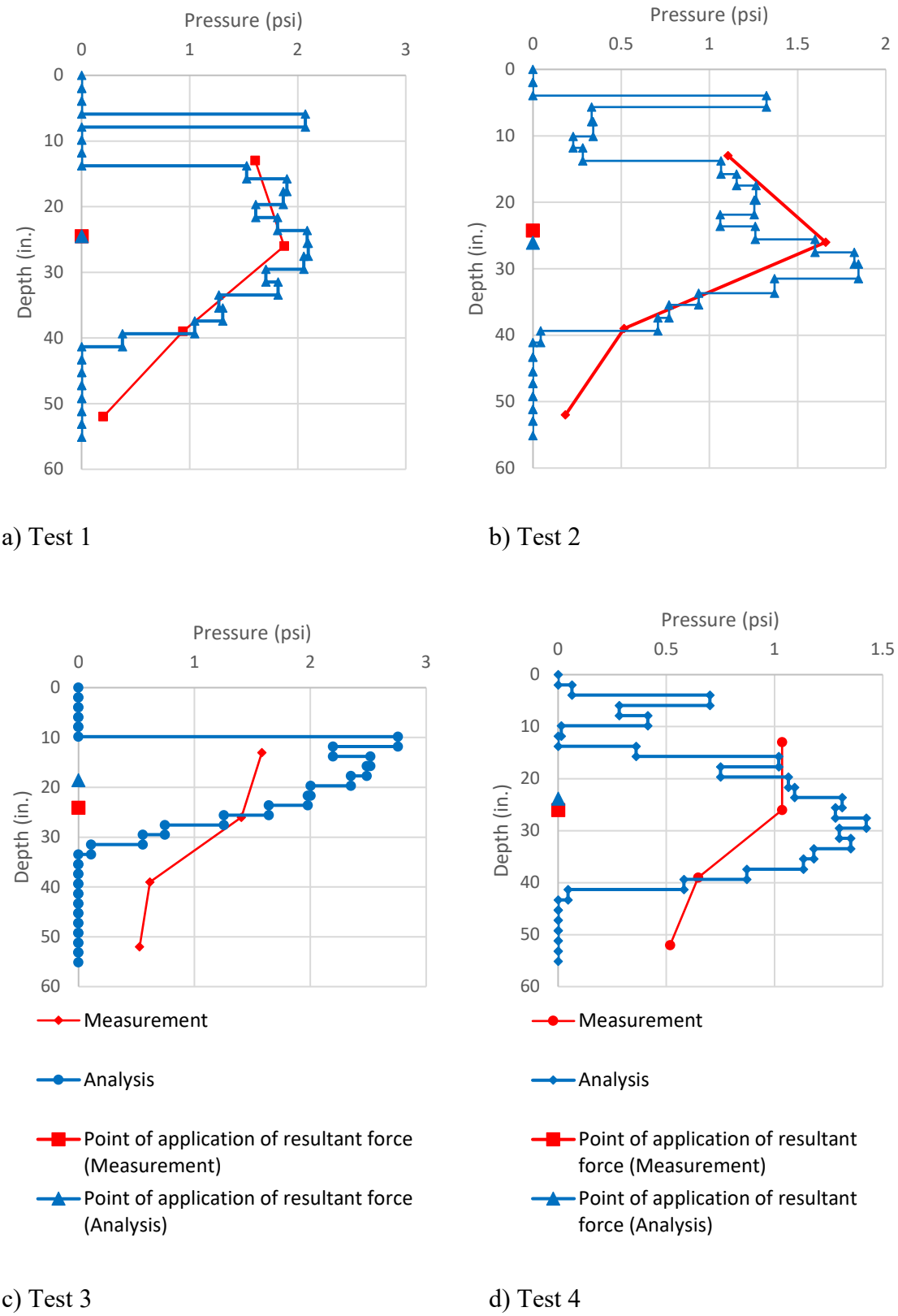

a) Test 1

b) Test 2

c) Test 3

d) Test 4

Figure 57. Comparison of lateral pressures on the concrete wall

The lateral pressures on the concrete wall are shown in Fig. 57 for all analysis cases. The pressures are slightly higher along the wall with 12-inch spacing than the wall with 4-inch spacing. The wall with wrapped-around geosynthetics resulted in smaller lateral earth pressures than the wall without a wrapped-around geosynthetics. The comparison between FEA and test results for the lateral pressures also can be made as shown in Fig. 57. For the geosynthetic with wrapped around, the lateral pressures from measurement are slightly lower than those from FEA. Similarly, the lateral pressures from test results for the geosynthetic without wrapped around are slightly less than those from FEA. The lateral pressures computed from FEA are close to the lateral pressures in soil without reinforcement calculated from coefficient of earth pressure at rest: 14x0.17=2.38 psi for the wall without wrapped around geosynthetics. Figures 58 show the maximum shear strain that occurred in the GRS wall under surcharge. It can be seen that those strains are located at the interface between backfill soil and concrete wall. Figure 59 shows the distribution of axial forces in geosynthetics. The theoretical failure line may intersect them at the locations of the maximum forces.

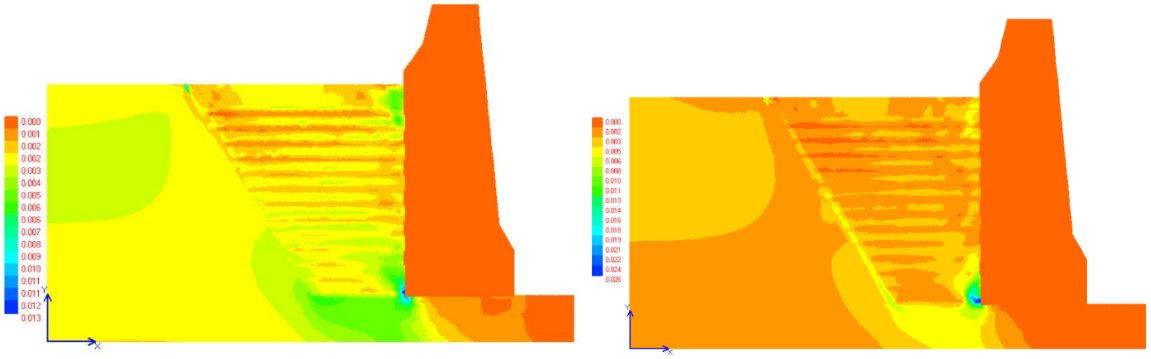

a) Test 1 b) Test 2

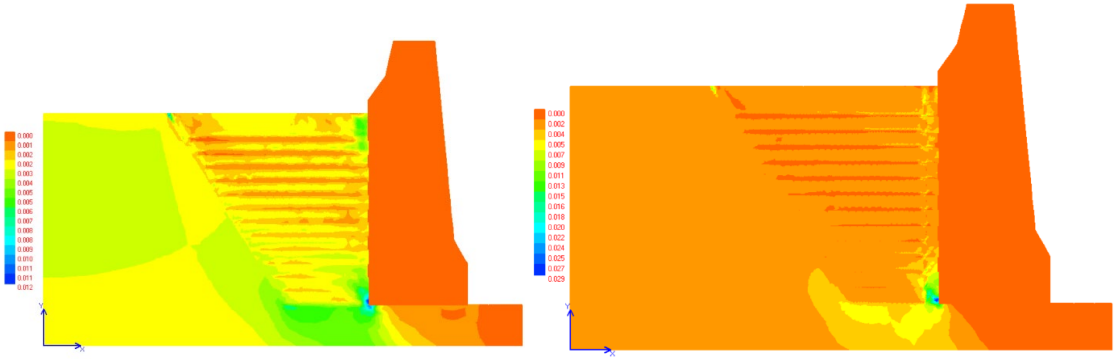

c) Test 3 d) Test 4

Figure 58. Maximum shear strains

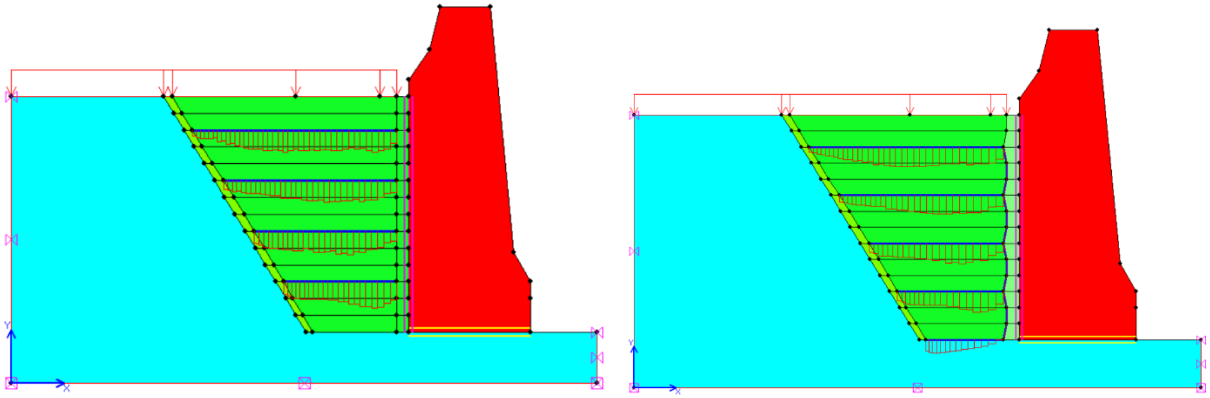

a) Test 1 b) Test 2

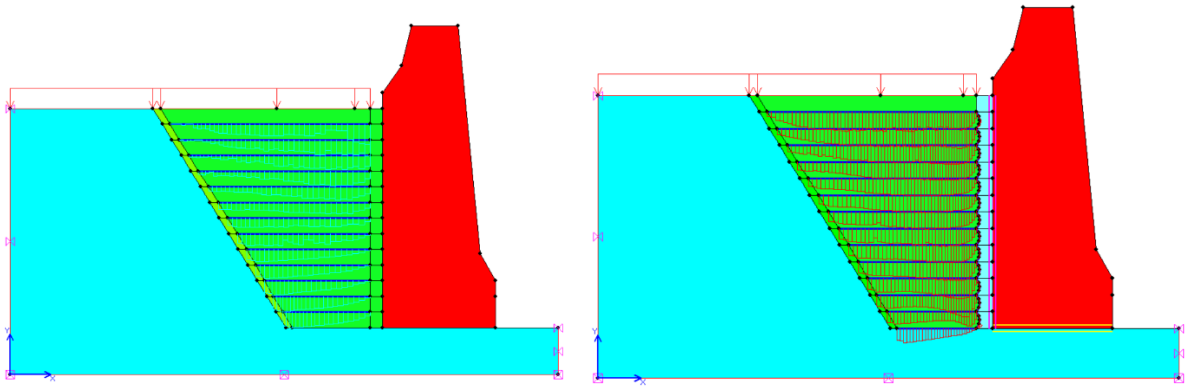

c) Test 3 d) Test 4

Figure 59. Axial forces in geosynthetics

Load transferred from soil to the concrete wall not only in the lateral direction but also in the vertical direction due to friction between soil and wall. For all tests, the measurements of the vertical loads were obtained from four load cells located at the bottom of the wall (as shown in Figs. 46 through 49). The measurements of lateral pressures from the pressure cells behind the concrete wall were used to compute lateral loads. Both vertical and lateral loads from FEM were obtained from internal stresses in the interface elements between the backfill and concrete wall. Table 13 summarized the comparison between measurement and analyses of vertical and lateral loads that transfer from soil to the concrete wall through their interface along the wall. The differences of lateral earth pressures between the T7B-GRS walls with and without wrap-around geosynthetic are not significant.

Table 13. Comparison of load transfer from soil to wall

Test	Vertical forces (lb/ft)		Lateral forces			
	Measurement	Analysis	Measurement		Analysis	
			Value (lb/ft)	Distance from the wall base to the point of application (in.)	Value (lb/ft)	Distance from the wall base to the point of application (in.)
1	700	808	706	24.5	580	24.5
2	500	476	526	26	440	23.8
3	660	699	503	24.3	487	18.5
4	400	405	464	24	384	26

5. ANALYTICAL METHOD FOR GRS WALL PRESSURE

The lateral pressure from GRS on the walls (sheet pile, concrete, block facing) depends on soil properties, geosynthetic properties, geosynthetic spacing, lateral wall deformation. The following analytical method is for the assessment of lateral earth pressures on GRS walls.

5.1 Governing equations

Geosynthetic spacing is "S" as shown in Fig. 60. Each geosynthetic reinforcement contributes to the horizontal stress at a vertical spacing of "S/2" above and below its location. The main stress direction remains unchanged under load application. According to Hooke's law, the strain-stress relationship is given by:

$$\begin{Bmatrix} \varepsilon_x \\ \varepsilon_y \\ \gamma_{xy} \end{Bmatrix} = \frac{1}{E_s} \begin{bmatrix} (1-\nu_s)^2 & -\nu_s(1+\nu_s) & 0 \\ -\nu_s(1+\nu_s) & (1-\nu_s)^2 & 0 \\ 0 & 0 & 2(1+\nu_s) \end{bmatrix} \begin{Bmatrix} \sigma_x \\ \sigma_y \\ \tau_{xy} \end{Bmatrix} \quad (25)$$

where ε_x and ε_y are normal strains in X and Y directions, respectively; γ_{xy} is shear strain; σ_x and

σ_y is vertical stresses in soil, respectively; τ_{xy} is shear stress; E_s is Young's modulus and ν_s Poisson's ratio of backfill. The normal stresses and strains are positive when soil is in compression.

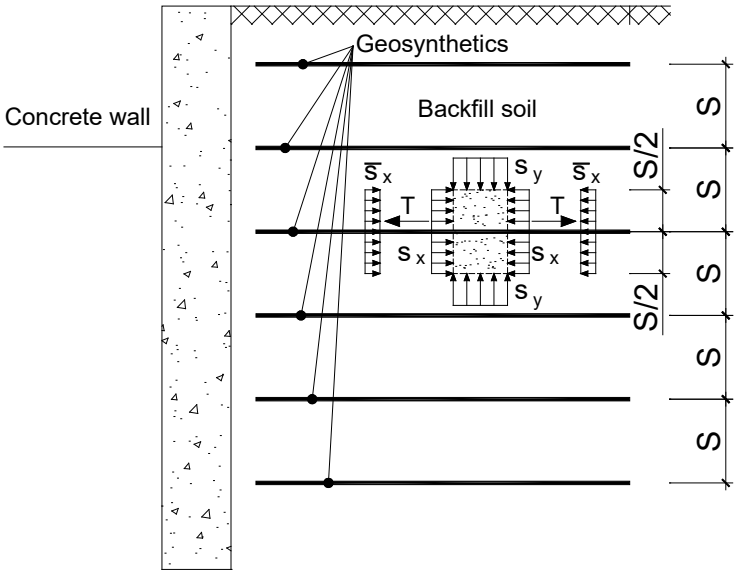

Figure 60. Stresses in GRS

Stress in soil is related to stress in GRS by the following equation:

$$\sigma_x = \bar{\sigma}_x + \frac{T}{S} \tag{26}$$

where S is the spacing between neighboring geosynthetics; T is tension force in a geosynthetic, $T \le T_f$ where E_r and A_r are Young's modulus and cross-sectional area of the geosynthetic, T_f is the tensile strength of geosynthetics; and $\bar{\sigma}_x$ is horizontal stress in GRS (Fig. 60).

Substituting Eq. (26) into Eq. (25) leads to:

$$\begin{Bmatrix} \varepsilon_x \\ \varepsilon_y \\ \gamma_{xy} \end{Bmatrix} + \begin{Bmatrix} \frac{E_r A_r}{E_s S}\left(1-\nu_s\right)^2 \varepsilon_x \\ -\frac{E_r A_r}{E_s S}\nu_s\left(1+\nu_s\right)\varepsilon_x \\ 0 \end{Bmatrix} = \frac{1}{E_s}\begin{bmatrix} \left(1-\nu_s\right)^2 & -\nu_s\left(1+\nu_s\right) & 0 \\ -\nu_s\left(1+\nu_s\right) & \left(1-\nu_s\right)^2 & 0 \\ 0 & 0 & 2\left(1+\nu_s\right) \end{bmatrix}\begin{Bmatrix} \bar{\sigma}_x \\ \sigma_y \\ \tau_{xy} \end{Bmatrix} \tag{27}$$

Equation (27) is rearranged as:

$$\begin{bmatrix} 1+\dfrac{E_r A_r}{E_s S}(1-\nu_s)^2 & 0 & 0 \\ -\dfrac{E_r A_r}{E_s S}\nu_s(1+\nu_s) & 1 & 0 \\ 0 & 0 & 1 \end{bmatrix} \begin{Bmatrix} \varepsilon_x \\ \varepsilon_y \\ \gamma_{xy} \end{Bmatrix} = \frac{1}{E_s} \begin{bmatrix} (1-\nu_s)^2 & -\nu_s(1+\nu_s) & 0 \\ -\nu_s(1+\nu_s) & (1-\nu_s)^2 & 0 \\ 0 & 0 & 2(1+\nu_s) \end{bmatrix} \begin{Bmatrix} \bar{\sigma}_x \\ \sigma_y \\ \tau_{xy} \end{Bmatrix} \quad (28)$$

From Eq. (28), the stress-strain relationship for plane strain condition of GRS from Hooke's law can be expressed as:

$$\begin{Bmatrix} \sigma_x \\ \sigma_y \\ \tau_{xy} \end{Bmatrix} = \begin{bmatrix} \dfrac{E_s(1-\nu_s)}{(1+\nu_s)(1-2\nu_s)} + \dfrac{E_r A_r}{S}\dfrac{(1-3\nu_s+2\nu_s^2-2\nu_s^3)}{(1+\nu_s)(1-2\nu_s)} & \dfrac{\nu_s E_s}{(1+\nu_s)(1-2\nu_s)} & 0 \\ \dfrac{\nu_s E_s}{(1+\nu_s)(1-2\nu_s)} - \dfrac{E_r A_r}{S}\dfrac{2\nu_s^2(1-\nu_s)}{(1+\nu_s)(1-2\nu_s)} & \dfrac{E_s(1-\nu_s)}{(1+\nu_s)(1-2\nu_s)} & 0 \\ 0 & 0 & 2(1+\nu_s) \end{bmatrix} \begin{Bmatrix} \varepsilon_x \\ \varepsilon_y \\ \gamma_{xy} \end{Bmatrix} \quad (29)$$

If $\varepsilon_x < 0$ then the coefficient of the lateral earth pressure is dependent on geosynthetic modulus, thickness, and vertical spacing as shown in Eq. (29). The coefficient of the lateral earth pressure at the rest of GRS is the same as that of the soil as shown in Eq. (30) if $\varepsilon_x = 0$:

$$\frac{\bar{\sigma}_x}{\sigma_y} = \frac{\nu_s}{1-\nu_s} \quad (30)$$

At failure, the vertical stress is related to the horizontal stress as the following equation based on Mohr-Coulomb criterion:

$$\sigma_{yf} = \sigma_{xf} K_p + 2c\sqrt{K_p} \quad (31)$$

Substituting Eq. (26) into Eq. (31) leads to:

$$\sigma_{yf} = \left(\bar{\sigma}_{xf} + \frac{T}{S_v}\right) K_p + 2c\sqrt{K_p} \quad (32)$$

Equation (32) can be rewritten as:

$$\sigma_{yf} = \bar{\sigma}_{xf} K_p + 2\left(c + \frac{T}{2S_v}\sqrt{K_p}\right)\sqrt{K_p} \quad (33)$$

As presented in Eq. (33), the equivalent cohesion of GRS is obtained as:

$$c_{eq} = c + \frac{T}{2S_v}\sqrt{K_p} \tag{34}$$

If the vertical pressure on GRS is known, the lateral pressure on the wall can be determined as the following procedures.

The lateral pressure in soil can be calculated as:

$$\sigma_{xf} = \sigma_{yf} K_a - 2c\sqrt{K_a} \tag{35}$$

At failure, Young's modulus of soil is assumed to be zero, from Eq. (29), the lateral strain in soil caused by the vertical pressure is:

$$\varepsilon_x = -\frac{\sigma_{yf} - \sigma_{xf}}{\frac{E_r A_r}{S_v}\frac{2\nu_s^2(1-\nu_s)}{(1+\nu_s)(1-2\nu_s)}} \tag{36}$$

The axial force in the geosynthetic:

$$T = -E_r A_r \varepsilon_x = S_v\left(\sigma_{yf} - \sigma_{xf}\right)\frac{(1+\nu_s)(1-2\nu_s)}{2\nu_s^2(1-\nu_s)} \le T_f \tag{38}$$

Then the horizontal stress in GRS is given by:

$$\overline{\sigma}_x = \sigma_x - \frac{T}{S_v} \tag{39}$$

Equation (39) can be used in CDOT Worksheet B504 to improve the design of the T7B-GRS wall.

5.2 Strength of geosynthetic

Strength of geosynthetic T_f is a minimum value of allowable tensile strength of the material and pullout resistance:

$$T_f = \min\left(\phi R_c T_a, \phi R_c T_i\right) \tag{40}$$

where ϕ is the resistance factor for reinforcement pullout, $\phi = 0.9$ (Table 11.5.7-1, AASHTO, 2017) for both pullout and tensile strengths; R_c is reinforcement coverage ratio.

Pullout resistance

The pullout resistance of the reinforcement per unit width of reinforcement is given by (FHWA-NHI-99-025 and AASHTO, 2017):

$$T_i = \phi F^* \alpha \sigma_{v0} L_i C \tag{41}$$

where F^* is the pullout resistance factor; for geosynthetic sheet reinforcement $F^* = 2/3 \tan\varphi$; α is a scale effect correction factor (Table 14); σ_{v0} is the effective vertical stress at the soil-reinforcement interface; L_i is the embedment or adherence length of the reinforcement in the resisting zone behind the failure surface, sometimes the termed resisting length of the reinforcement; and C is the reinforcement effective unit perimeter, $C = 2$ for strips, grids, and sheets.

Table 14. Scale effect correction factor

Reinforcement Type	Default Value for α
All steel reinforcements	1
Geogrids	0.8
Geotextiles	0.6

Tensile strength of reinforcement

The initial stress-strain characteristics of geosynthetic reinforcement depend on the geometry and tensile properties of their load-carrying elements. The characteristics of geosynthetic reinforcing elements manufactured with the same base polymer may vary widely. The tensile capacity of the reinforcements is further affected by creep, temperature, construction damage, aging, and other factors. The ultimate (or, yield) tensile strength of the geosynthetic reinforcement is usually determined from the wide strip tensile strength test (ASTM D 4595). When used in the design, however, an allowable tensile strength is computed by applying reduction factors to the ultimate strength to account for the above-mentioned factors. The maximum tensile strength is computed as follows:

$$T_{\max} \le \phi T_a R_c = \phi \frac{T_{ult}}{RF} R_c = \phi \frac{T_{ult}}{RF_{CR} RF_D RF_{ID}} R_c \quad (42)$$

where T_a is nominal long-term reinforcement design strength; T_{ult} is ultimate (or yield tensile strength) from wide strip tensile strength test (ASTM D 4595) based on minimum average roll value (MARV) for the product; RF is a dimensionless product of all applicable reduction factors; RF_{CR} is creep reduction factor; RF_D is durability reduction factor; RF_{ID} is installation damage reduction factor; and $\phi = 0.9$ is resistance factor for reinforcement tension in Table 11.5.7-1 (AASHTO, 2017).

Creep reduction factor

This reduction factor is obtained from long-term laboratory creep testing. Creep testing is essentially a constant load test on multiple product samples, loaded to various percentages of the ultimate product load, for periods up to 10,000 hours. The creep reduction factor is the ratio of the ultimate load to the maximum sustainable load within the design life. Typical reduction factors as a function of polymer type are indicated in Table 14.

Table 15. Creep reduction factors

Polymer Type	Creep Reduction Factors
Polyester	2.5 to 2.0
Polypropylene	5.0 to 4.0
Polyethylene	5.0 to 2.5

Durability Reduction Factor

This factor (RF_D) is dependent on the susceptibility of the geosynthetic to attack by microorganisms, chemicals, ultraviolet radiation, thermal oxidation, hydrolysis, and stress cracking, and can vary from 1.1 to 2.0.

Installation Damage Reduction Factor

The placement and compaction of backfill material against geosynthetics may damage and reduce

its tensile strength. The level of damage for each geosynthetic reinforcement is summarized in the damage reduction factor, which is the function of weight and type of construction equipment, and geosynthetic material type. The installation damage is also influenced by the lift thickness and type of soil present on either side of the reinforcement. Where granular and angular soils are used for backfill, the damage is more severe than where soft, finer soils are used.

The installation damage factor ranges from 1.1 to 3.0 depending on backfill gradation and product mass per unit weight. To account for installation damage strength loss, where full-scale product-specific testing is not available for geotextile, a minimum product weight of 270 g/m3 should be specified for reinforcement applications and a default value of 3.0 is recommended for a reduction factor.

Reduction factor

For wall applications which are defined as not having severe consequences should the poor performance of failure occur, having nonaggressive soil conditions, and if the geosynthetic product satisfies the minimum requirement listed in Table 11.10.6.4.3b-1 (AASHTO, 2017), the long-term tensile strength of the reinforcement may be determined using a default reduction factor $RF = 7$ as provided in Table 11.10.6.4.3b-1 (AASHTO, 2017) instead of product-specific test results.

5.3 Application to T7B-GRS wall

Consider the T7B-GRS walls with 4”-4’ height (similar to the full-scale models) and with maximum height as presented in B504-S7 (CDOT, 2018). The layers of geosynthetic are placed at a spacing of 12”. The calculation is based on B504-H2 (CDOT, 2018) and the proposed equations for active lateral earth pressure (Eq. 39). The T7B-GRS walls with 4”-4’ height was selected because it meets the design requirements for overturning and minimum bearing pressure. The calculation results of tensile, pullout strength of the geosynthetics, and applied forces on the concrete wall are given in Appendix B and the lateral earth pressures along the walls are shown in Figs. 61 to 63.

The active lateral earth pressure of GRS reduced significantly in comparison to that of backfill soil at the top layers because of the tension force of the geosynthetic (Figs. 61 to 63). The active lateral pressures are calculated by the proposed equation for GRS and the classical equation for soil that increases linearly with depth. It is in good agreement with the measurements and the results of FEA from the surface to the mid-depth of the wall and much higher beyond (Fig. 57 and Fig. 61).

This means that the overturning moment from the analytical method will be greater than those from measurements and FEAs. In the FEA and lab tests, the concrete wall was allowed to move and the soil was deformed mainly on the upper part of the GRS wall while the analytical solution did not consider the movement of the concrete wall. As a result, the lateral earth pressure calculated by using the analytical method was significantly higher than those in comparison to the FEA and measurements at the lower part of the concrete wall.

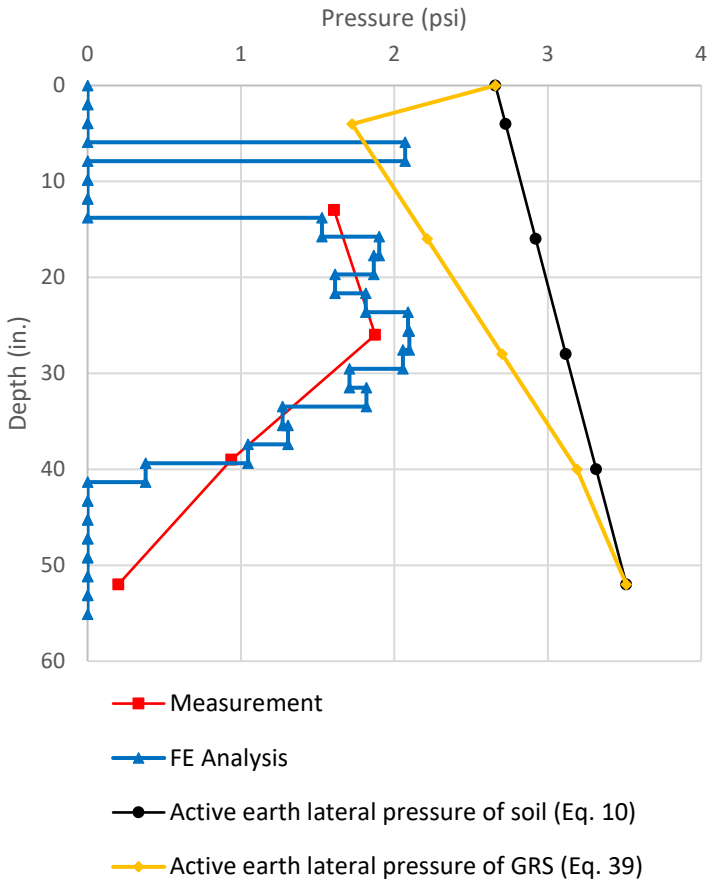

Figure 61. Lateral earth pressures (4'-4" height) under 14psi surcharge

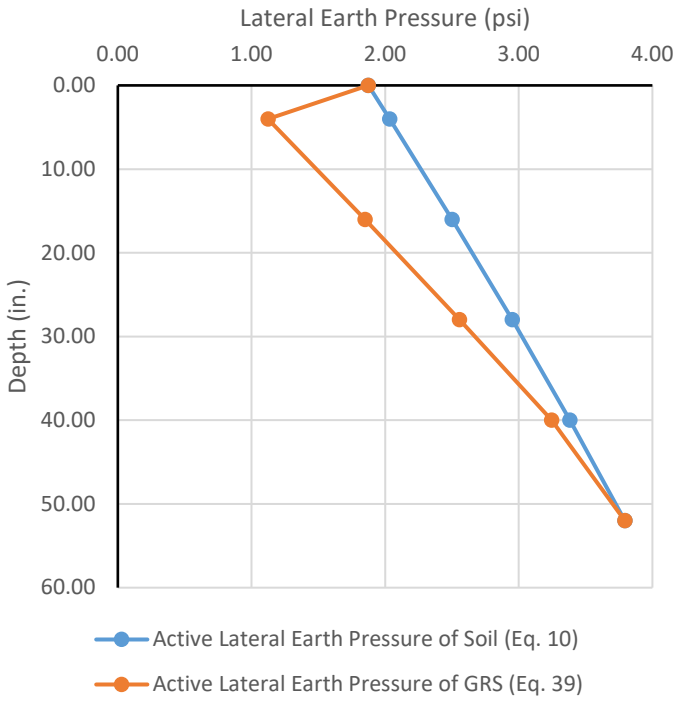

Figure 62. Lateral earth pressures (4'-4" height)

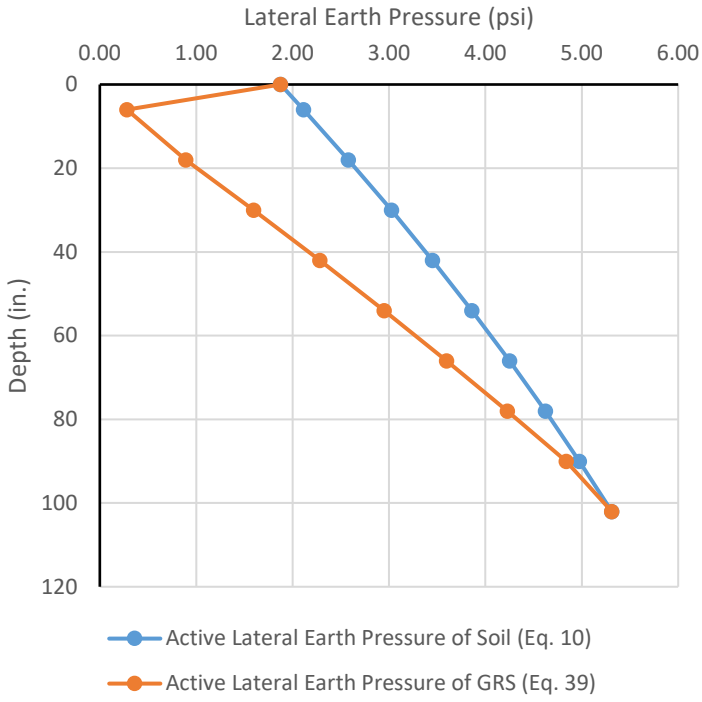

Figure 63. Lateral earth pressures (8'-6" height)

5.4 Optimum wall shape and maximum wall height

The wall shape and maximum height should be satisfied all requirements of 1) Overturning; 2) Bearing capacity; and 3) Sliding. The current design method found that the maximum height of T7B-GRS wall is 8'-6" based on the design criteria: 1) GRS wrap around phased wall is self-standing and applied no (or minimum) pressure to the adjacent concrete rail; 2) Earthquake detail is required for stability regardless to seismic performance zone. The optimal wall shape (or the base width) and the maximum wall height are mainly contributed by overturning moment from lateral earth pressure of GRS. Load factors for bearing resistance and overturning are used in the calculation according to AASHTO (2017).

For checking the overturning effect, the righting moment is greater than the overturing moment when the minimum base width is 39" while the original design of the wall base width is 32". The wall base increased 26" to satisfy the condition minimum bearing pressure, $q_{\min} \geq 0$:

$$q_{\min} = \frac{F_V}{A}\left(1 - \frac{6e}{B}\right) \geq 0$$

The maximum bearing pressure is calculated as:

$$q_{\max} = \frac{F_v}{A}\left(1 + \frac{6e}{B}\right)$$

where F_v is vertical load; A is wall base area; B is wall base width; and e is eccentricity.

Table 16 shows all loads applied on the wall, bearing pressures, and concrete wall weights. The original and modified wall shapes are shown in Fig. 64. The wall needs to be checked with the bearing and sliding conditions with the maximum bearing pressure and the minimum required resisting force as shown in Table 16.

Table 16. Factored load on the concrete wall

Base width (in.)	Righting moment, M_r (lb.in./in.)	Overturning moment, $1.5M_{o,GRS}$ (lb.in./in.)	Vertical force, F_v (lb/in.)	Horizontal force, $F_{h,GRS}$ (lb/in.)	q_{max} (psi)	q_{min} (psi)	Concrete wall weight, W_w (lb/in.)
32	11927	15025	560	427	98	-63	264
39	15254	15025	578	427	73	-37	278
58	23743	15025	624	427	40	0	314

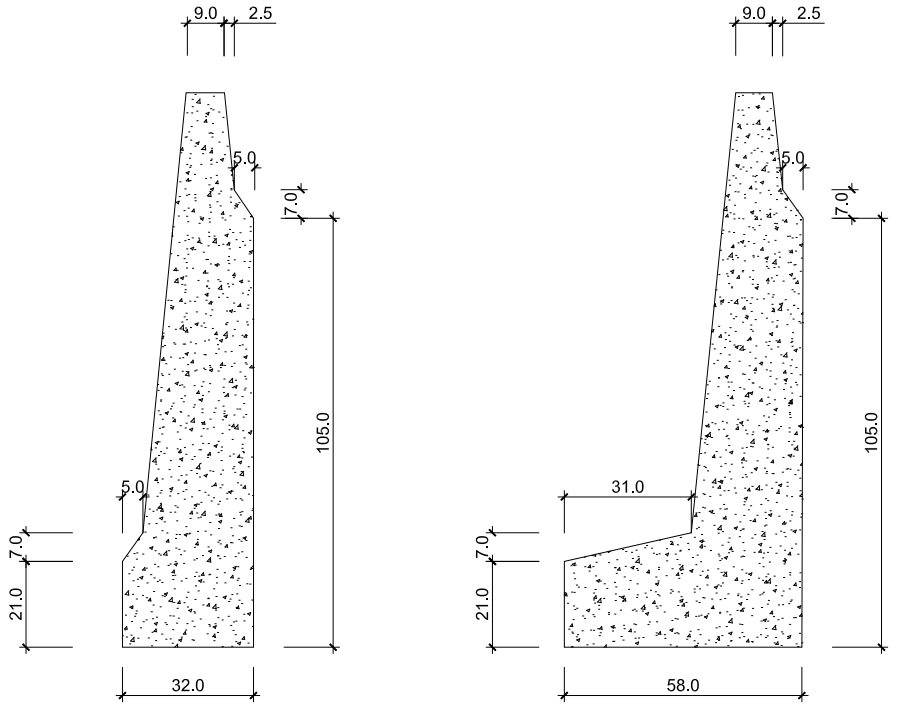

a) Original shape b) Modified shape

Figure 64. Wall shape for the maximum height

5.5 Impact load

The findings of NCHRP Report 663 (2010) may be used to determine equivalent static forces for sliding and overturning stability on MSE walls (CDOT Bridge Design Manual, 2020). Over the last decade, the design load for such barriers has changed from 10 kips to 54 kips and raised the question that which load should be used. In the NCHRP Report 663 (2010), the stability of the barrier system was investigated using static and dynamic analytical solutions, full-scale static and dynamic impact load tests, and numerical modeling. It was found that barrier stability can be satisfied using static equilibrium analyses with an equivalent static load of 10 kips while the dynamic barrier load of 54 kips is appropriate for the strength design of the barrier but will result in an overly conservative design of the moment slab.

The current design of the T7B-GRS wall with the maximum wall height of 8-6" did not meet the requirements of overturning and minimum bearing pressure whether or not accounting for impact load. The proposed wall shape with righting moment much higher overturing moment so it can support the impact load. CDOT (2018) showed that the vehicular horizontal impact of 10 kips that may refer to NCHRP Report 663 (2010). This design load is used in this study as a reference and the load distribution and overturning moment caused by vehicular impact load are calculated based on Chapter 11 in CDOT Bridge Design Manual (2020).

The equivalent length of load distribution is:

$$L_{im,eq} = 5 + 2 \times (8.5 + 1.8) = 25.6 \text{ ft}$$

Overturning moment caused by vehicular impact load is given by:

$$M_t = \frac{F_t}{L_t + 2(H + H_e)}(H + H_e) = \frac{10000}{4 + 2(8.5 + 2)}(8.5 + 2) = 4080 \text{ lb.in./in.}$$

where H is wall height below the ground surface; H_e is the distance from the ground surface to the applied load location; L_t is the length of the vehicle in contact with the rail; F_t is transverse impact force.

$$M_t < M_r - M_o = 23743 - 15025 = 8718 \text{ lb.in./in.}$$

The T7B-GRS wall satisfied the requirement of overturning. Other checks should be conducted for bearing and sliding capacities.

6 SUMMARY AND CONCLUSIONS

This report presents the findings of tests from four large-scale physical models of T7B-GRS walls with comprehensive instrumentation. A research team of six MS and Ph.D. students conducted the tests under the supervision of two professors in the Center for Geotechnical Engineering Science (CGES) at the University of Colorado Denver. The walls were identical except with/without wrap-around for the geosynthetic reinforcements at different spacing. The backfill is the Colorado Class I backfill of crushed granite widely used for GRS walls in Colorado. The four T7B-GRS walls loaded to pressures higher than the service load without visible damage. Four FE models simulated the performance of the four walls using the SSI2D program. Results of the FE analyses compared well with the measured model performance.

The analytical method for the active earth pressure of GRS is developed and applied for the T7B-GRS wall with maximum height. The findings of this study are summarized as follows:

- For the T7B-GRS walls with wrap-around geosynthetics, lateral pressures on the concrete walls are small and yet exist due to the lateral stiffening effects of GRS with reduced deformation. However, the resultant lateral forces are less than those from the T7B-GRS walls without wrap-around effects, but the differences were not significant.
- The load cells along the wall base measured the vertical load transferred from the backfill to the concrete wall through the soil-concrete interface. The wall foundation design and overturning stability analysis should take into account the effect of this vertical load.
- The lateral earth pressures from the FE analyses are in good agreement with measurements.
- The active lateral earth pressure of GRS proposed in this study can improve the current design method.
- The T7B-GRS wall with a maximum height of 8’-6” without wrapped around does not satisfy the current CDOT design requirements. The improved wall shape includes a 56-inch wall base. Following the current CDOT design method and the proposed active earth pressures can provide an optimal shape and a maximum height of the T7B-GRS wall.

- It is time to conduct full-scale field studies of GRS walls with a comprehensive instrumentation program to further check the proposed wall shape optimization and stability of all walls, including T7B-GRS and truncated-base walls.

REFERENCES

AASHTO T-180. Standard Method of Test for Moisture–Density Relations of Soils Using a 4.54-kg (10-lb) Rammer and a 457-mm (18-in.) Drop.

AASHTO (2017). AASHTO LRFD Bridge Design Specifications.

AASHTO (2020). AASHTO LRFD Bridge Design Specifications.

Abu-Hejleh, Zornberg, J., N., Wang, T., McMullen, M., and Outcalt, S. (2000). "Performance of Geosynthetic- Reinforced Walls Supporting the Founders/Meadows Bridge and Approaching Roadway Structures, Report 2: Assessment of the Performance and Design of the Front GRS Walls and Recommendations for Future GRS Abutments." Report No. CDOT-DTD-R-2001-12, Colorado Department of Transportation.

Abu-Farsakh, M.Y., Ardah, A. and Voyiadjis, G.Z., 2019. Numerical parametric study to evaluate the performance of a Geosynthetic Reinforced Soil–Integrated Bridge System (GRS-IBS) under service loading. Transportation Geotechnics, 20, p.100238.

Adams, M., Nicks, J., Stabile, T., Wu, J.T., Schlatter, W. and Hartmann, J., 2011. Geosynthetic reinforced soil integrated bridge system, synthesis report (No. FHWA-HRT-11-027). The United States. Federal Highway Administration.

Adams, M., Nicks, J., Stabile, T., Schlatter, W. and Hartmann, J., 2012. Geosynthetic reinforced soil integrated bridge system, interim implementation guide (No. FHWA-HRT-11-026). Federal Highway Administration.

Ahmadabadi, M. and Ghanbari, A. (2009). New procedure for active earth pressure calculation in retaining walls with reinforced cohesive-frictional backfill. Geotextiles and Geomembranes 27 456-463.

Ardah, A., Abu-Farsakh, M. and Voyiadjis, G., 2017. Numerical evaluation of the performance of a Geosynthetic Reinforced Soil-Integrated Bridge System (GRS-IBS) under different loading conditions. Geotextiles and geomembranes, 45(6), pp.558-569.

ASTM D-4595. Standard Test Method for Tensile Properties of Geotextiles by the Wide-Width Strip Method.

Bathurst, R.J., 2014. Reinforced soil walls e design and construction. Bridge Struct. Eng. 44 (3), 15-24.

Bligh, R.P., Briaud, J., Kim, K.M. and Abu-Odeh, A., 2010. Design of roadside barrier systems placed on MSE retaining walls (NCHRP Report 663). Washington, DC: Transportation Research Board.

Carrubba, P., Moraci, N., Montanelli, F., 1999. Instrumented soil reinforced retaining wall: analysis of measurements. In: Proceedings of Geosynthetics, vol. 2. IFAI, Boston, Massachusetts, USA, pp. 921e934. April 1999.

CDOT (2018). MSE Wall Sheets LRFD.

CDOT Bridge Design Manual (2020).

Chang, Nien-Yin, Abu-Hassan, Mohamed, 2006 "Anisotropic Properties of MSE Geo-composite," Proceedings, ASCE Geo-Congress, Atlanta, GA.

Chang, Nien-Yin, K. Lee, T. Wang. 2004, "Hybrid T Walls under Seismic Loads, Geotechnical Special Publication No. 126, pp 1239-1248, ASCE GeoTransportation 2004, UCLA.

Chang, Nien-Yin, Lee, Zeh Zon, Wang, Trever, "Hybrid T Walls under Seismic Loads, Geotechnical Special Publication No. 126, pp 1239-1248, ASCE GeoTransportation 2004, UCLA.

Chang, N.Y., Nghiem, H.M., and Lee, K., (2020a). Performance of a GRS-IBS Bridge Abutment: Colorado Case Study. Report CDOT-2020-07.

Chang, N.Y., Nghiem, H.N., and Wang, S., (2020b). Analyze and Validate Bearing Pressure Requirements for Truncated Base Mechanically-Stabilized Earth/Geosynthetically-Reinforced Soil (GRS) Walls. Report CDOT-2020-01.

Chang, Nien-Yin, Oncul, Fatih, and Wang, Trever (2004), "Colorado Type 7 and Type 10 Rails under High Test Level Loads, (1st author with F. Oncul, T. Wang, et al,), Geotechnical Special Publication No. 126, pp 1610-1620, ASCE GeoTransportation 2004, UCLA.

Chang, Nien-Yin, Wang, T., Suiidimanan, O. 2004, "Multi-directional Seismic Responses of Hybrid Tee Walls, Geotechnical Special Publication No. 126, pp 1701-1710, ASCE GeoTransportation 2004, UCLA.

Elias, V., Christopher, B.R., Berg, R.R. and Berg, R.R., 2001. Mechanically Stabilized Earth Walls and Reinforced Soil Slopes: Design and Construction Guidelines (Updated Version) (No. FHWA-

FHWA (1999). Earth Retaining Structures. Reference Manual. FHWA NHI-99-025

FHWA (2001). Load and Resistance Factor Design (LRFD) for Highway Bridge Substructures. FHWA HI-98-032

Farzaneh, O., Askari, F.,and Fatemi J. (2014). Active earth pressure induced by strip loads on a backfill. International Journal of Civil Engineering, Vol. 12, No. 4, Transaction B: Geotechnical Engineering, December.

Greco, V. G. (2006). Lateral earth pressure due to backfill subject to a strip of surcharge. Geotechnical and Geological Engineering 24: 615–636.

Greco, V. G. (2005). Active earth thrust by backfills subject to a line surcharge. Can. Geotech. J. 42: 1255–1263.

Ghanbari, A., and Taheri, M. (2012). An analytical method for calculating active earth pressure in reinforced retaining walls subject to a line surcharge. Geotextiles and Geomembranes 34 1-10.

Jaky, J., (1944). The coefficient of earth pressure at rest. J. of the Society of Hungarian Architects and Engineers, pp.355-358.

Jarquio R. Total lateral surcharge pressure due to strip load, Journal of the Geotechnical Engineering Division, 1981, No. 10, Vol. 107, pp. 1424-1428.

Liu, Hsing Cheng (199x), Triaxial Tests of Geotextile Reinforced Sand, MS Thesis, Center for Geotechnical Engineering and science (CGES), University of Colorado Denver.

NAVFAC DM7-02 (1982). Foundations and Earth Structures.

NHI-00-043. The United States. Federal Highway Administration.

Nicks, J.E., Adams, M.T., Ooi, P.S.K. and Stabile, T., 2013. Geosynthetic reinforced soil performance testing - Axial load-deformation relationships (No. FHWA-HRT-13-066).

Rahmouni, O., Mabrouki, A., Benmeddour, D. and Mellas, M., 2016. A numerical investigation into the behavior of geosynthetic-reinforced soil segmental retaining walls. International Journal of Geotechnical Engineering, 10(5), pp.435-444.

Rankine, W.J.M. (1857). On the stability of loose earth. Philosophical Transactions of the Royal Society of London, Vol. 147, p. 9 - 27.

Saghebfar, M., Abu-Farsakh, M., Ardah, A., Chen, Q. and Fernandez, B.A., 2017. Performance monitoring of geosynthetic reinforced soil integrated bridge system (GRS-IBS) in Louisiana. Geotextiles and Geomembranes, 45(2), pp.34-47.

Soong, T-Y., and Koerner, R.M., "On the Required Connection Strength of Geosynthetically Reinforced Walls," Geotextiles and Geomembranes, 15, 1997, pp. 377–393.

Wu, J.T.H., (2001). Revising the AASHTO Guidelines for Design and Construction of GRS Walls, Colorado Department of Transportation, Report No. CDOT-DTD-R-2001-16, 2001.

Wu, J.T. and Ooi, P.S., 2015. Synthesis of Geosynthetic Reinforced Soil (GRS) Design Topics (No. FHWA-HRT-14-094). The United States. Federal Highway Administration.

Yu, Y., Bathurst, R.J. and Allen, T.M., 2017. Numerical modeling of two full-scale reinforced soil-wrapped-face walls. Geotextiles and Geomembranes, 45(4), pp.237-249.

APPENDIX A

Table A1. Soil properties used in the analyses

Properties	Units	Value
Friction angle, ϕ	(^{0})	43
Cohesion, c	(psi)	14.4
Dilatancy angle, ψ	(^{0})	8.7
K_L	-	1300
n_L	-	0.477
K_{ur}	-	1975.6
n_{ur}	-	0.344
ν	-	0.145

Table A2. Properties of the base foundation soil

Properties	Units	Value
Young's Modulus	(psi)	4124
Undrained shear strength	(psi)	17
Poisson's Ratio	-	0.3

Table A3. The interface between soil and concrete wall

Properties	Units	Value
Friction angle	(^{0})	38

Cohesion	(psi)	0

Table A4. Geosynthetic properties

Properties	Unit	Value
EA_i	lb/ft [kN/m]	44250 [659]
EA_{ur}	lb/ft [kN/m]	69000 [1028]
Fmax	lb/ft [kN/m]	4353 [65]

Table A5. Point coordinates

Point	X (in.)	Y (in.)	Point	X (in.)	Y (in.)	Point	X (in.)	Y (in.)
1	0.00	0.00	19	90.55	59.06	37	43.00	55.12
2	137.80	0.00	20	93.50	59.06	38	40.61	59.06
3	137.80	11.81	21	69.29	11.81	39	38.22	62.99
4	93.50	11.81	22	35.83	66.93	40	90.55	31.50
5	93.50	66.93	23	66.14	19.69	41	90.55	39.37
6	0.00	66.93	24	61.81	27.56	42	90.55	47.24
7	90.55	11.81	25	57.09	35.43	43	90.55	55.12
8	90.55	66.93	26	52.36	43.31	44	90.55	62.99
9	90.55	19.69	27	47.24	51.18	45	86.61	66.93
10	93.50	19.69	28	42.52	59.06	46	66.93	66.93
11	90.55	27.56	29	64.51	19.69	47	122.05	11.81

12	93.50	27.56	30	59.73	27.56	48	122.05	23.62
13	90.55	35.43	31	57.34	31.50	49	118.11	30.51
14	93.50	35.43	32	54.95	35.43	50	112.60	87.76
15	90.55	43.31	33	52.56	39.37	51	100.79	87.76
16	93.50	43.31	34	50.17	43.31	52	98.43	77.76
17	90.55	51.18	35	47.78	47.24	53	93.50	70.87
18	93.50	51.18	36	45.39	51.18	54	122.05	19.69
Point	X (in.)	Y (in.)	Point	X (in.)	Y (in.)	Point	X (in.)	Y (in.)
55	90.55	15.75	62	93.50	23.62	69	93.50	47.24
56	90.55	23.62	63	62.12	23.62	70	49.80	47.24
57	37.80	66.93	64	63.98	23.62	71	93.50	55.12
58	70.87	11.81	65	93.50	31.50	72	44.88	55.12
59	93.50	15.75	66	59.45	31.50	73	93.50	62.99
60	66.90	15.75	67	93.50	39.37	74	40.16	62.99
61	68.50	15.75	68	54.72	39.37			

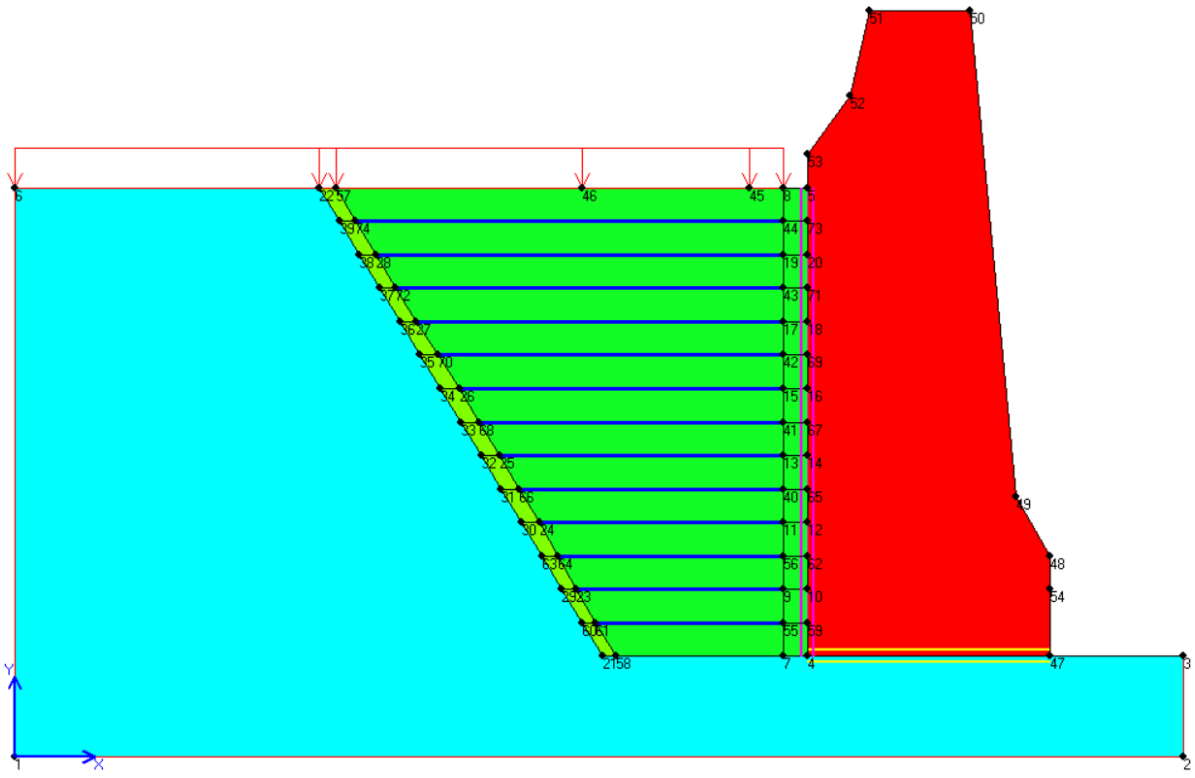

Figure A1. The geometry of the model

APPENDIX B

B.1 Design criteria

CDOT parameters used in MSE Wall LRFD (CDOT 2018) are shown in Table 2 (from B-504-H2). The geometry of the concrete wall and applied forces are shown in Figs. B1 and B2.

Active earth pressure coefficient:

$$K_a = \frac{1-\sin\varphi}{1+\sin\varphi} \qquad \text{(B1)}$$

At rest earth pressure coefficient:

$$K_0 = 1 - \sin\varphi \tag{B2}$$

$$K_r(z) = K_0 - \frac{z}{20}(K_0 - K_a) \text{ if } z < 20', \text{ otherwise } K_r(z) = K_a \tag{B3}$$

Factored vertical stress:

$$\sigma_{v1}(z) = \gamma_v \gamma_{soil}(z - HMAthk) + \gamma_{HMA,Max}\gamma_s(HMAthk) + LS\gamma_{soil}LLSurg \tag{B4}$$

Lateral pressure of soil only:

$$\sigma_{h,soil} = K_r \sigma_{v1} \tag{B5}$$

The proposed lateral pressure of GRS (from Eq. 39):

$$\sigma_{h,GRS} = \sigma_{h,soil} - \frac{T}{S_v} \tag{B6}$$

Tension force in the ith geosynthetic layer (from Eq. 11.10.6.3.2-1, AASHTO LRFD, 2020):

$$T_i = \phi F^* \alpha \sigma_{v0} L_i C \tag{B7}$$

Maximum tension force of geosynthetic (from Eqs. 11.10.6.4.1-1 and 1.10.6.4.3b-1, AASHTO LRFD, 2020):

$$T_i \le T_{\max} = \phi T_a R_c = \phi \frac{T_{ult}}{RF} R_c = \phi \frac{T_{ult}}{RF_{CR} RF_D RF_{ID}} R_c \tag{B8}$$

The factored friction force between soil and concrete wall at a depth:

$$F_{v,f,i} = \frac{1}{2}\left(\sigma_{vl,GRS,2} + \sigma_{vl,GRS,1}\right)\left(z_2 - z_1\right)\tan\delta \tag{B9}$$

where δ is friction angle between soil and concrete wall, $\tan\delta = 0.8\tan\varphi$.

Total factored friction force:

$$F_{v,f} = \sum F_{v,f,i} \tag{B10}$$

Factored lateral force at a depth:

$$F_{h,GRS,i} = \frac{1}{2}\left(\sigma_{h,GRS,2} + \sigma_{h,GRS,1}\right)\left(z_2 - z_1\right) \tag{B11}$$

Total factored lateral force:

$$F_{h,GRS} = \sum F_{h,GRS,i} \tag{B12}$$

Factored overturning moment at a depth:

$$M_{0,GRS,i} = \sigma_{h,GRS,1}\left(z_2 - z_1\right)\left(H - \frac{z_2 + z_1}{2}\right) + \frac{1}{2}\left(\sigma_{h,GRS,2} - \sigma_{h,GRS,1}\right)\left(z_2 - z_1\right)\left(H - \frac{2z_2 + z_1}{3}\right) \tag{B13}$$

Total factored overturning moment:

$$M_{0,GRS} = \sum M_{0,GRS,i} \tag{B14}$$

Righting moment:

$$M_r = 0.9W_w\left(B - d_w\right) + F_{v,f}B \tag{B15}$$

Check for the overturning moment:

$$M_r \geq 1.5M_{0,GRS} \tag{B16}$$

Eccentricity at the concrete wall base:

$$e = \frac{\sum M}{F_v} = \frac{1.5M_{0,GRS} - 1.5F_{v,f}B - 1.25W_w\left(B - d_w\right)}{F_v} \tag{B17}$$

Maximum and minimum bearing pressures at the wall base:

$$q_{\max,\min} = \frac{F_v}{A} = \frac{1.5F_{v,f} + 1.25W_w}{A}\left(1 \pm \frac{6e}{B}\right) \tag{B18}$$

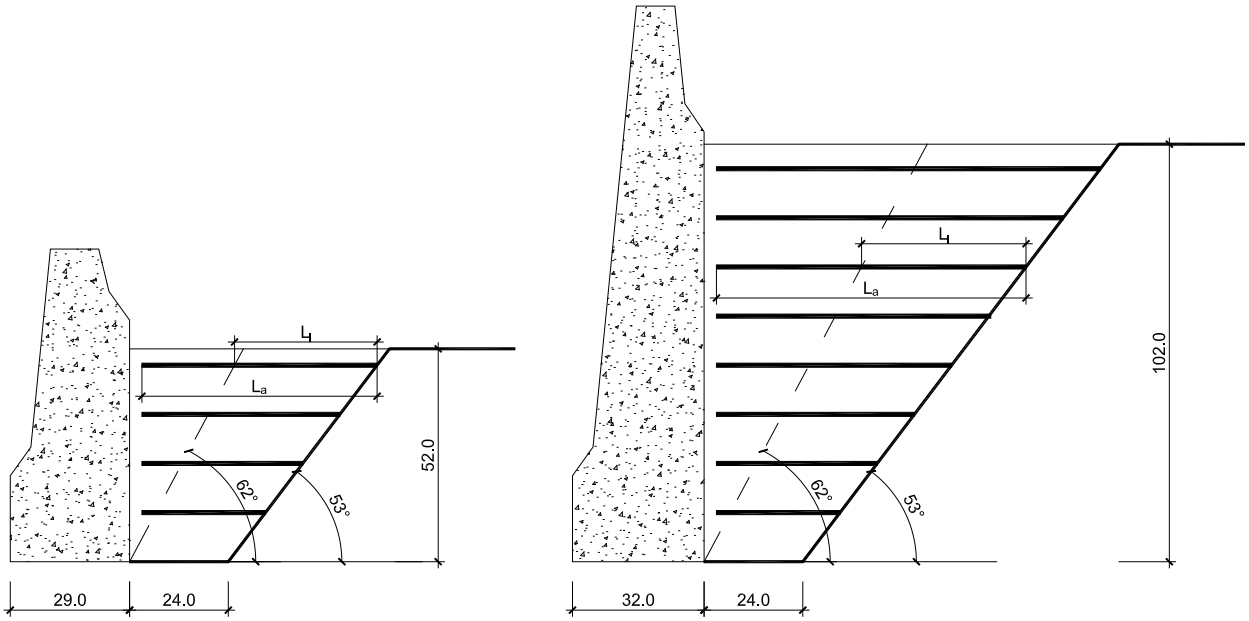

a) 4’-4” height a) 8’-6” height

Figure B1. Geometry of the T7B-GRS walls

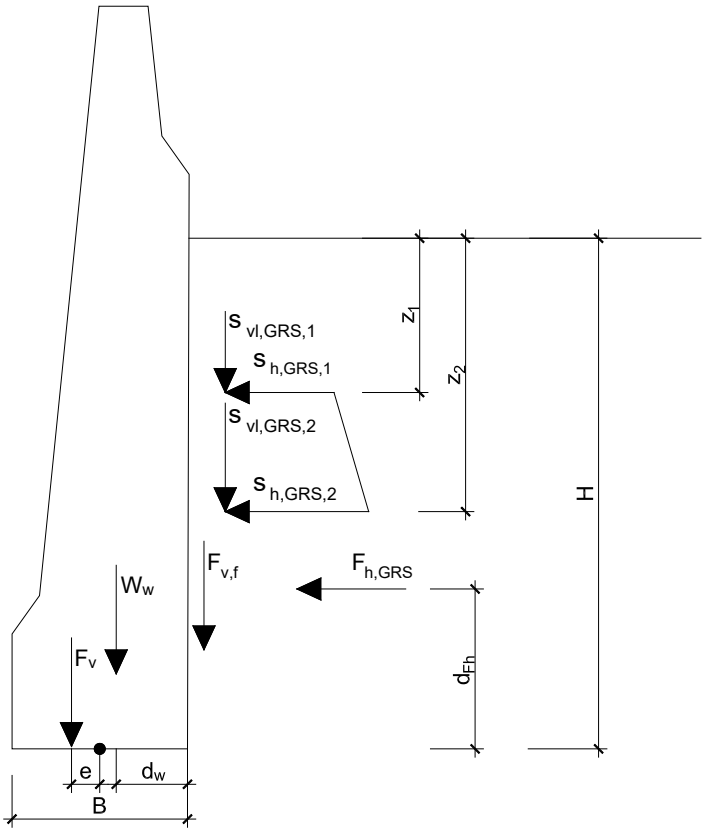

Figure B2. Forces on the concrete wall

B.2 T7B-GRS wall under design load

Table B1. Parameters used in CDOT Work Sheet

Property	Value
φ	34^0
Υ_{soil}	125 pcf
Υ_h	1.5
Υ_v	1.35
LS	1.75
$LL_{Surcharge}$	2’
d_{max}	2”
HMA_{thk}	10”
hma	140 pcf
Υ_{HMA}	Max.=1.5 Min.=0.65
F*	0.449672

Table B2. Concrete wall properties

Wall height	Concrete wall weight (lb/in)	Base width (in.)	Wall height (in.)	d_w (in.)
4’-4”	136	29	52	12.7
8’-6”	264	32	102	12.8

Table B3. Coefficients of lateral earth pressures

K_a	K_p	K_0
0.282715	3.537132	0.440807

Table B4. Design tensile strength of geosynthetic

RF	ϕ	R_c	T_{ult} (lb/ft)	$\phi T_a R_c$ (lb/in)
7	0.9	1	4800	51.42

Table B5. Factors for calculating tension force in the geosynthetic

C	α	R_c	φ
2	0.6	1	0.9

B.2.1 4’-4” height

Table B6. Design pullout strength of geosynthetic (4’-4” height)

z (in.)	σ_v (psi)	L_a (in.)	L_i (in.)	L_a-L_i (in.)	Min (L_i,L_a-L_i) (in.)	φ$T_i R_c$ (lb/in.)
0	2.55					
4.00	2.84	57.17	34.65	22.52	22.52	10.94
16.00	3.70	48.13	31.99	16.14	16.14	7.84
28.00	4.57	39.09	29.32	9.76	9.76	4.74
40.00	5.44	30.04	26.66	3.38	3.38	1.64
52.00	6.31	0.00	0.00	0.00	0.00	0.00

Table B7. Calculation of lateral earth pressures (4’-4” height)

z (in)	σ_{vl} (psi)	K_r	$\sigma_{h,soil}$ (psi)	$\sigma_{h,GRS}$ (psi)	$F_{h.GRS,i}$ (lb/in.)	$M_{0,GRS,i}$ (lb.in./in.)	$F_{v,f,i}$ (lb/in.)
0.00	4.25	0.44	1.87	1.87			

4.00	4.64	0.44	2.03	1.12	6.00	300.84	3.24
16.00	5.82	0.43	2.50	1.85	17.84	740.39	9.62
28.00	6.99	0.42	2.95	2.56	26.43	784.51	14.26
40.00	8.16	0.41	3.38	3.25	34.81	618.29	18.78
52.00	9.33	0.41	3.79	3.79	42.23	246.81	22.79

$F_{h,GRS} = 127$ lb/in., $d_{Fh} = 21$ in.

Table B8. Bearing pressure (4'-4" height)

F_v (lb/in)	$\sum M$ (lb.in./in.)	e (in)	B' (in.)	q_{max} (psi)	q_{min} (psi)
273.50	2242.92	7.75	16.50	24.55	-5.69

B.2.1 8'-6" height under design load

Table B9. Design pullout strength of geosynthetic (8'-6" height)

z (in.)	σ_v (psi)	L_a (in.)	L_i (in.)	L_a-L_i (in.)	Min (L_i,L_a-L_i) (in.)	$\varphi T_i R_c$ (lb/in.)
0	2.55					
6.00	2.98	93.34	45.30	48.04	45.30	22.00
18.00	3.85	84.30	42.63	41.66	41.66	20.23
30.00	4.72	75.26	39.97	35.28	35.28	17.14
42.00	5.58	66.21	37.31	28.90	28.90	14.04
54.00	6.45	57.17	34.65	22.52	22.52	10.94
66.00	7.32	48.13	31.99	16.14	16.14	7.84
78.00	8.19	39.09	29.32	9.76	9.76	4.74
90.00	9.06	30.04	26.66	3.38	3.38	1.64

Table B10. Calculation of lateral earth pressures (8'-6" height)

z (in)	σ_{vl} (psi)	K_r	$\sigma_{h,soil}$ (psi)	$\sigma_{h,GRS}$ (psi)	$F_{h.GRS,i}$ (lb/in.)	M_0 (lb.in./in.)	$F_{v,f,i}$ (lb/in.)
0	4.25	0.44	1.87	1.87			

6.00	4.84	0.44	2.11	0.28	6.47	645.08	3.49
18.00	6.01	0.43	2.58	0.89	7.04	626.25	3.80
30.00	7.18	0.42	3.02	1.60	14.93	1156.36	8.06
42.00	8.36	0.41	3.45	2.28	23.27	1527.71	12.56
54.00	9.53	0.41	3.86	2.95	31.39	1686.93	16.94
66.00	10.70	0.40	4.25	3.60	39.28	1642.03	21.20
78.00	11.87	0.39	4.62	4.23	46.95	1401.02	25.34
90.00	13.04	0.38	4.98	4.84	54.40	971.89	29.36
102.00	14.21	0.37	5.31	5.31	60.90	359.74	32.86

$F_{h,GRS} = 286.6$ lb/in., $d_{Fh} = 35$ in.

Table B11. Bearing pressure (8'-6" height)

F_v (lb/in)	$\sum M$ (lb.in./in.)	e (in)	B' (in.)	q_{max} (psi)	q_{min} (psi)
560.16	10289.79	24.65	-17.30	98.42	-63.41

B.2.3 4'-4" height T7B-GRS wall under 14psi surcharge

Table B12. Parameters used in CDOT Work Sheet

Property	Value
φ	43^0
Υ_{soil}	150 pcf
Υ_h	1.0
Υ_v	1.0
LS	1.0
Surcharge	14 psi
F*	0.621677

Table B13. Factors for calculating tension force in the geosynthetic

C	α	R_c	φ
2	0.6	1	0.9

Table 14. Design pullout strength of geosynthetic (4'-4" height)

z (in.)	σ_v (psi)	L_a (in.)	L_i (in.)	L_a-L_i (in.)	Min (L_i,L_a-L_i) (in.)	$\varphi T_i R_c$ (lb/in.)
0	14.06	0	0	0	0	0.00
4.00	14.41	57.17	39.30	17.87	17.87	12.00
16.00	15.45	48.13	35.47	12.65	12.65	8.50
28.00	16.49	39.09	31.65	7.44	7.44	4.99
40.00	17.53	30.04	27.82	2.22	2.22	1.49
52.00	18.58	0.00	0.00	0.00	0.00	0.00

Table B15. Calculation of lateral earth pressures (4'-4" height)

z (in)	σ_{vl} (psi)	K_r	$\sigma_{h,soil}$ (psi)	$\sigma_{h,GRS}$ (psi)	$F_{h.GRS,i}$ (lb/in.)	M_0 (lb.in./in.)	$F_{v,f,i}$ (lb/in.)
0	14.06	0.19	2.66	2.66			
4.00	14.41	0.19	2.72	1.72	8.77	439.56	6.54
16.00	15.45	0.19	2.92	2.21	23.63	986.44	17.63
28.00	16.49	0.19	3.12	2.70	29.49	878.92	22.00
40.00	17.53	0.19	3.32	3.19	35.36	630.60	26.38
52.00	18.58	0.19	3.51	3.51	40.22	237.46	30.00

$F_{h,GRS} = 127$ lb/in., $d_{Fh} = 21$ in.

Table B16. Bearing pressure (4'-4" height)

F_v (lb/in)	$\sum M$ (lb.in./in.)	e (in)	B' (in.)	q_{max} (psi)	q_{min} (psi)
324.28	2229.81	6.90	18.21	27.14	-4.77

B.3 Optimum wall shape of 8'-6" height T7B-GRS wall

Total lateral force: $F_{h,GRS} = 286.6$ lb/in.

Factored lateral force: $1.5 \times 284.6 = 427$ lb

Table B7. Load characteristics on the concrete wall (8'-6")

Base width (in.)	Distance from the wall base to point of application of lateral resultant force (in.)	Eccentricity at the wall base (in.)
32	35	24.7
39	35	19.9
58	35	9.7